Field-deployable system for the detection and measurement of micronutrients

Edward Lo

A dissertation

submitted in partial fulfillment of the

requirements for the degree of

Doctor of Philosophy

University of Washington

2014

Reading Committee:

Buddy D. Ratner, Chair

David G. Castner

Lara J. Gamble

Program Authorized to Offer Degree: Bioengineering

University of Washington

Abstract

Field-deployable system for the
detection and measurement of micronutrients

Edward Lo

Supervisory Committee Chair:
Professor Buddy Ratner
Department of Bioengineering

Micronutrient deficiency is a global problem affecting billions of people world-wide. A lack in any of vitamin A, zinc, iron, folic acid or iodine can result in major health defects which can greatly reduce quality of life. While nutrient supplementation can reduce these deficiencies, other diseases can also occur when nutrient intake is too high. Although accurate systems exist to measure micronutrient status, they are unsuitable for wide scale studies in developing countries due to various drawbacks. In particular, tests are usually specific (capable of analyzing only one, or at most 2 nutrients), expensive, cumbersome and time consuming. To solve these issues, in this work, a compact system capable of measuring multiple nutrients quickly is developed.

Initial work focused on developing a proof-of-concept. Here, a laboratory scale mass spectrometer, Low Temperature Plasma ionization source, and multivariate analysis were combined to create a new system, Plasma Pencil Atmospheric Mass Spectrometry (PPAMS). PPAMS was used to study sample matrices containing nutrients at three different levels spanning the blood range. Individual nutrients were studied by varying single nutrients and holding the

other nutrients constant. In these cases, principal component analysis was capable of classifying data based on nutrient concentration by performing a cube root transformation on the data. The spectra, however, could not be compared for sample data collected on different days due to the appearance of new contamination peaks, caused by using shared equipment.

With detection differences achieved on a laboratory scale instrument, a compact MS, the Advion Express**ion**, was purchased. After system optimizations, individual peaks indicative of nutrient content were observed for Vitamin A, Iron and Zinc. Furthermore, individually quantifying Vitamin A and Zinc was achieved by constructing mathematical models to predict independent data sets in controlled samples at blood levels. The remaining nutrients, and multi-nutrient samples, however, could not be accurately quantified. Overall, PPAMS has been shown to be capable of detecting and quantifying select nutrients at nanogram quantities, even in the presence of a high salt background. Furthermore, with additional system improvements and advances in technology, this method may be capable of simultaneously measuring all 5 micronutrients.

Acknowledgments

I would like to thank everyone for their help and support throughout this process. First, I would like to thank Dr. Buddy Ratner for giving me the opportunity to work on this project. Your vision, support and feedback have helped me to grow not only as a scientist, but as a person as well. To Dr. Dave Castner, thank you for co-advising this project, your insight has been imperative for driving this work forward, as has your support in being a member of my supervisory committee. To my remaining committee members, Drs. Lara Gamble and Michael MacCoss, your expertise and suggestions have been vital contributions and I appreciate all the guidance. Dr. Jeanette Stein and Joelle Rolfs, working with you has been an honor and a pleasure. I have learned so much through our shared discussions and long days in lab. I would also like to acknowledge the Bill and Melinda Gates Foundation for making this work possible through their generous funding.

To the others who have also helped with this project, thank you for your dedication and for all the support throughout. Thank you to all the Ratner lab members and friends I have made during this program. You have made this a truly memorable experience and I could not have spent this time with better people. Finally, I would like to thank my family – my parents, brother, Cheryl and Elmer who have provided me with all the love and support I could hope for.

Table of Contents

List of Abbreviations

AC	Alternating current
Ag	Silver
BSA	Bovine serum albumin
CAR	Central African Republic
CH_3COOH	Acetic Acid
cPBSz	Citrate phosphate buffered saline with sodium azide
Ctrl	Control
DART	Direct analysis in real time
dH2O	Deionized/distilled water
DMEM	Dulbecco's Modified Eagle Medium
DMSO	Dimethyl sulfoxide
DNA	Deoxyribonucleic acid
DPCA	Discriminant Principal Component Analysis
DRC	Democratic Republic of the Congo
ESI	Electrospray ionization
EtOH	Ethanol
Fe	Iron
FolA	Folic Acid
H_2O	Lab grade water
HBL	High blood level concentration
HCl	Hydrochloric acid
Hcyst	Homocysteine
HPLC	High-pressure liquid chromatography
HV	High voltage
i.d.	Inner diameter
LBL	Low blood level concentration
LPM	Liters per minute
LTP	Low temperature plasma
M	Molecular fragment
m/z	mass-to-charge ratio
MALDI	Matrix-assisted laser desorption/ionization
MBL	Medium blood level concentration
MeOH	Methanol
MS	Mass spectrometer
MS/MS	Tandem mass spectrometry
o.d.	Outer diameter
PBS	Phosphate buffered saline
PC	Principal Component
PCA	Principal Component Analysis
PLSr	Partial least squares regression
PPAMS	Plasma pencil atmospheric mass spectrometry

ppb	parts per billion
ppm	parts per million
RBC	Red blood cell
RDA	Recommended daily allowance
RMSEP	Root mean squared error of prediction
RT	Room temperature
S/N	Signal-to-noise ratio
SEM	Scanning electron microscopy
SIM	Selected ion monitoring
Thyr	Thyroxine
ToF-SIMS	Time-of-Flight secondary ion mass spectrometry
UV	Ultraviolet
VitA	Vitamin A
Zn	Zinc

List of Figures

List of Tables

List of Equations

1 Introduction

1.1 Micronutrient Status

Micronutrient deficiency is a global concern, affecting more than 2 billion people worldwide.[1] Deficiencies in key micronutrients, in particular iron, zinc, iodine, vitamin A and folic acid, are major detractors to the quality and length of life. Individuals with sub-optimal levels of micronutrients suffer an increased amount of preventable ailments[2] that cause a significant decrease in both overall life expectancy and disability-adjusted life years. This is a particularly significant problem in developing countries, where a high degree of poor diet and poor micronutrient intake exists.[3]

Each micronutrient is critical for the health of individuals, and a lack in any can cause severe health effects. For example, low iron levels have been shown to increase maternal mortality during birth[4] and decrease cognitive and motor development in infants[5,6] and low zinc levels have been linked to growth retardation,[7] reduced immune system function[8] and hypogonadism in males[9]. In addition to the standard health deficiencies that are caused, deficiencies in folic acid, iron and zinc have been shown to damage DNA, and may be a major cause of cancer.[10]

Many studies have been completed to show that nutrient addition can vastly improve the quality of life. By ensuring a population has sufficient micronutrients, many ailments, including those previously mentioned, can be reduced.[11] In developed countries, extensive programs are in place to increase the amount of micronutrient intake. For example iodine deficiency was prevalent in many regions of the United States in the early 1900s, however with the addition of iodine into table salt in 1924, immediate improvements were observed for thyroid disorders.[12] Another example of fortification was completed more recently in 1998, when the Food and Drug Administration mandated the addition of folic acid to enriched grain products.[13] This in turn led to a significant decrease in the occurrence of neural tube defect births.[14] This effect was further supported by studies of folic acid supplementation in Canada.[15]

Supplementation of appropriate micronutrients is a cost effective way of improving overall health,[16] particularly for the developing world. However, while studies have shown the importance of nutrient addition into food staples, the implementation of this on a wide scale, for example across all of Africa, is complicated by the fact that an excess of micronutrients can also cause severe problems. Similar to iodine deficiency, a chronic excess of iodine can also result in

hypothyroidism,[17] however, in other cases, excess can also lead to hyperthyroidism.[18] Both of these can result in further health complications and decrease the overall quality of life. Thus, care must be taken to ensure that populations will not become burdened with an excess of micronutrients. Specifically, each nation, and subpopulations within each nation, will require different amounts of nutrients added into their food. This can be highlighted by a world map of iodine health status from a study by de Benoist et. al.,[19] shown in Figure 1-1.

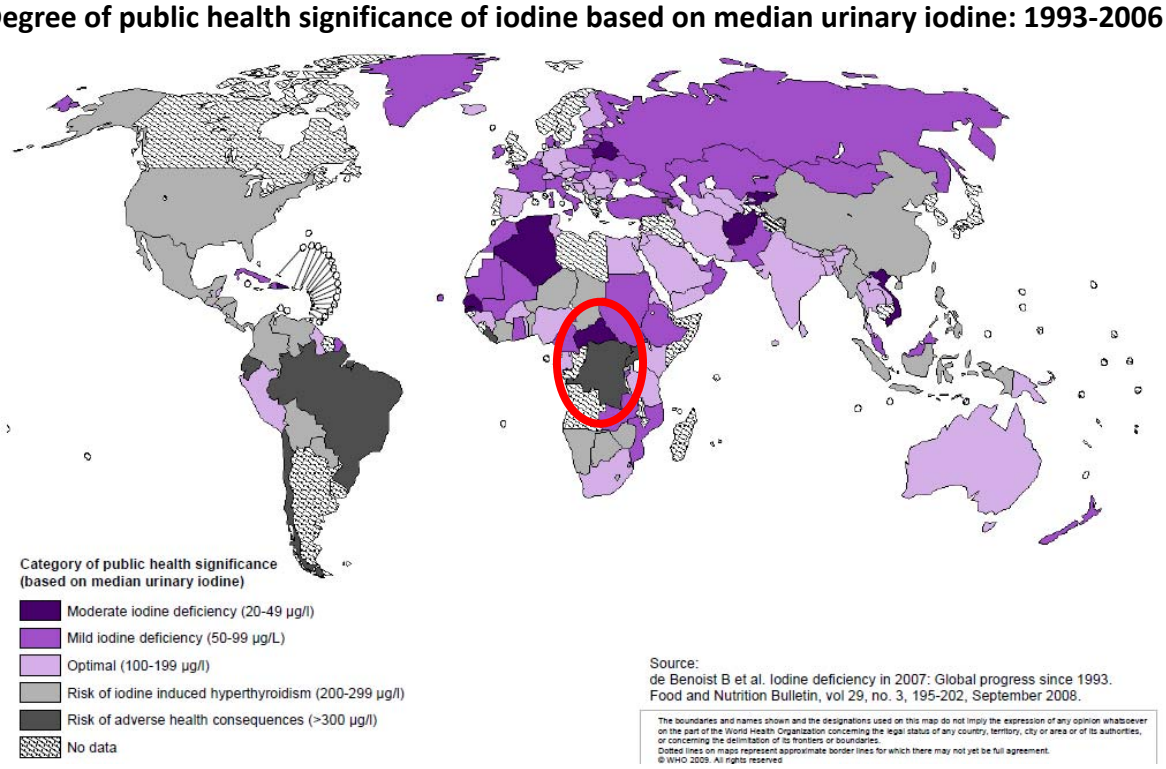

Figure 1-1 Iodine nutrition status map Circled in red are neighboring nations, the Central African Republic (upper, dark purple) and the Democratic Republic of the Congo (lower, dark grey). Figure reproduced with permission from The Food and Nutrition Bulletin, from de Benoist et. al.[19]

This figure shows that in Africa, many neighboring countries have different levels of iodine health status, ranging from dark purple which is a moderate iodine deficiency, up to dark grey which is an iodine excess, to the point where they are at risk for health consequences.[19] While the excess of iodine can be explained by government programs in place for the iodization of salt, this is a clear example of how greater control is required. Furthermore, while this map gives a general idea of a nation's nutrient status, within each country, differences will also exist on the community, and perhaps even individual level. For example, while de Benoist's study

showed an overall excess of iodine in the Democratic Republic of the Congo (DRG), caused by their established salt iodization programs, further studies have shown that the actual iodine distribution within the country is still well outside the acceptable range. In particular, studies have shown that the iodine content in salt in the DRG varies from below the minimum accepted value in 36% of the country's salt, to above the maximum allowable amount in 19% of salt.[20] This study indicated that over half of the population is receiving an inappropriate amount of iodine, and may still be at risk for health defects. Thus, experts agree that a great need exists to control the level of micronutrient fortification required to properly address nutrition.[21] Furthermore, to ensure that the amount of nutrients supplemented reflects the need of the population, we must continually monitor the effect of the supplementation.

1.2 Micronutrient detection and measurement

To ensure the proper amounts of micronutrients are added into food, the baseline nutrient level prior to fortification must be known. Current standards in micronutrient detection and measurement require laboratory scale techniques.[22] Furthermore, no single technique can be used to measure all 5 micronutrients of interest in these studies. Thus, to determine the nutrient levels, samples must be collected and properly stored on site, prior to being shipped to a testing facility. Upon receipt, different techniques will be used, such as atomic absorption spectroscopy for zinc[23] and high performance liquid chromatography (HPLC) for Vitamin A.[24] These results could then be transported back to the researchers to be analyzed to determine whether or not fortification is necessary. The required sample and data handling and transport can quickly become cost and time prohibitive for developing regions, particularly for large scale studies and studies on isolated populations.

Other challenges also exist for micronutrient measurement, due to a lack of agreement about which markers best indicate nutrient status. For example, traditionally, retinol, the most prevalent form of Vitamin A in the blood, is used to measure Vitamin A status[25,26] and can be detected using the aforementioned HPLC. However, recently, some researchers are now using retinol binding protein (RBP), the retinol carrier in blood, to determine Vitamin A status instead.[27] RBP is seen as an inexpensive alternative to retinol,[28] and is commonly measured using the enzyme linked immunosorbent assay test to achieve quantitation.[29] Both these methods, however, may have confounding factors, such as diseases which can alter their blood concentrations.[30] Furthermore, all of the other nutrients also have various potential markers to

indicate status. Thus, in this work, information about the entire blood based sample will be collected. By collecting information from the entire sample, results from the different markers might be detected, which may improve the overall accuracy of the test.

1.2.1 On-site measurement

While some progress has been made for the on-site measurement of most of the nutrients of interest, no solution exists to assess multiple nutrients at once. For example, Iron detection has seen some success. While several method involve the collection of blood on site, to be transported to a lab for analysis,[31] a portable method has also been developed. Here, the use of a portable surface plasmon resonance system, along with a microfluidic device[32] allowed researchers to determine transferrin levels, which is the iron carrier in serum. Portable zinc measurements have also been investigated. For example, Hanna Instruments (Smithfield, RI) produces the Zinc Portable Photometer. However, this system is used only for measurements of Zinc in water, not biological fluids. Developments for Vitamin A detection have come in the form of test strip fabrication, using an enzyme immunoassay.[33] This method, however, still requires extensive sample preparation and needs 40 minutes to complete a single test. For iodine, success has been achieved in the analysis of real samples using an adapted commercially available radioimmunoassay,[33] however, this method requires the use of radioactive substances, and several hours to complete each test. Furthermore, while somewhat adaptable for field use, extensive sample preparation is required. While no methods for portable or on-site detection of Folic Acid were found, none of the current solutions can address the need of efficiently measuring multiple nutrients.

1.3 Mass Spectrometry

While current analysis methods have limited applicability and limited ability for real-time, on-site use, mass spectrometry may provide a viable solution as a single test for all five micronutrients. Mass spectrometry is made up of two key components, the ionization source and the mass spectrometer (MS). Sample ionization must occur in order for the sample constituents to be determined. These ionization sources impart energy to the sample to form positive and negative ions as well as neutral particles. The ions are then transported towards the detector through methods such as pressure gradients and electric fields.[34] To identify the sample ions, the different species from the sample are then separated from each other, using a mass analyzer. To accomplish this, normally, the mass analyzer separates the ions based on the mass-to-charge ratio

(*m/z*), through filtering, trapping, or time-of-flight. After the masses have been separated, the detector will determine the intensity of the each ion. While many different ionization sources and MSs are currently available the ones utilized in these studies will be presented in later sections.

Mass spectrometry is an extremely versatile technique with applications in a variety of areas and is one of the most sensitive techniques available.[35] Several systems have been developed to analyze samples in real world settings. One of the most visible areas for ion mobility spectrometry applications can be seen with explosives detection. These systems can be seen across the world in airports, as well as more portable systems designed for field detection for the military.[36] While these systems for explosives detection are very fast (analysis within seconds), they are traditionally used only for detection and not measurement.[37] Other methods, however, have been developed for quantitative analysis as well. In particular, quantitation has been a key focus for mass spectrometry based proteomics. Here, biological samples are measured to determine protein concentration levels through both labeled (isotopic) and unlabeled methods.[38] These systems, however, generally utilize large, laboratory based instruments and are often very time consuming to complete. This study aims to combine the strengths of these different systems to form a quantitative, yet fast and portable mode of analysis.

1.4 Overview and specific aims

This project aims to develop a field deployable system that can be used to analyze and measure five of the most important micronutrients for child development and health, iron, zinc, iodine, vitamin A and folic acid. This study will focus on the analysis of samples with controlled levels of nutrients to mimic individuals with various health statuses. The capability of studying all 5 micronutrients will allow for broad surveys of entire populations and subgroups within these populations in order to determine the nutrients required to improve their quality and length of life. Specific Aim 1 will focus on system development as well as initial proof of concept testing. Specific Aim 2 will focus on further testing and verification by varying nutrients at blood levels. Specific Aim 3 will focus on further system development (miniaturization) as well as model building using known samples.

Specific Aim 1: To develop and test a mass spectrometry based system for sample analysis, and compare to traditional lab scale techniques

Specific Aim 2: To develop a physiologically-relevant nutrient model based on adult human blood levels and analyze with Plasma Pencil Atmospheric Mass Spectrometry (PPAMS)

Specific Aim 3:

A. To acquire a compact mass spectrometer and optimize system settings for Vitamin A detection and demonstrate quantitation using partial least squares analysis
B. To utilize the compact mass spectrometer and improve detection of iron, zinc, folic acid and thyroxine (a biomarker for iodine)

2 Experimental materials and general methods

2.1 Materials

2.1.1 Micronutrients

Micronutrient powders were purchased from Sigma-Aldrich Chemical Co. (St. Louis, MO) as iron (II) chloride (Fe), zinc (II) chloride (Zn), and folic acid (FolA). Vitamin A was purchased as retinol (VitA), which is the dominant biological form. When available, VitA was purchased at 99% purity, however, 97% purity was also used. Iodine was also purchased from Sigma-Aldrich in the form of thyroxine (Thyr), which is the main iodine-containing molecule through the body.

2.1.2 Solvents, biological fluids and chemicals

In depth protocols for specific experiments can be found within the Methods sections of each specific aim. Here, the use of each chemical will be described in brief. VitA, FolA and Thyr have relatively low to no water solubility and were thus normally dissolved at high concentrations in suitable solvents, prior to addition to the final samples. Ethanol (EtOH, Decon Labs Inc., King of Prussia, PA), for VitA, dimethyl sulfoxide (DMSO, Sigma Aldrich), for FolA and ammonium hydroxide (NH_4OH, Fisher Scientific, Pittsburgh, PA), for Thyr were used to dissolve the respective nutrients at high concentrations, as described later. Bovine serum albumin (BSA, Sigma-Aldrich) was used as a model for blood for time-of-flight secondary ion mass spectrometry (ToF-SIMS) experiments. Porcine plasma (PL26009, Innovative Research, Novi, Mi) is used as an initial blood model in plasma pencil atmospheric mass spectrometry (PPAMS) experiments. Bovine whole blood (IR1-040N, Li Heparin, Lot 11916, Innovative Research) was for further experiments using the PPAMS. Baseline nutrition in samples were measured at the University of Washington Research Testing Service, as discussed in section 4.2.1.

Sodium azide (Sigma Aldrich), sodium citrate (Fisher Scientific, Waltham, MA), sodium phosphate (Fisher Scientific), sodium chloride (Mallinckrodt Chemical Company, St. Louis, MO), sodium iodide (Sigma Aldrich), citric acid monophosphate (Baker Mallinckrodt, Phillipsburg, NJ), water (Macron Chemical company) were used to make citrate phosphate buffered saline. Sodium hydroxide (Mallinckrodt Chemical Company), hydrochloric acid (EMD Millipore, Philadelphia, PA) and acetic acid (Fisher Scientific) were used for pH adjustment experiments. 50% gluteraldehyde (Electron Microscopy Sciences, Fort Washington, PA) was used for cell fixation. Triton x-100 (Sigma Aldrich) was used for cell lysis. Glass slides were

cleaned with dichloromethane (Fisher Scientific), acetone (Sigma Aldrich) and methanol (Sigma Aldrich).

2.1.3 Substrates

Different sample substrates were used dependent on analysis technique. Round, 12 mm diameter, thickness #1 glass coverslips were purchased from Ted Pella and were used for time-of-flight secondary ion mass spectrometry (ToF-SIMS) experiments. Initial PPAMS experiments were completed using 60x15 mm petri dishes from VWR (Radnor, PA) for liquid based samples, and glass cover slips for dried samples. Later experiments in Chapters 5 and 6 as well as cell lysis experiments were performed on 12.7 mm, grade 40 filter paper from Whatman (Maidstone, Kent, UK).

2.1.4 Gas supply

Gas for the plasma source was purchased as standard helium from Praxair (Danbury, CT). Nitrogen and standard air for additional gas flow experiments were also purchased from Praxair.

2.2 General Methods

2.2.1 Glass Cleaning

Glass substrates were cleaned prior to sample deposition via sequential submersion in dichloromethane, acetone and methanol. Glass was placed in a suitable holder and submerged in solvent. Each wash was completed two times for 10 minutes in a sonicator. Samples were then loosely covered with aluminum foil and allowed to dry overnight in a laminar flow hood. Just prior to sample deposition, glass slides were treated for 30 minutes with ultraviolet/ozone to make it more hydrophilic allowing for even distribution of the sample.

2.2.2 Buffers

Citrate phosphate buffered saline with sodium azide (cPBSz) was used as a diluent for porcine plasma. Initially 10x cPBSz was made by adding 64.30 g NaCl, 14.99 g NaI, 21.02 g citric acid monohydrate and 13.8 g monobasic Na phosphate in 1 L water. The pH of the solution was then adjusted to 6.93, requiring approximately 15.75 g solid NaOH. After pH adjustment, 2.0 g sodium azide was added to the solution. For experimental use, the overall solution was diluted to 1x, to obtain a pH 7.4 solution. Phosphate buffered saline (PBS, Sigma Aldrich) was used as a rinsing agent and was constituted from powder form in distilled, deionized water from

a Barnstead/Thermolyne deionizer unit (Nanopure, minimum 18.2MΩ·cm resistivity, Dubaque, IA).

2.2.3 Surface Analysis

2.2.3.1 Time-of-Flight Secondary Ion Mass Spectrometry (ToF-SIMS)

ToF-SIMS is a highly sensitive surface analysis technique, sampling from the first 2 nm of a surface.[39] This technique is performed under ultrahigh vacuum, and works by striking the surface of the sample with an ion beam (primary ion), Bi_3^+ in these experiments, which causes ions from the sample to be emitted (secondary ions),[40] which can then be analyzed. In this work, static SIMS is performed to analyze the surface molecules (total dose $<10^{13}$ ions/cm^2).[41] This ensures that only the top most layer of the surface is analyzed. Experiments were performed on a TOF.SIMS 5-100 time-of-flight spectrometer (ION-TOF, Münster, Germany). Samples were prepared by adding in nutrients based on the recommended daily intake, as well as values expected to be found in human blood. Nutrients were added to a 1 mg/ml bovine serum albumin solution in distilled, deionized water, and deposited on clean glass slides. Samples were then dried for at least 2 days in a desiccator, prior to loading into the ToF-SIMS system the night prior to data collection. Additional details regarding ToF-SIMS experiments can be found in section 3.2.2.

2.2.3.2 Electrospray Ionization Mass Spectrometry (ESI-MS)

ESI-MS is a well-established ambient MS technique, capable of analyzing liquid samples.[42] The sample is flowed through a needle with a kilovolt potential, which charges the liquid and causes it to disperse as a spray which can be analyzed using the attached MS.[43] For ESI-MS experiments, samples were prepared by adding nutrients into methanol, at values based on the concentrations found in human blood. Nutrients were dissolved in solvents as required prior to diluting in a MeOH solution with 0.1% acetic acid. Samples were then injected into the ESI at 90 μl/min Additional details regarding ESI-MS experiments can be found in section 3.2.3.

2.2.3.3 Plasma Pencil Atmospheric Mass Spectrometry (PPAMS)

PPAMS is a novel technique combining a low temperature plasma (LTP) with an atmospheric mass spectrometer and a multivariate analysis method. The LTP was constructed at the University of Washington, based on work by Harper et. al.[44] In summary, a Teflon block was machined to have two inlets, one for the gas flow and one for the high voltage electrode, both feeding in to one outlet with a glass tube attached. This design allowed the gas to flow over the

high voltage electrode, which was then guided by the glass tube to the sample, shown in Figure 2-1. The LTP-probe consists of a glass tube (o.d. 6.35 mm, i.d. 3.75 mm) with an internal grounded electrode (stainless-steel; diameter 1.33 mm) centered axially and an outer electrode of copper tape surrounding the tube's exterior. The wall of the glass tube serves as the dielectric barrier. The plasma plume was created by applying an alternating high voltage of 3-6 kV at a varying frequency of 2-5 kHz to the inner electrode, leaving the outer electrode grounded to generate the dielectric barrier discharge. The discharge AC voltage was provided by a custom built power supply utilizing a square-type waveform with adjustable frequency and amplitude. The total power consumption was below 3 W. Helium discharge gas was fed through the tube's interior to form the plasma, as well as to force the plasma plume out of the tube to strike and ionize the sample, and sequentially to transport the analyte ions to the MS inlet. The plasma source was placed at an angle of approximately 60° from the sample surface. Gas flow was kept at approximately 1.6 liters/minute (LPM) using a 1-2.5 LPM flow meter from key instruments (Trevose, PA).

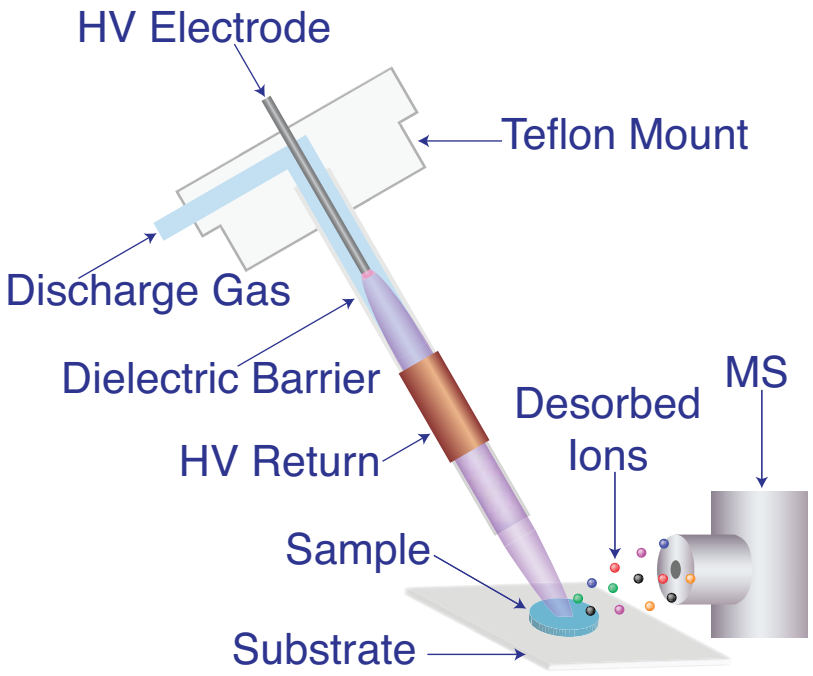

Figure 2-1 Plasma pencil atmospheric mass spectrometer schematic. The discharge gas is flowed through the Teflon mount, and passes across the high voltage (HV) electrode to form the energetic plasma. The dielectric barrier guides the plasma to ionize the sample, which is analyzed by the mass spectrometer. Figure provided courtesy of S. Herschbein.

For most experiments in Chapters 3 and 4, PPAMS was performed using the Bruker Esquire Ion trap, which is the MS coupled to the ESI from section 3.2.3. The exception,

described in section 4.3.7, had the LTP coupled to a Finnigan LTQ Orbitrap mass spectrometer. The orbitrap, a high accuracy mass spectrometer, was used to verify the presence of ions of interest from the samples. In Chapters 5 and 6, PPAMS was performed using a compact MS, Advion's Express**ion** (Ithaca, NY).

2.2.4 Data Analysis

2.2.4.1 Principal Component Analysis (PCA)

Principal component analysis (PCA) is a multivariate technique used for data reduction. This technique takes information in the form of variance from the original variables (in the case of mass spectra, the individual *m/z* intensities), to make a new set of variables, called principal components (PCs). The PCs are linear combinations of the *m/z* intensities and each proceeding PC is orthogonal to the last. The sum of all the PCs will give 100% of the variance expressed in the original spectra.[45] Principal components are comprised of two sets of information, the scores and the loadings. The scores are used to show how the original samples are related to each other, while the loadings show the amount of influence of each *m/z* intensity.[46]

The key advantage of using PCA is that often only a few PCs are required to account for the majority of the variance in the original data. This allows the study of a smaller set of variables while still maintaining most or all of the key information. All data from ToF-SIMS, ESI-MS and PPAMS experiments were studied using PCA. PCA was completed using the NESAC/BIO MVA Toolbox (Seattle, WA) for MATLAB (the MathWorks, Inc., Natick, MA). Unless noted otherwise, all data was normalized to the sum of selected peaks (equal to the total intensity of the spectrum for unsupervised analysis), to account for ion yield fluctuations between experiments. All data was mean centered prior to PCA. Square root and cube root transformations were also applied to some data sets, which will be discussed in sections 4.3.2 and 4.3.4.

Data from each instrument was analyzed slightly differently as follows. For ToF-SIMS, data was initially analyzed via unsupervised PCA, where a complete peak list, with all peaks with intensities > 100 counts for $m/z < 100$, > 50 counts for *m/z* between 100-200, and > 5 counts for $m/z > 200$ were used. Further analysis was completed by forming a peak list of the protein and nutrient peaks to perform supervised PCA. This peak list selection will be discussed in section 3.3.1. For ESI-MS, unsupervised PCA was performed using data from the entire spectra. For PPAMS, data was analyzed via binned (to unit mass) and instrument default (one data point

for each 0.1 *m/z*) formats. PPAMS data was initially analyzed using unsupervised PCA, after which supervised PCA was also performed. Peak list formation for PPAMS data will be discussed in sections 4.3.3 and 5.4.3.1.

2.2.4.2 Discriminant PCA (DPCA)

Discriminant PCA (DPCA) is a modified PCA technique. Here, rather than separating data purely based on a maximization of variance, scaling is completed to account for both within group variance, and between group variance.[47] This is accomplished by computing the standard deviation within each group of samples (i.e. samples with a specific level of nutrients added), then dividing the group by the standard deviation.[47] Thus, data that has high within group variance will be scaled lower and be given a smaller significance during analysis. These analyses were also completed using the NESAC/BIO MVA Toolbox.

2.2.4.3 Partial least squares regression (PLSr)

Partial least squares regression (PLSr) is a regression based technique used to relate two matrices. In most cases, PLSr is utilized to relate the **X** measured matrix to the **Y** predicted matrix, using a linear multivariate model. Regression analysis differs from PCA in that PCA analyzes data only in the **X** block. The advantage of this analysis is the ability to analyze data that has many correlated variables (i.e. variable that change with each other), while also modeling the response variables.[48] This is completed by maximizing the covariance between the **X** and **Y** matrices.[49] To create a PLSr model, a training or calibration set is used. The training data set is split into groups, and model parameters are then adjusted to minimize the prediction error. Model testing can then be completed using a verification data set. PLSr was completed on PPAMS data using the PLS_Toolbox (Eigenvector, Inc., Wenatchee, WA).

3 Specific Aim 1: To develop and test a mass spectrometry based system for sample analysis, and compare to traditional lab scale techniques

3.1 Background

3.1.1 Motivation

The ability of MS to sensitively analyze a variety of samples makes it a good technique for analyzing nutrients in blood, however, numerous potential ionization sources and mass spectrometers are available that may be suitable. Here, we will evaluate several techniques through published literature, then select the most promising to test further. Prior to an extensive assessment, an initial group of samples will be evaluated to determine the method's feasibility. This will be completed by comparing groups of samples with different nutrients to see if consistent differences can be observed in the spectra. Simultaneously, the selected combination of MS and ionization source will also be compared to other well characterized, highly sensitive MS techniques.

3.1.2 Ionization source

Many ionization methods are currently used, however, not all are viable for this application. A suitable ionization source should be useable in ambient conditions, amenable to test a blood based sample and safe for use by a relatively inexperienced, minimally trained operator. While several sources were examined, 3 will be discussed here to select the ideal source. First, electrospray ionization (ESI), which is one of the earliest[50] and most commonly used ambient techniques. This method analyzes liquid samples, often with little sample preparation, and can achieve sensitivity in the femto to attomole range for some sample types.[41] While this sensitivity is far beyond our requirements of measuring micronutrients in blood, ESI systems are known to have difficulty with high salinity samples[51] such as the 150mM sodium found in blood.[52] While desalting is possible using columns, their use would cause an increase in the per test cost, and the experiment time and complexity. Another commonly used ambient technique is direct analysis in real time (DART).[53] DART is able to analyze samples directly, with no sample preparation required. This method has been used for various applications, including in the area of drug detection and the analysis of self-assembled monolayers.[54] Of particular interest, DART has been shown to be amenable for use on high salt, biological

samples through its application in the detection of drugs in blood plasma, with no sample cleanup or filtering.[55] This method, however, normally applies a high temperature plasma for ionization, commonly reaching 250-350°C.[44,56] This could lead to potentially unsafe conditions for inexperienced users if the ionization source is contacted, and can also lead to sample burning, or even ignition in filter paper based samples.[57]

Recently, a novel technique involving the production of a low temperature plasma (~30°C) has been introduced.[44] Like DART, this technique can be applied to a variety of sample types in both liquid and solid states. This technique is less established and less characterized compared to the other discussed techniques, but has still been applied to many different sample types. Specifically, studies have included the investigation of samples such as pharmaceuticals,[58] drugs of abuse,[59] explosives[44,60] and food.[61] Furthermore, in the drugs of abuse study, this low temperature plasma has been applied to the detection and quantification of narcotics in complex samples (such as urine), down to the ng/ml range.[59] The ability of this technique to not only detect the analyte of interest in a high salt background, but also provide quantitative information (currently through the use of spiked standard) makes it an ideal candidate for the detection of micronutrients.

3.1.3 Mass spectrometer

For the ionization technique selected, a variety of MSs are also amenable for analysis. For this application, the most important characteristic is that the inlet of the MS must be able to be exposed to atmospheric pressure to allow for sample analysis. Next, to increase our ion capture efficiency, the distance between the sample and the inlet should be minimized, to decrease the ion travel distance and increase the capture efficiency. Similarly, to increase capture and detection efficiency, a relatively short inlet is desirable, to prevent gas phase molecules from attaching to the inlet walls. Additionally, with the use of helium as the ionization gas, the MS must have a suitable pump. In some cases, helium can cause an increase in inlet pressure which will decrease MS functionality.[62] Overall, the system must be tested in order to ensure suitability for this application. In this aim, the cost of the MS is not an important issue as initially shared equipment can be used for technique verification. In later aims, however, a cost effective solution will be required to make the detection and measurement method feasible for wider scale use. Thus, a MS with comparable specifications to a MS we can purchase later is ideal. Two mass spectrometer types are particularly suitable for this application, the quadrupole (or triple

quadrupole) mass spectrometer as well as an ion trap mass spectrometer. These two instrument types are promising since they can be configured to sample at ambient conditions and they have been miniaturized, such as the Express**ion** CMS by Advion (Ithaca, NY) and the Griffin 400 by FLIR Systems (Wilsonville, OR). A compact size will be imperative for the final, transportable product.

3.1.4 Data analysis

Here, we hope to combine three key elements, the ionization source, mass spectrometer and data analysis method to form our PPAMS system. Initially, particularly for samples in simple solutions, data can first be analyzed primarily by studying mass spectra and determining peaks indicative of nutrients, by finding peaks with greater expression when the nutrient is present compared to control samples. The identity of these peaks can then be verified via tandem mass spectrometry (MS/MS) to confirm the breakdown of the isolated *m/z* peak. For more complex samples, however, additional analysis will likely be required. With many additional peaks present in the spectra from the background solution, the actual peaks of interest may be confounded or masked.[63] Furthermore, sample recombinations may occur due to reactions of the nutrients in solution, to form new complexes that may not be present in simpler sample solutions. To improve and facilitate data analysis, a multivariate technique, principal component analysis (PCA), will be used, as described in section 3.2.5. Here, different samples will be compared in order to determine differentiating factors in the samples.

3.2 Materials and Methods

3.2.1 General procedures and supplies

Details concerning general sample preparation methods as well as common supplies and chemicals used throughout the three aims can be found in Chapter 2.

3.2.2 Time-of-Flight Secondary Ion Mass Spectrometry (ToF-SIMS).

ToF-SIMS data were obtained with a TOF.SIMS 5-100 (ION-TOF, Münster, Germany). While both positive and negative mode data were collected, as positive spectra produced the strongest data trends, only positive ion ToF-SIMS data will be presented. Data was collected below the static SIMS limit using a Bi_3^+ primary ion source. The resulting spectra were analyzed with the Surface Lab 6 software package from ION-TOF. Peak lists were constructed starting with a base of protein-related peaks adapted from Brown et. al.,[64] and were supplemented with nutrient-related peaks. Nutrient-related peaks were determined through one of two methods,

either the presence of the peak in the nutrient samples and absence of the peak in the control sample or a peak that showed a changing intensity proportional (or inversely proportional) to the nutrient concentration in the sample.

A sample preparation protocol was developed for these experiments with standard concentrations of the micronutrients dissolved in a 1 mg/ml BSA in dH_2O solution. Initially, standard concentrations were based on adding 100% of the recommended daily allowance (RDA) of each nutrient in 1 cup (236 ml) of protein solution to simulate nutrient detection in a food source. The final RDA levels used were 1.7 parts per million (ppm) FolA, 3.8 ppm VitA, 625 parts per billion (ppb) Thyr, 75 ppm Fe and 46 ppm Zn. A secondary preparation protocol was developed based off of the concentrations of nutrients expected in the blood of an adult human. These samples were based on the upper levels expected in healthy human blood (HBL) and were also prepared in a 1 mg/ml BSA/dH_2O solution. The final HBLs used were 50 ppb FolA, 650 ppb VitA, 105 ppb Thyr, 2 ppm Fe and 20 ppm Zn. A 10 μL droplet of each solution was pipetted onto a 12 mm diameter, clean glass coverslip and allowed to dry for two days in a vacuum desiccator prior to analysis. Higher concentrations, up to 1000x the RDA levels, were also used in cases where peaks could not be found using RDA and HBL concentrations, only

3.2.3 Electrospray Ionization Mass Spectroscopy (ESI-MS).

To perform a comparison with an established ambient technique, ESI-MS was performed. Positive ion electrospray MS and MS/MS spectra were obtained on a Bruker-Esquire LC-ion trap MS (Bruker/Hewlett-Packard, Billerica, MA). Samples were infused by flow injection at 1.5 μL/min via a syringe pump (Cole Parmer Model 74900, Vernon Hills, IL) and ionized in a standard orthogonal Bruker ionizer. The mass spectrometer settings for the ESI-MS experiments were as follows: electrospray capillary, 100 V; transfer capillary, 70 V; drying gas temperature, 250 °C; skimmer 1, 20 V; skimmer 2, 6.0 V; octopole I, 3 V; octopole II, 1 V; octopole radiofrequency, 100 V; peak-to-peak lens I voltage, -5 V; lens II voltage, -60 V. Mass spectra were obtained by ejecting trapped ions in the range of *m/z* 50-1100 for all samples. Approximately 100 scans were accumulated and averaged to provide the spectra used for analysis. Spectra were exported using the Bruker data analysis software for further analysis. Mixed solutions of nutrients were prepared at previously listed HBL values for four nutrients and at 10x HBL for the remaining nutrient in methanol, for each of the five nutrient types. When required, nutrients were first dissolved in a separate solvent. Specifically, FolA was dissolved in

DMSO at 0.5 mg/ml, VitA was dissolved in EtOH at 6.5 mg/ml and Thyr was dissolved in 4M NH_4OH at 1.1 mg/ml. Samples were then infused by flow injection and analyzed via ESI-MS.

3.2.4 Plasma Pencil Atmospheric Mass Spectrometry (PPAMS).

Initially, experiments were performed on a quadrupole MS, the Hiden Analytical HPR20 MS (Warrington, UK), however, due to an inability of the system's pumps to handle helium (data not shown), no signal was observed. Thus, an alternate MS, the Bruker Esquire Ion Trap from the ESI-MS system, was used instead. To perform PPAMS, the ESI portion of the system (the front end) was removed as the ionization system is substituted with the LTP. This allowed for the ionization of the sample directly into the MS inlet. As with the ESI-MS, data was acquired and analyzed with the associated Bruker software. PPAMS was performed in the positive and negative-ion mode on pure micronutrient stock powders. As positive mode yielded the best data, only positive ion PPAMS data are presented. The MS settings for the PPAMS experiments were as follows: peak-to-peak lens I voltage, -5 V; lens II voltage, -60 V; skimmer 1, 15 V; skimmer 2, 4.0 V, octopole I, 3 V; octopole II, 2 V. The spectrometer was programmed to collect spectra for a maximum ion trap injection time of 200 ms with 2 microscans per spectrum. The scans were averaged over 30 seconds of acquisition time. An in-house low-temperature plasma probe (LTP-probe) was constructed as described elsewhere[59,65-68] for the generation of an atmospheric plasma at low temperatures (~30 °C). This instrument enables the analysis of samples without visibly noticeable sample decomposition or destruction. Samples were placed on a sample holder 5 mm away from the MS inlet, and 3-5mm away from the plasma source. An example experimental set up can be viewed in Figure 3-1. A more detailed description of the LTP-probe can be found in section 2.2.3.3.

Initial experiments were completed using pure nutrient powders attached to double sided tape. The tape was placed onto a 12 mm diameter glass slide, nutrient powder was layered on top of the tape. Excess powder was removed by cleaning with a stream of nitrogen gas. Additional samples were analyzed as solutions, based in MeOH or 10% porcine plasma in citrate phosphate buffered saline (cPBSz), dried on glass slides. The citrate is added for use as a calcium chelator to inhibit the calcium-dependent proteases common to blood and blood products.[69,70] Nutrients were added at levels based on earlier HBLs as well as an additional level based on the lower limit expected in healthy human blood (LBL). LBL samples were doped at: 5 ppb FolA, 288 ppb VitA, 46 ppb Thyr, 0.5 ppm Fe, and 10 ppm Zn. Additional control samples included plain glass,

plain 10% porcine plasma solution, all 5 nutrients at LBL in 10% porcine plasma, and all 5 nutrients at HBL in 10% porcine plasma. Like the ESI-MS experiments, nutrients were first dissolved in appropriate solvents while Fe and Zn were dissolved into porcine plasma solution directly.

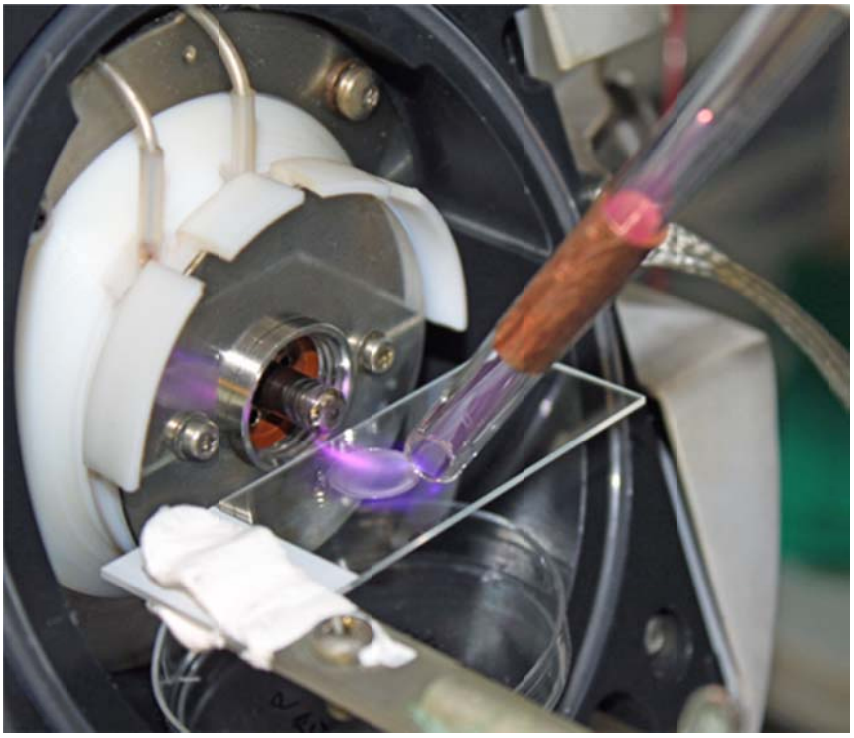

Figure 3-1 PPAMS sample set up. The helium plasma (purple) strikes the sample and ionizes particles into the mass spectrometer.

Several different sample groups were tested. The first test had samples doped with single nutrients at 10x HBL in MeOH, which was completed to determine peaks that may be indicative of specific nutrients at levels similar to those found in humans. Next, samples were tested with four nutrients added at 1xHBL, and the remaining nutrient added at 10xHBL in MeOH. The next experiment was completed to mimic a "relatively healthy" individual, with one nutrient at LBL, and the other four at HBL in 10% porcine plasma. Finally, a "relatively unhealthy" individual was tested, with one nutrient at HBL and the other four at LBL in 10% porcine plasma. Each of these experiments was repeated for all studied nutrients. 10µl of each sample solution was deposited onto 12mm, cleaned glass cover slips, and placed in a desiccator overnight prior to analysis.

3.2.5 Principal Component Analysis (PCA).

A multivariate analysis technique, PCA,[59] which captures the linear combination of peaks that describe the primary sources of variance in a given dataset (known as principal components, PCs) was employed to analyze the resulting spectral data using a Matlab (The MathWorks, Inc., Natick, MA) program written by D. Graham.[71] For ToF-SIMS data, initially, a complete peak set was created for data analysis which included all peaks whose intensities were > 100 counts for *m/z* < 100, > 50 counts for *m/z* between 100-200, and > 5 counts for *m/z* > 200. Then, to further analyze the data, the peak list was reduced to include only the protein and nutrient peaks as described in Section 3.2.2. With these supervised peak lists, data was normalized to the sum of the selected peaks. For all other analyses the entire spectra was normalized to the total intensity of the spectrum. Normalization is required to account for fluctuations in yield between spectra, while attempting to reduce the influence of background noise on the analysis. PCA was performed using the NESAC/BIO MVA Toolbox (Seattle, WA) for MATLAB (the MathWorks, Inc., Natick, MA). All spectra were mean-centered before running PCA. Further data treatment prior to PCA is described as needed.

As the data sets used in PCA are made up of several different types of samples, statistical limits were employed to differentiate the sample types. The scores were assumed to follow a normal distribution as the sample groups consist of replicate spectra from the same sample type. A *t* distribution was utilized to calculate 95% confidence ellipses and confidence intervals about each data group's PC scores. A more in-depth explanation is found in the literature.[71,72]

3.3 Results

3.3.1 ToF SIMS

ToF-SIMS experiments were performed in both positive- and negative-ion modes. As noted in the methods section, this study focuses on the positive ion results. All of the nutrients were found to be detectable in the BSA solution beyond a certain concentration range, using the protein/nutrient peak lists. The metal ion nutrients (Fe and Zn) were readily detectable at the listed HBLs and could be separated from the BSA controls using PCA. Representative ToF-SIMS positive ion scores and loadings plots from iron are shown in Figure 3-2. Scores and loadings plots of PC 1 (capturing 80% of the total variance between the samples) comparing three samples: a plain BSA sample, a sample doped with iron at HBL and a sample doped with all five nutrients at HBL are shown in Figure 3-2.

The other nutrients could also be detected, though they required concentrations higher than the listed HBLs. VitA and FolA could be separated when the concentration was raised to 5x and 1000x HBL, respectively, as shown in Figure 3-3. Thyroxine also required a raised concentration, to 500x HBL (data not shown). In all cases, including the metals, separation required the use of supervised PCA. As previously described, a base peak list was formed using known peptide peaks, to which nutrient peaks were also added. Nutrient peaks were determined by studying mass spectra, and identifying peaks specific to the nutrient, or, peaks which had an easily identifiable change with concentration, examples of which is shown in Figure 3-4.

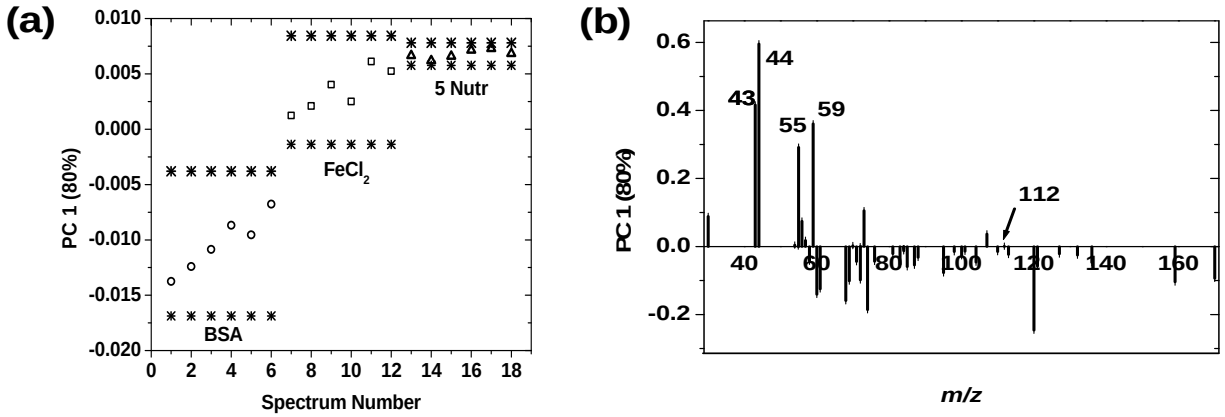

Figure 3-2 PCA on Fe data from ToF-SIMS. (a) Scores plot from PCA of the positive ion spectra comparing peaks from a plain BSA solution sample, a BSA solution doped with HBL Fe sample and a sample containing all five nutrients at HBL. PC1 captures 80% of the variance in the samples and positive a positive score represents the addition of Fe into the solutions. (b) The loadings plot for PC1 clearly shows that peaks typically linked to iron are present in the positive PC loadings. Characteristic iron peaks are present in the iron-containing samples from *m/z* 55-57 (Fe^+, FeH^+), and 112 (Fe_2^+) verifying that the addition of iron is responsible for PC 1. Peaks at 43, 44, and 59 are ions that display improved ionization upon the addition of iron into the system.

3.3.2 ESI-MS

ESI-MS was performed on samples of methanol with all 5 nutrients added. In each sample, one nutrient was added at 10x HBL to determine changes in the *m/z* intensities. Figure 3-5 shows the positive-ion ESI-MS spectra from these experiments. While most peaks are present in all spectra, certain peaks show an increased intensity in the spectra in which an excess of a single micronutrient is added (Figure 3-5 (a) through (e)). For visibility purposes, only up to 300 *m/z* is shown, however, more peaks were also found in the higher mass region. Several peaks were identified as being linked to a nutrient and have been labeled in Figure 3-5.

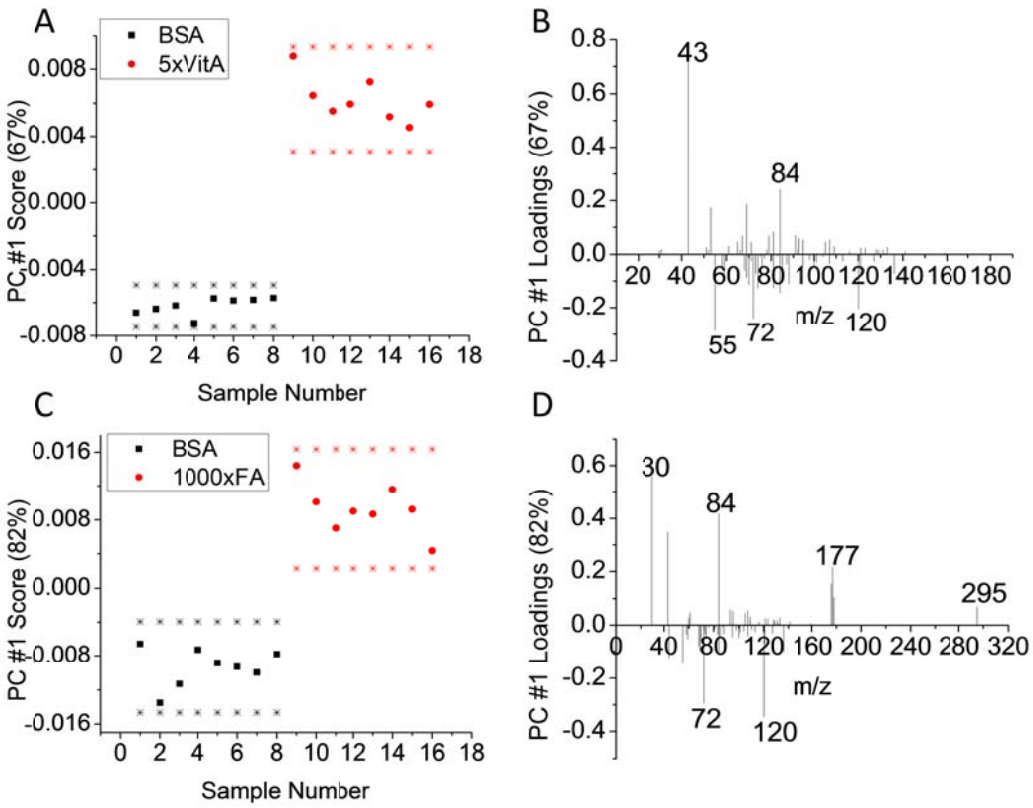

Figure 3-3 PCA on VitA and FolA samples from ToF-SIMS. An experiment was performed to determine whether micronutrients were separated by ToF-SIMS data at physiological nutrient concentrations. Only two nutrients, iron and zinc effectively separated from the control samples at the HBL concentration. The remaining three nutrients required concentration levels much higher than the HBL values to display significant separation. PC #1 scores and loadings plots from ToF-SIMS data illustrating the separation between the BSA controls and nutrient-doped samples are shown for: A, B) 5x HBL VitA and C, D) 1000x FolA. Specific peaks in the loadings plots (B, D) which were determined to originate from the nutrients had the expected loadings, trending to the same side as the nutrient in the scores plot. In particular, for VitA (B), peaks at *m/z* 43, 69 and 81, and FolA (D) peaks at *m/z* 176-178 and 295 had positive loadings, which correspond to the scores plots.

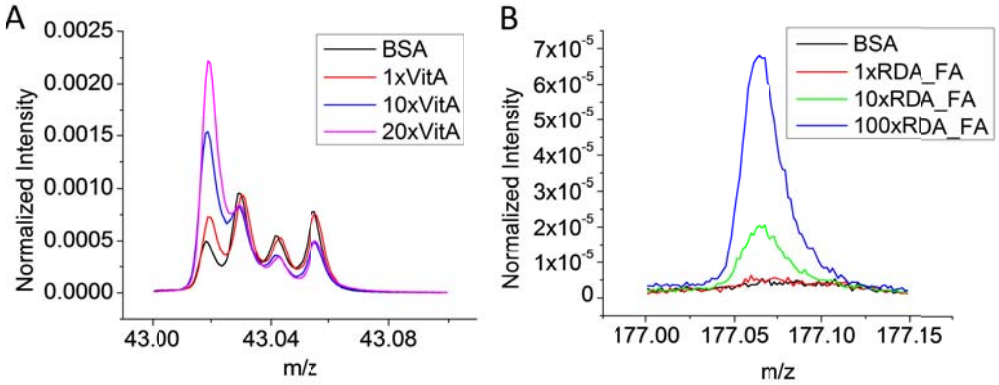

Figure 3-4 Normalized VitA and FolA nutrient peaks from ToF-SIMS. ToF-SIMS peak intensities sketches, indicating gradients of expression as the concentration of the analytes are increased. A) Comparison between 0, 1x RDA, 10x RDA and 20x RDA vitamin A concentrations. B) Comparison between 0, 1x RDA, 10x RDA and 100x RDA levels for folic acid. Note that 1x RDA is equivalent to 5x HBL for VitA, and 76x HBL for FolA.

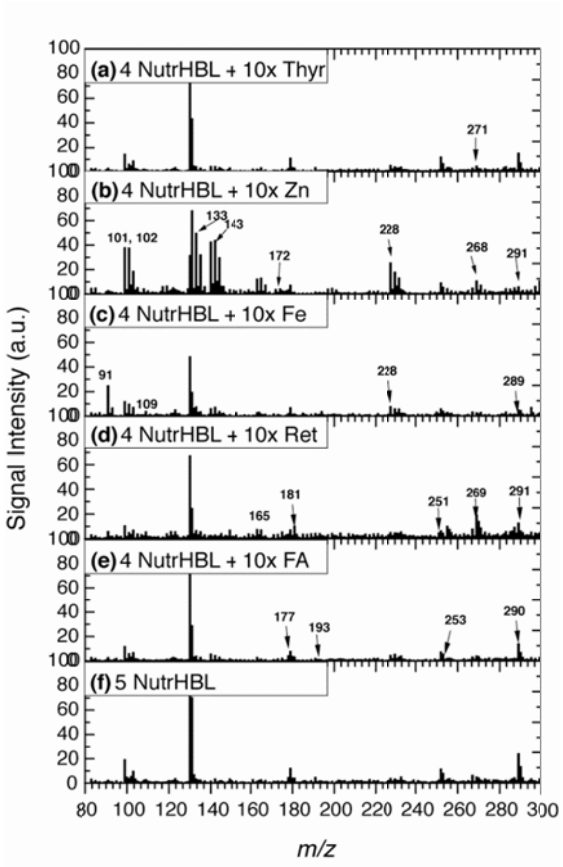

Figure 3-5 Positive ion ESI-MS data of mixed micronutrient samples prepared in methanol. Solutions are multi-component mixtures consisting of one nutrient at a 10x concentration of its HBL and the remaining four nutrients at a 1x HBL (4 NutrHBL samples). Changes in each spectrum versus the control 5 NutrHBL spectrum (f) were assumed to be due to the presence of the excess nutrient. The major ions believed to be from the fragmentation of each nutrient are labeled, and potential identities are listed: (a) The majority of Thyr's fragments are above *m/z* 300. Only *m/z* 271 was visible in the 80-300 range shown; (b) *m/z* 101 ($ZnCl^+ + H_2$) , 133 ($ZnCl^+ + O_2 + H_2$), 143 ($ZnCl^+ + C_2H_2O + H_2$), 172 ($ZnCl_2^+ + HCl + H_2$) , 228 ($ZnCl_2 + FeCl^+ + H_2$) and 291 ($2ZnCl_2 + H_2O + H_2 + H^+$) were attributed to Zn; (c) *m/z* 91 ($FeCl^+$), 109 ($FeCl^+ + H_2O$), 228 ($ZnCl_2 + FeCl^+ + H_2$), and 289 ($2FeCl_2 + 2H_2O + H^+$) represented Fe; (d) *m/z* 165 ($C_{11}H_{17}O^+$), 181 ($C_{11}H_{17}O_2^+$), 251 ($C_{15}H_{23}O^+ + O_2$), 269 ($C_{15}H_{23}O^+ + O_2 + H_2O$), and 291 ($C_{18}H_{27}O_3^+$) indicated VitA; and (e) *m/z* 177 ($C_7H_7N_5O^+$), 193 ($C_7H_9N_6O^+$), 253 ($C_{12}H_{13}NO_5^+$), and 290 ($C_{13}H_{11}N_6O_2 + Na^+$) represented FA.

PCA of the positive ion ESI-MS data from Figure 3-5 readily distinguishes between the solutions with the excess micronutrient. The scores plot for PC 1 vs. PC 2 is shown in Figure 3-6 (a). The first two PCs account for 95% of the total variance in the data set. The loadings plot for PC 1, which captures 70% of the total variance, is shown in Figure 3-6 (b). Select loading peaks are marked by colored dots that indicate the peak's potential contributing nutrients (black for the control sample, red for FolA, olive for VitA, blue for Fe, orange for Zn, and magenta for Thyr).

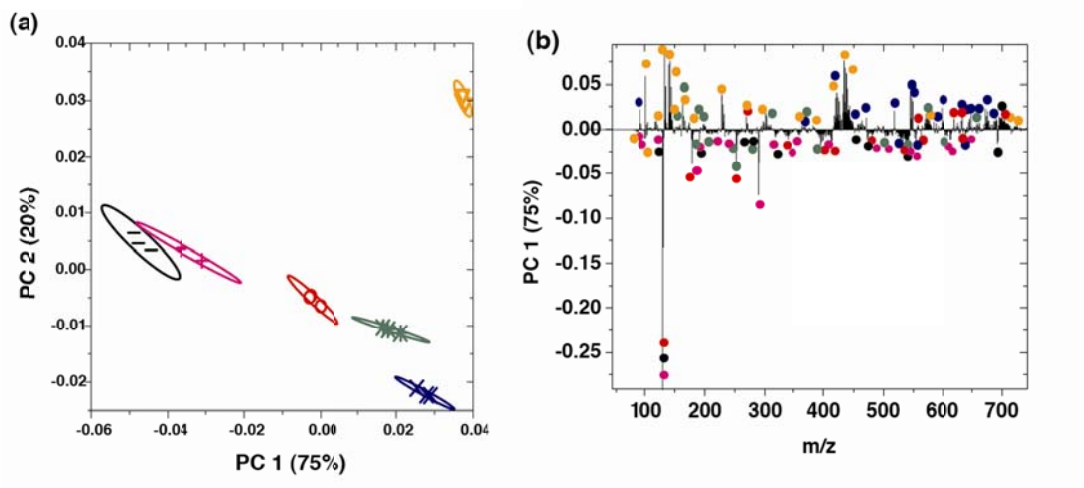

Figure 3-6 PCA on ESI-MS data. The PCA results for the ESI-MS positive ion spectra shown in Figure 3-5 are presented as a) scores and b) loadings plots. (a) The scores plot displays an excellent separation of each of the micronutrients present in the HBL mixed solutions. Ellipses drawn around each of the groups represent the 95% confidence limit for that group on PCs 1 and 2.[71] (b) The loadings associated with PC 1, capturing 75% of the system variance, show how the original ESI-MS peaks relate to the location of the spectra on the scores plot. Colored dots indicate the potential nutrient associated with a given peak as determined through a plot of the raw nutrient mass peaks at each mass number. In comparing (a) and (b), we can see more contributing peaks for Zn and Fe in the positive loadings, and more Thyr, and FolA in the negative loadings. Colors and symbols: (-, black) 5 NutrHBL; (o, red) 4 NutrHBL + 10x FA; (*, olive) 4 NutrHBL + 10x VitA; (X, blue) 4 NutrHBL + 10x Fe; (∇, orange) 4 NutrHBL + 10x Zn; and (+, magenta) 4 NutrHBL + 10x Thyr (n=3).

3.3.3 PPAMS

Initial experiments were performed on pure powders of the individual nutrients which were suspended on double sided tape and analyzed. Then, a solution of all five nutrients at HBL was prepared in methanol, as previously described, dried onto a glass surface, and analyzed. As shown in Figure 3-7 (a), mass spectra were acquired from the samples with a good signal to noise ratio. Several key fragments were observed for each of the nutrients. The peaks shown in Figure 3-7 (a) were first observed in the PPAMS (and MS/MS) data of the raw nutrient powders suspended on tape (data not shown). As an example, single MS/MS spectra acquired from each of the nutrients are presented in Figure 3-7 (b)-(e), and will be further discussed in section 3.4.3. Samples of the five micronutrients were prepared for PPAMS in a 10% porcine plasma solution in cPBSz, as described in section 3.2.4. Unsupervised PCA (PCA performed with all the peaks in the spectra) was performed on the resulting spectra to determine if the samples could be separated based on the nutrients at LBL and HBL levels, even in the complex solutions. In the "relatively healthy" sample, with 4 nutrients at HBL and 1 nutrient at LBL, the data can be completely separated using the scores from PC1 and PC2 (Figure 3-8 (a)) to 95% confidence. In

the "relatively unhealthy" sample, with 4 nutrients at LBL and 1 nutrient at HBL, the data is mostly separable when plotting PC1 and PC2 scores (Figure 3-8 (c)). In the unhealthy samples, while some of the 95% confidence ellipses do overlap, the actual data points are separated.

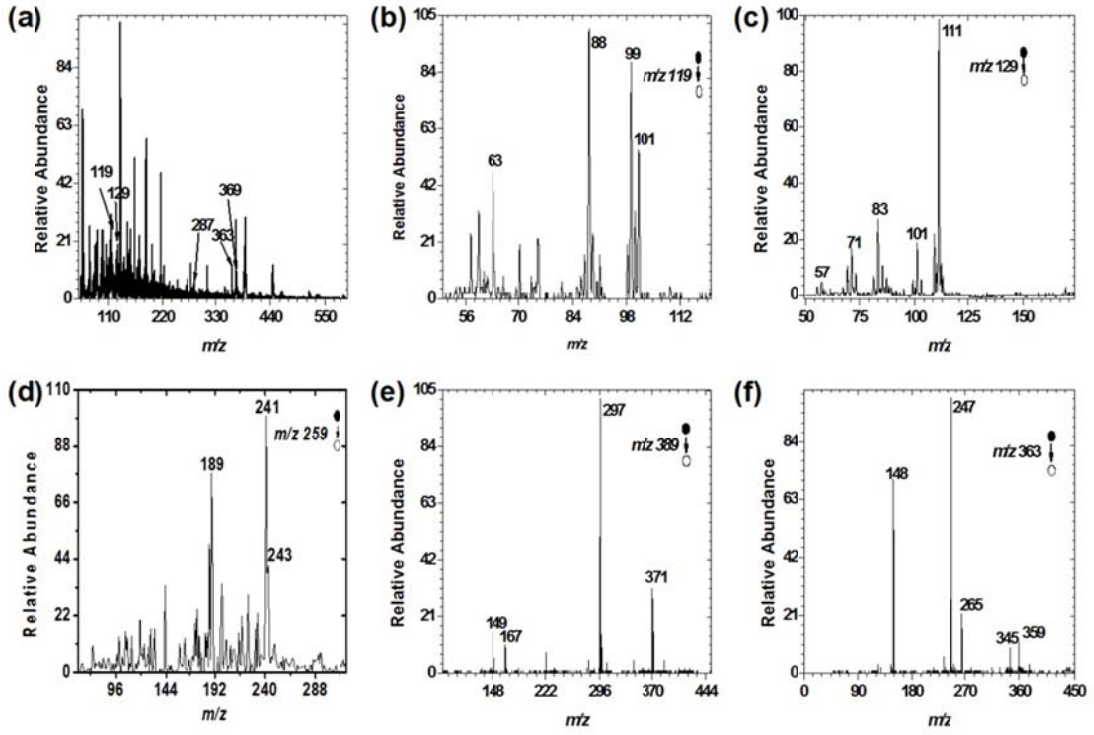

Figure 3-7 PPAMS of nutrients with MS/MS spectra. (a) Raw positive ion PPAMS data of a mixed micronutrient sample of all five micronutrients at HBL concentration in methanol spotted and dried on a glass disk. While multiple MS/MS spectra were taken on each sample, a single peak and accompanying MS/MS plot has been included for each micronutrient. The PPAMS/MS product ion positive-ion mode spectra taken on raw single nutrient powders fixed on double stick tape included: (b) Zn: MS/MS of *m/z* 119 ($ZnCl^+ + H_2 + H_2O$); (c) Fe: MS/MS of *m/z* 129 ($CHNFe^+ + N_2 + H_2O$); (d) VitA: MS/MS of *m/z* 259 $M_{VitA}^+ - 2\ CH_2$ (formula: $C_{18}H_{26}O^+$) (e) FolA: MS/MS of *m/z* 389 ($C_{12}H_{13}N_2O_5^+ + O_2 + 2N_2 + 2H_2O$); and (f) Thyr: MS/MS of *m/z* 363, ($C_6H_5I_2O_2^+$). See the text for additional breakdown peaks.

3.4 Discussion

3.4.1 ToF-SIMS

For HBL concentration nutrients, two could be separated and detected at the 1xHBL level. For example, in the case of Fe, the plots from Figure 3-2 show that the primary difference between the three sample groups is the addition of Fe into the BSA solution, as both the Fe containing samples (the Fe only and the 5 nutrient samples) separate towards the positive scores and the sample without Fe (BSA only) separates towards the negative. This was confirmed in the

loadings as well, as common fragments for this nutrient showed the expected trends; in particular, peaks such as Fe^+, FeH^+ and Fe_2^+ were shown as positive loadings. Additional peaks appearing in the positive loadings, such as those at 43 and 44 *m/z*, were likely influenced by other nutrients in the 5 nutrient sample, such as VitA which is seen to influence peaks at 43 *m/z* in Figure 3-4. This is also likely the reason the 5 nutrient samples are further separated from the control sample. Inspection of the PC 1 plots for samples containing additional zinc presence also showed separation which could be correlated well to the addition of that nutrient. Specifically, the Zn and ZnH ions heavily influenced the separation. For both these metals, various isotopes were detectable and used to clarify differences between samples which enhanced their separations in PCA.

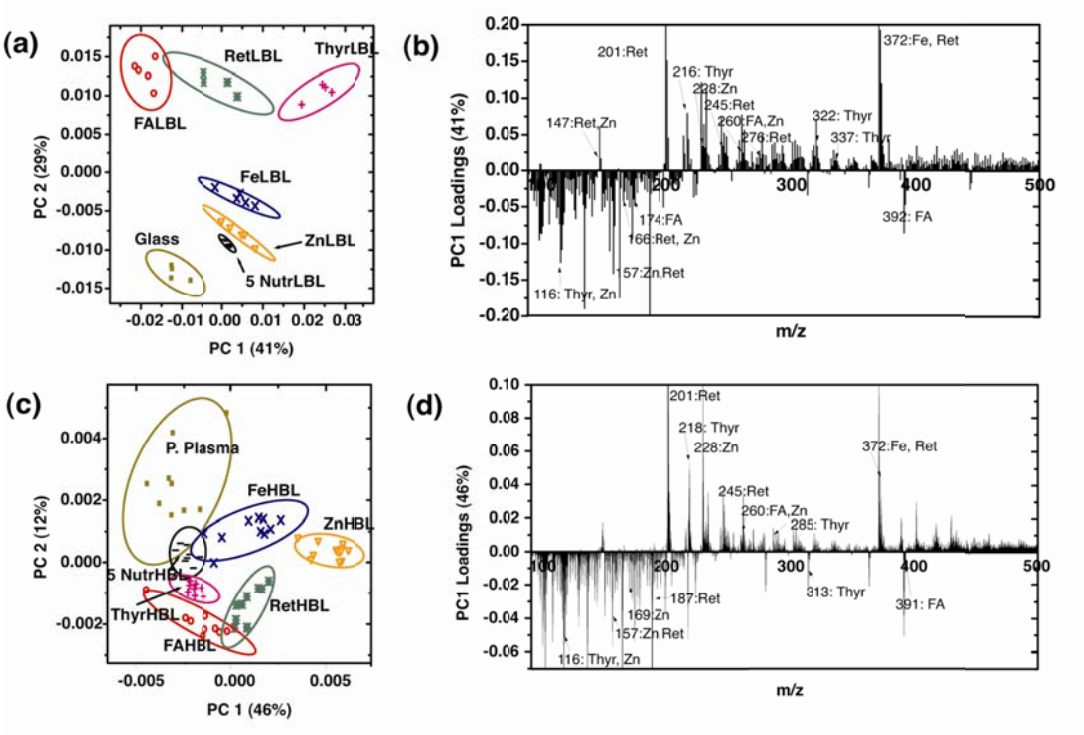

Figure 3-8 PCA on PPAMS healthy and unhealthy data. (a) PC1 vs PC2 Scores plot from PCA of the PPAMS positive ion spectra of a set of solutions modeling a relatively "healthy" individual in which four nutrients are at HBL and the remaining one is at LBL as indicated. Almost all samples separate to 95% confidence. Symbols: (-) 5 NutrLBL; (o) 4 NutrHBL + FALBL; (*) 4 NutrHBL + RetLBL; (X) 4 NutrHBL + FeLBL; (∇) 4 NutrHBL + ZnLBL; and (+) 4 NutrHBL + ThyrLBL. (b) Loadings plot for PC 1 (41%) from PCA of positive ion spectra for the "Healthy" blood model. Peaks have been labeled and the potential nutrient(s) associated with them were determined through plots of the raw spectra for each mass. (c) Scores plot from the positive ion spectra of the inverse set of samples, modeling a relatively "unhealthy" individual in which four of the nutrients are at LBL and only one is at HBL as indicated. Data points for each sample type separate, however, confidence intervals have significant overlap. Symbols: (-) 5 NutrHBL; (o) 4 NutrLBL + FAHBL; (*) 4 NutrLBL + RetHBL; (X) 4 NutrLBL + FeHBL; (∇) 4 NutrLBL + ZnHBL; and (+) 4 NutrLBL + ThyrHBL. (d) Loadings plot for PC 1 (46%) for the "unhealthy" blood model. All solutions were formed in a 10% porcine plasma solution in cPBSz buffer.

Other nutrients VitA, FolA and Thyr, required higher than HBL concentrations. Here, while several peaks could be identified as nutrient-related peaks, most were not visible or only slightly visible at 1x levels. These peaks are likely covered by the surrounding BSA solution. In the ultra-high vacuum conditions of ToF-SIMS, these nutrients, and in particular the hydrophilic FolA, may re-orient away from the exposed surface. At higher concentrations, these peaks begin to re-appear due a higher probability of localizing at the surface. This can be seen as the intensity of the unique peak at *m/z* 177 increases as FolA concentration increases (Figure 3-4(b)). Some fragments, such as those seen at *m/z* 43 from VitA in Figure 3-4 (a), while not unique to the nutrient, were shown to be produced by the breakdown of the nutrients. For future quantitation efforts, a combination of peaks which are unique to the nutrient and others which show a trend with nutrient concentration will likely be required.

3.4.2 ESI-MS

An initial experiment was performed on the Bruker-Esquire LC-ion trap MS to characterize nutrient fragmentation. The mixed nutrient mass spectra, with single nutrients at 10x HBL were cross-compared to a control solution spectrum taken on a solution of all five nutrients at HBLs. Unlike ToF-SIMS and PPAMS, methanol was chosen over a BSA or porcine plasma solution for the dilutions due to the signal saturation caused by high salt content in BSA or plasma (data not shown), which has also been shown in literature.[51] The number of peaks present in these spectra complicates the analysis of nutrient concentration. This process will become even more challenging in later experiments containing porcine plasma, due to the addition of protein and salt in solution, which are at concentrations 1000x higher than the nutrients. Multivariate techniques assist in performing this analysis by reducing many variables to a small number of variables best expressing the greatest degrees of variance.

Visually, the addition of excess Zn (the most concentrated micronutrient in this experiment) appears to account for the separation demonstrated in PC 2, seen in Figure 3-6. This trend continues with excess Fe and VitA correlating to the separation in PC 3 (shown in Section 9.1, Appendix A). Additional PCs were also seen to separate the nutrients with lower blood concentrations (see Appendix A). Overall, PCA was able to separate the nutrients in the expected manners, with initial PCs separating nutrients with higher concentrations, and later PCs separating out nutrients with lower concentrations. This is expected because the higher concentration nutrients should also account for a larger degree of variance, in comparison to

lower concentration nutrients. From these spectra, several peaks were identified. Some examples include *m/z* 101 ($ZnCl^+ + H_2$) for Zn, *m/z* 91 ($FeCl^+$), *m/z* 165 ($C_{11}H_{17}O^+$) for VitA, and *m/z* 193 ($C_7H_9N_6O$) for FolA.

It is noted that while the linear correlation appears to be strong for this particular set of samples analyzed with ESI-MS, the PCA scores represent a multivariate combination of several peaks that have increased or decreased intensities, depending on fragmentation patterns. With the addition of a physiological solution in future experiments, the scores may not yield as linear of a correlation between the abundance of the individual micronutrients as the fragmentation patterns may change.

3.4.3 PPAMS

As mentioned in section 3.2.4, the Hiden MS was inadequate for sample analysis using our PPAMS approach. Low signal intensities were observed and were attributed to the pumping system's inability to remove helium. This was confirmed by testing the headspace above a MeOH sample. When air was flowed over the sample, the MeOH signal was still visible, however, this signal was greatly reduced when helium was flowed over the sample instead.

Following the ESI-MS results, a test was conducted with the PPAMS coupled to the Bruker-Esquire LC-ion trap MS to determine if the LTP-probe was capable of ionizing the nutrients. Using samples of nutrients doped in methanol, differences in spectra were observed, and fragments originating from the nutrients were found. In particular, for Zn, the peak at *m/z* 119 was identified as $ZnCl^+ + H_2 + H_2O$. PPAMS/MS results are shown in Figure 3-7 (b), and the breakdown is characterized by the expected adducts *m/z* 99 ($ZnCl^+$), and *m/z* 101 ($ZnCl^+ + H_2$). For Fe, the peak at *m/z* 129 was identified as $CHNFe^+ + N_2 + H_2O$, and the resulting PPAMS/MS spectrum is shown in Figure 3-7 (c). The resulting MS/MS spectra contained peaks at *m/z* of 57 (FeH^+), 71 ($FeNH^+$), 83 ($CHNFe^+$), and 111 ($CHNFe^+ + N_2$), corroborating the initial identification.

The organic nutrients were also identified in the methanol samples. For VitA, the ion at *m/z* 259 was observed. This was identified as $M_{VitA}^+ - 2\ CH_2$ (net formula: $C_{18}H_{26}O^+$) as shown in Figure 3-7 (d). Upon analysis with tandem mass spectrometry, the identity was corroborated with several smaller fragments identified, such as *m/z* 243 (M_{259}^+ - OH + H, $C_{18}H_{26}^+$) and the cleavage of C_4H_7O from M_{259}^+ to give *m/z* 189 ($C_{14}H_{20}$). For FolA, determination of the PPAMS/MS peak at *m/z* 389 (shown in Figure 3-7 (e)) was accomplished through the

identification of the ion present at *m/z* 297 as the larger fragment produced by cleavage of FolA at the peptide bond ($C_{12}H_{13}N_2O_5^+ + O_2$). Additionally, the peaks at *m/z* 167 and *m/z* 149 were assigned to the cleavage of the second peptide bond removing ($C_5H_7O_4$) and an additional water molecule, respectively. As representative of the Thyr, Figure 3-7 (f) shows *m/z* 363 consisting of one of the ring structures present in the full thyroxine molecule. The Thyr spectrum also showed expected fragments at *m/z* 345 ($M_{363}^+ - H_2O$), *m/z* 247 ($M_{363}^+ + O - I - H_2O + CH$) and *m/z* 232 ($M_{363}^+ - H_2O - I + CH_2$). Structures of all the nutrients can be found in Section 9.2, Appendix B.

The efficacy of using PPAMS for ambient sampling of blood plasma with little or no sample preparation is demonstrated using a series of model solutions. As anticipated, the scores did not yield a linear correlation between the abundance of the individual micronutrients with the addition of the buffer and protein solutions. However, the nutrients were separable at both high and low blood plasma concentrations and the PCA scores shifted based upon nutrient concentration. In addition, some of the peaks that were dominant in the loadings plot for the "healthy" plasma model were also present in the loadings plot for the "unhealthy" model (Figure 3-8 (b) and (d)). For the unhealthy model, an overlap in the confidence intervals can be seen, which is not surprising due to the lower concentrations of nutrients in these samples. Overall, as samples can largely be separated without any additional spectra filtering, this method seems capable of the analysis of micronutrients in blood based samples.

3.5 Conclusions

In this specific aim, we determined that plasma pencil atmospheric mass spectrometry is a promising technique for the analysis of nutrients in blood. This technique has shown separation ability equal to or better than the thoroughly studied, laboratory scale techniques of electrospray ionization mass spectrometry and time of flight secondary ion mass spectrometry. Here, we saw that in clean solutions, clear peaks originating from the nutrients could be isolated and identified at levels found in blood. Furthermore, with the addition of a complex background using porcine plasma, separation can still be achieved. While a significant degree of background signal occurs, this does not eliminate our ability to differentiate between samples. Based on the results obtained here, with differences in samples clearly visible at blood levels using PPAMS for analysis, we anticipate that future analysis using multivariate techniques will allow for quantitation of the nutrients.

4 Specific Aim 2: To develop a physiologically-relevant nutrient model based on adult human blood levels and analyze with PPAMS

4.1 Background

4.1.1 Motivation

While we have shown that this system can be used to determine differences in samples with micromolar levels of nutrients, more studies are necessary to further characterize the nutrients. In particular, additional sample groups must be analyzed and compared to determine if consistent differences can be observed and used to separate samples based on nutrient concentration. If consistent differences in the spectra can be found which are dependent on nutrient concentration, these spectral characteristics may then be useable to help with nutrient quantitation in unknown samples. Due to the wide variations in blood and blood plasma content from person to person, a set of tightly controlled samples will be used first. Here, a complete set of samples will be studied in order to determine the ability of the PPAMS system to separate samples based on nutrient level. Specifically, nutrients will be added to a porcine plasma solution at various levels spanning the blood range to study the resulting change in mass spectra.

4.1.2 Nutrients in plasma

Nutrients are present in the body at regulated levels, however, when a chronic insufficient or excessive level of nutrients is consumed, this will cause an imbalance and cause the blood level of the nutrient to deviate from the normal. From the University of Washington's Laboratory test catalog, the ideal serum nutrient levels for adults are as follows: iron, 40-155 µg/dL, zinc, 60-120 µg/dL, thyroxine, 4.8-10.8 µg/dL, vitamin A, 30-65 µg/dL and folic acid, >0.58 µg/dL. In order to test a full set of regulated samples, nutrients will be added into solution manually. For this system, testing whole blood from multiple individuals may have too many confounding factors as the other blood components such as proteins[73], hematocrit[74] and salt[52] can also have varying levels, all of which are present at much higher concentrations compared to the micronutrients. By having controlled samples, we hope to be able to isolate the peaks which vary only due to changes in nutrient concentration.

4.1.3 Mass spectrometry

4.1.3.1 Ionization Source

In most of the work in this aim, as with the work from aim 1, a helium-based LTP will be used for sample ionization. This gas has been used extensively in other studies[44,60,75] and provides a very clear visualization of the plasma as shown in Figure 3-1. While gases such as N_2 or air can be used for ionization purposes, He has been shown to be the most effective.[76] Furthermore, the apparatus is a non-permanent setup, as the system must be disassembled after each use due to the shared MS. Thus, a clear plasma, such as that produced using air as the source gas, would make aligning the sample with the plasma more difficult.

4.1.3.2 Mass spectrometer

While the main MS for this system was selected in the previous aim, further work for peak verification may be required. The consistent availability of the ion trap, as well as its sufficient performance (similar to some of the more portable MSs commercially available, as discussed in Aim 3) make its use much more convenient, however, the mass resolution and accuracy of the ion trap are not ideal for initial model building[41]. The resolution is typically about 2000 ($m/\Delta m$, Δm = Full width of peak at half the maximum value, though a resolution of up to 30,000 can be achieved), and accuracy is 30 ppm in ideal conditions, which make the identification of specific compounds difficult because many compounds can have the same mass at a resolving power of 2000. While tandem mass spectrometry (MS/MS) can be performed for verification, determining which peaks to study can be very difficult, and many important peaks can be overlooked. Thus, in this work, we will utilize an orbitrap MS as well. The orbitrap MS, while not as easily accessible, has much better resolution and accuracy. Here, the resolving power is 130,000 (at 400 m/z) and mass accuracy can be as low as 2 ppm, which can uniquely identify peaks.

4.2 Materials and Methods

4.2.1 Sample preparation

As in the work from specific aim one, nutrients were first dissolved in an appropriate solvent to form stock solutions. FolA was dissolved in DMSO at 0.5 mg/ml, VitA was dissolved in EtOH at 6.5 mg/ml and Thyr was dissolved in 4M NH_4OH at 1.1 mg/ml. Fe and Zn were dissolved into porcine plasma solution directly at 1.55 mg/ml and 1.2 mg/ml, respectively. These stock solutions could then be further diluted into porcine plasma solutions. Two separate sample

matrices were prepared for experimental analysis. The first sample set consisted of varying Fe, Zn and VitA at 3 different levels while holding FolA and Thyr constant (at the lowest concentration), and the second set consisted of varying FolA, Thyr and VitA at 3 different levels while holding Fe and Zn constant (at the lowest concentration). Each set of samples consisted of a matrix of 27 test samples, plus additional control samples. The nutrient levels for each nutrient were labeled as low blood level (LBL), healthy blood level (HBL) or medium blood level (MBL), with LBL corresponding to a borderline deficient level, HBL corresponding to the upper end up a healthy individual, and MBL corresponding to an intermediary value between low and high. A sample matrix can be found in section 9.3, Appendix C. The exact concentrations added to the samples can be found in Table 4-1. The solvents, DMSO, EtOH and NH_4OH were held at constant concentrations across the different samples to ensure this was not a differentiating factor for analysis. Further testing was also completed with varied pH levels. Here, the pH of the samples was adjusted from 7.4 with an acid to pH 6 or a base to pH 9. Two separate experiments were completed. In the first experiment, 12M hydrochloric acid and 6M sodium hydroxide were used. In the second experiment, glacial acetic acid and 14M ammonium hydroxide were used. In each case, pH was verified using pH paper.

Table 4-1: Nutrient levels tested

Nutrient	HBL	MBL	LBL
Fe	27.8 μM (155 μg/dL)	17.5 μM (97.7 μg/dL)	7.2 μM (40.3 μg/dL)
Zn	18.3 μM (120 μg/dL)	13.8 μM (90 μg/dL)	9.2 μM (60 μg/dL)
VitA	2.3 μM (65 μg/dL)	1.7 μM (47.5 μg/dL)	1.1 μM (29.9 μg/dL)
FolA	113 nM (5 μg/dL)	63 nM (2.8 μg/dL)	11.3 nM (0.5 μg/dL)
Thyr	139 nM (10.8 μg/dL)	102 nM (7.9 μg/dL)	63 nM (4.9 μg/dL)

Due to the natural presence of these nutrients in the porcine plasma used in the experiments, nutrient addition is calculated based on making each of the values in Table 4-1 the final concentration of the nutrient in solution. The porcine plasma was tested using the University of Washington Department of Laboratory Medicine Research Testing Service. A set of example results obtained from a porcine plasma sample can be seen in section 9.4, Appendix D.

4.2.2 Data Collection

PPAMS experiments were completed in a similar fashion as in aim 1. For the ion trap MS, the same collection settings were kept constant. Positioning of the samples was varied, dependent on the requirements of the sample type. For samples dried and spotted on glass or filter paper the positions were kept constant with samples resting 1-2mm below the MS inlet. However, for liquid based samples (the majority of the samples), the sample stage was lowered due to physical limitations from the sample substrate. For the liquid samples, solution (1 ml) was deposited into the cover of a 60x15mm petri dish. Thus, the substrate holder was lowered to place the lip of the petri dish cover just below (~1 mm) the mass spectrometer inlet.

4.2.3 Data analysis

PCA was performed on collected data, as discussed in section 3.2.5. Data was separated into smaller sample groupings prior to analysis. Sample groupings were formed by varying a single nutrient across the three test levels (HBL, MBL and LBL), while holding the other two nutrients at a constant HBL, MBL or LBL concentrations. Thus, in each data matrix, each nutrient was analyzed three times. A summary of the three sample groupings for Fe can be seen in Table 4-2. Similar groupings were made for each of the nutrients. Initial analysis of grouped data was completed using unsupervised PCA.

Table 4-2: PCA data grouping

	Fe level	Zn level	VitA level
Fe group 1	**HBL**	**LBL**	**LBL**
	MBL		
	LBL		
Fe group 2	**HBL**	**MBL**	**MBL**
	MBL		
	LBL		
Fe group 3	**HBL**	**HBL**	**HBL**
	MBL		
	LBL		

Following initial analysis on normalized data, several additional analyses were completed. First, different transformations (square, and later cube root) were applied to the data set to increase the emphasis on lower intensity peaks. These were completed by taking the square

or cube root of all peak intensities, after normalization. Initial peak list formation was also completed by eliminating peaks from the full data set. Peak lists were formed by analyzing the loadings plot when the corresponding scores plot showed the expected trend in concentration, as discussed in section 4.4.3. When a trend was observed, loadings >|0.009| were kept to form a peak list. Thus, multiple peak lists were made for each nutrient. Peak lists constructed from the same nutrient across different days were then consolidated to form a single peak list for each nutrient by comparing peak lists, and keeping the common peaks. A comparison between unbinned and binned (to 1 amu) data was also performed.

4.3 Results

4.3.1 Raw analysis

Two key data set types were tested and studied in this aim. The first data set was a 27 sample matrix of nutrients with Fe, Zn and VitA varied; the second was a matrix with FolA, Thyr and VitA varied. Initial data analysis consisted of completing PCA on grouped data sets, like the groupings listed in Table 4-2, after normalization (total intensity of the spectra) and mean centering. In general, PCA was unable to separate samples from each other in the groupings for any of the nutrients. An example of Zn analysis, with Fe and VitA held at a constant LBL concentration, is shown in Figure 4-1 (A, B). In these analyses, the data points and 95% confidence intervals overlapped in all three sample types (Zn LBL, MBL and HBL). While only PC 2, which accounts for 11% of total variance is shown, data did not completely separate in PC 1 or any additional PCs either. In general, the peaks found in the initial experiments of nutrients in MeOH still appear, however, they do not show consistent trends in expression (i.e. higher expression at higher nutrient levels).

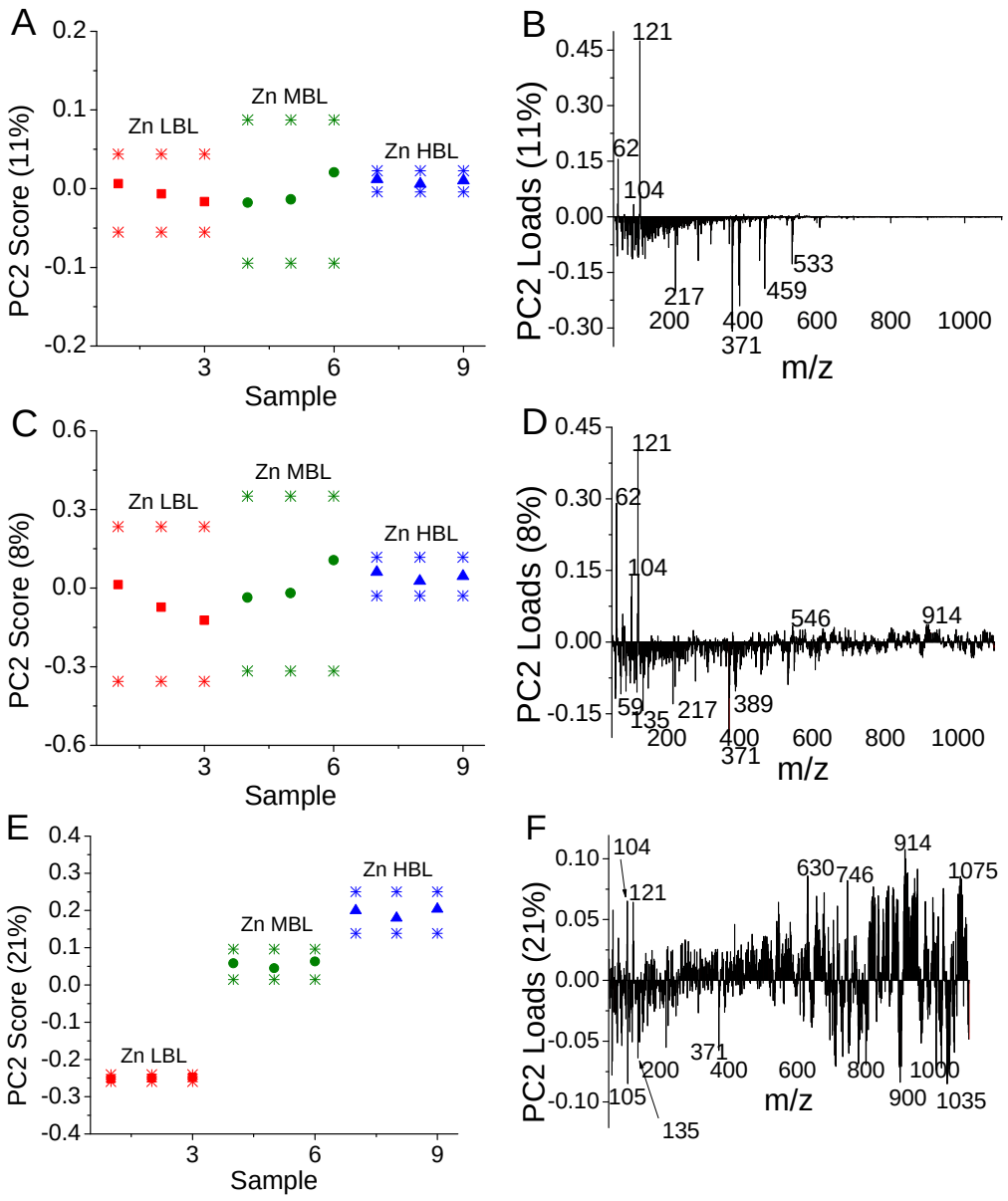

Figure 4-1 PCA on Zn concentration variation using different transformations. A, B) Scores and loadings with no transformation applied. Data is not separated in PC 2 (or other PCs) and has high overlap of data points between all levels of Zn. C, D) Scores and loadings with square root transformation applied. Data is still not separated in PC 2 (or other PCs). E, F) Scores and loadings with cube root transformation applied. Data is separated fully to 95% confidence, and displays a trend, with the scores increasing as concentration of Zn increases. Many of the high intensity loadings overlap between the 3 transformations, however, many more are present in the cube root transformation. * indicates 95% confidence intervals.

4.3.2 Square root transformation

After an unsuccessful separation of the data without data transformations, additional analyses were performed. In this section, a square root transformation was applied to the data set. An example of Zn analysis, with Fe and VitA held at a constant LBL is shown in Figure 4-1 (c-d). Again, as in the non-transformed data, the data points and 95% confidence intervals overlapped in all three sample types (Zn low, medium and high). Here PC 2 only accounts for 8% of the total variance, but again, data did not separate in PC 1 or any additional PCs either. While separation in some of the sample groupings was observed, for example in the analysis of Thyr shown in Figure 4-2, overall, the separation occurred infrequently. Furthermore, only one of the observed data separations was to 95% confidence. The square root transformed data analysis is summarized in Table 4-3, where 50% of the analyses resulted in the data separating in the expected manner showing a trend (labeled as "Y", with a green or yellow background, in Table 4-3), 3% of the data separated to 95% confidence (labeled as "Y" in green), and 47% had separation of the data points with different nutrient levels, but not to 95% confidence (labeled as "Y" with yellow background).

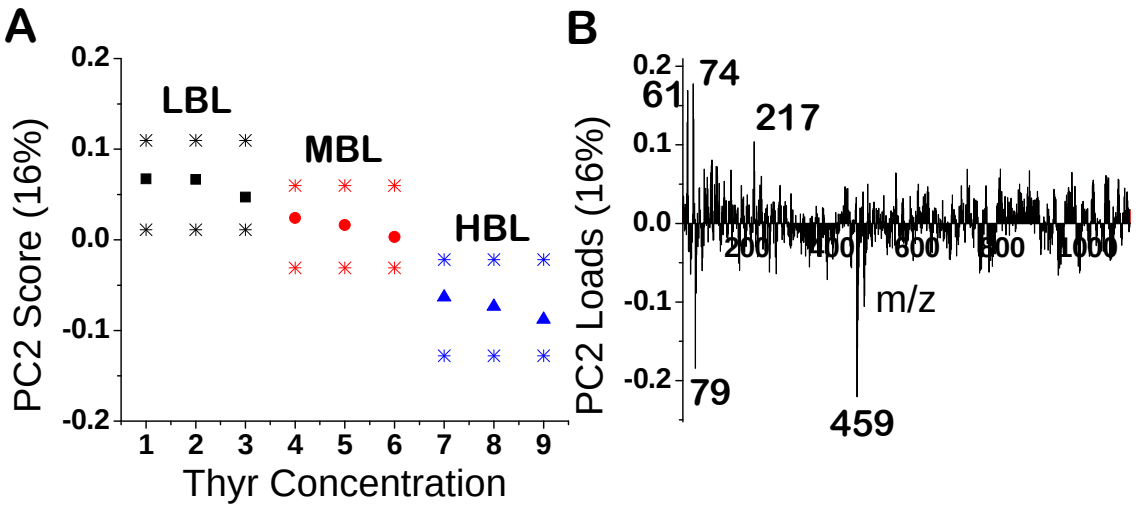

Figure 4-2 PCA on Thyr data with square root transformation. PC 2 scores plot and associated loadings. Data points separate from each other, and displays information about the trend based on Thyr concentration, though the separation is not to 95% confidence. Additional analysis, such as peak list formation may help with the separation of data to show statistical trends. * indicates 95% confidence intervals.

Table 4-3 Nutrient data summary after square root transformation

Nutrient varied	Fe	Fe	Fe	Zn	Zn	Zn	VitA	VitA	VitA
Other nutrients	LBL	MBL	HBL	LBL	MBL	HBL	LBL	MBL	HBL
Day 1	N	Y	N	Y	Y	N	N	N	Y
Day 2	Y	N	Y	N	N	Y	Y	N	N

Nutrient varied	FolA	FolA	FolA	Thyr	Thyr	Thyr	VitA	VitA	VitA
Other nutrients	LBL	MBL	HBL	LBL	MBL	HBL	LBL	MBL	HBL
Day 3	Y	Y	N	N	N	Y	N	Y	N
Day 4	N	Y	Y	Y	Y	Y	N	Y	N

Green: Separation of data points showing trend, to 95% confidence
Yellow: Separation of data points showing trend, not to 95% confidence
Red: Data points overlap or do not show trend

4.3.3 Peak list formation

To attempt to improve data separation, peak lists for each nutrient were formed, as described in section 4.2.3. In the initial peak list formation, only data with a square root transformation applied was been used. The peak lists have been able to slightly improve data separation, with a few exceptions where significant improvement has occurred. A sample comparison between raw PCA analysis, and PCA analysis of data with a peak list applied is shown in Figure 4-3. Here, the data without the peak list applied (Figure 4-3 (A,B)) does not show the expected trend. The LBL concentration Fe sample sits between the Fe HBL and Fe MBL concentrations, indicating that the PC1 scores do not change proportionally to the concentration of Fe (additional PCs also do not indicate a trend in score with the concentration). With the peak list applied, the separation was vastly improved, with the medium shifted between the LBL and HBL concentrations, thus, after the peak list was applied, the data began to show a trend based on Fe concentration, though not to 95% confidence. Overall, however, while improvement was seen after peak list application, the separation was still inconsistent across the other analyses, and separation was still not to 95% confidence, thus, additional analyses are required.

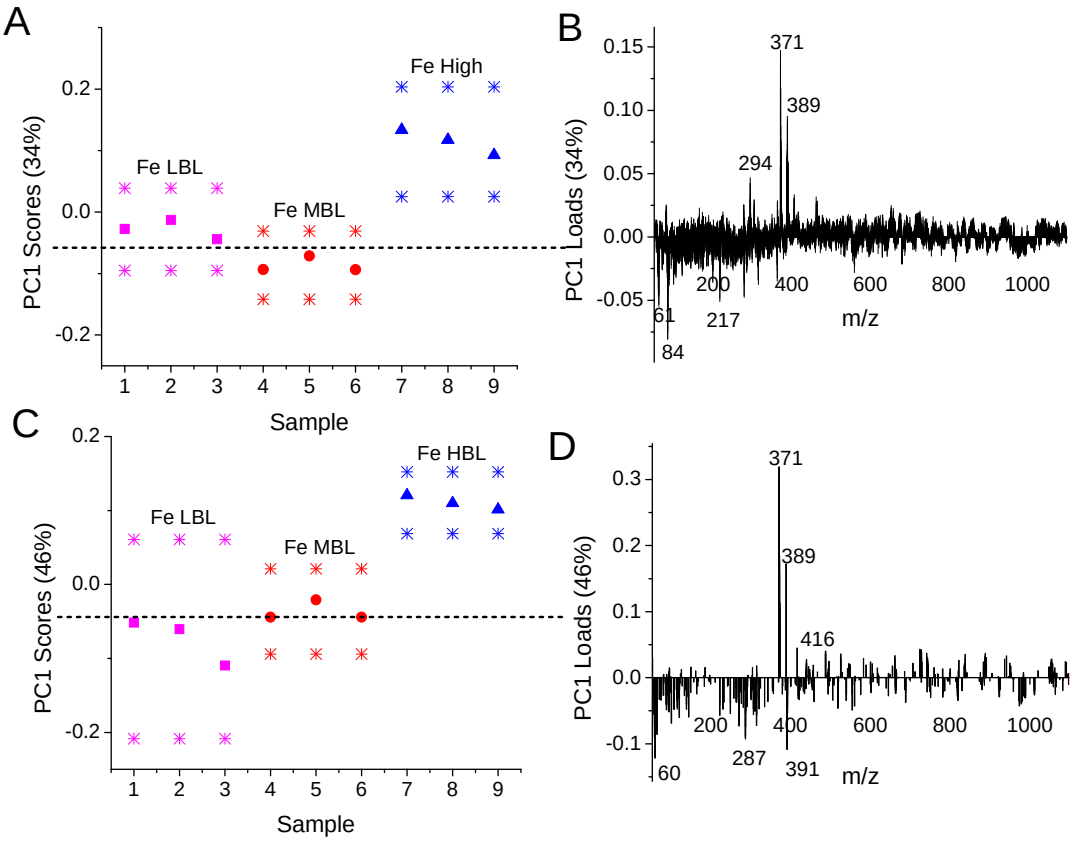

Figure 4-3 Effect of peak list on PCA of square root transformed data. A, B) Scores and loadings prior to peak list application. The scores show the low Fe concentration samples placed between the Fe medium and Fe high data points. C, D) Scores and loadings after peak list application. Fe medium data points are shifted slightly towards the positive loadings as the Fe low data points are shifted towards the negative loadings. This results in a slight trend being shown in the data points of the scores plot, based on concentration of Fe as the medium samples separate between the low and high, as shown with the dashed black line. Additional analysis and peak list development may result in further improvement to increase separation to 95% confidence. The method used for peak list construction is described in 4.2.3. * indicates 95% confidence intervals.

4.3.4 Higher order transformation

To further improve data separation, a cube root transformation was applied to the spectra. An example of Zn analysis, with Fe and VitA held at a constant LBL value, is shown in Figure 4-1 (E-F). In this case, separation is seen between all three sample types (Zn LBL, MBL and HBL) to 95% confidence. Separation occurs in PC 2 and accounts for 21% of the total variance and indicates a trend, with the score increasing as Zn concentration increases. Similar to the representative example in Figure 4-1, separation was improved for most analyses for all four other nutrients, compared to PCA on the no transformation and square root transformation data. A summary of the analysis after cube root data transformation can be seen in Table 4-4. Overall, 75% of the analyses resulted in the data separating in the expected manner showing a trend

(labeled as "Y", with a green or yellow background, in Table 4-4). 28% of the data separated to 95% confidence (labeled as "Y" in green), and 47% had separation of the data points with different nutrient levels, but not to 95% confidence (labeled as "Y" with yellow background), totaling 75%. This is much improved, relative to the square root data presented in Table 4-3. Overall after cube root transformation, Thyr and FolA had the best separation ability, followed by VitA, then Fe and Zn. In general, a trend in separation, like that seen in Figure 4-1 (E), occurred most often in PC 2. A comparison of the loadings plots (Figure 4-1 (B, D, F)) shows that the cube root transformation has more peaks with significant contribution to separation and that many of these peaks have higher masses than those seen in the other analyses. However, we also see that many of the important loadings from the raw and square root analyses carry over to the cube root, such as *m/z* 104, 121, 135 and 371.

Table 4-4 Nutrient data summary after cube root transformation

Nutrient varied	Fe	Fe	Fe	Zn	Zn	Zn	VitA	VitA	VitA
Other nutrients	LBL	MBL	HBL	LBL	MBL	HBL	LBL	MBL	HBL
Day 1	Y	Y	N	N	Y	Y	N	Y	Y
Day 2	Y	N	Y	Y	N	Y	Y	N	Y

Nutrient varied	FolA	FolA	FolA	Thyr	Thyr	Thyr	VitA	VitA	VitA
Other nutrients	LBL	MBL	HBL	LBL	MBL	HBL	LBL	MBL	HBL
Day 3	Y	Y	Y	Y	Y	Y	N	N	Y
Day 4	Y	Y	N	Y	Y	Y	Y	Y	Y

Green: Separation of data points showing trend, to 95% confidence
Yellow: Separation of data points showing trend, not to 95% confidence
Red: Data points overlap or do not show trend

Additional analyses were also completed with a control sample (10% porcine plasma without the added nutrients), and compared to analyses without the control sample, as shown in Figure 4-4. This example, taken from VitA being varied with the other nutrients held at the LBL concentration (data from "Day 3" in Table 4-4), shows that the initial analysis without the control sample has overlapping data points (Figure 4-4 (A,B), overlap between VitA MBL and VitA HBL). However, once the control sample is added, separation of the data points occurs in PC 2, shown in Figure 4-4 (E,F), though not to 95% confidence. Many of the chief loadings from the analysis with the control (Figure 4-4 (C,D)) overlap with those seen in analysis without the

control (Figure 4-4 (A,B)), such as m/z 676, 787, 817 and 954. With the control sample added, PC 1 largely separates out the porcine plasma control from the other samples (Figure 4-4 (C,D)).

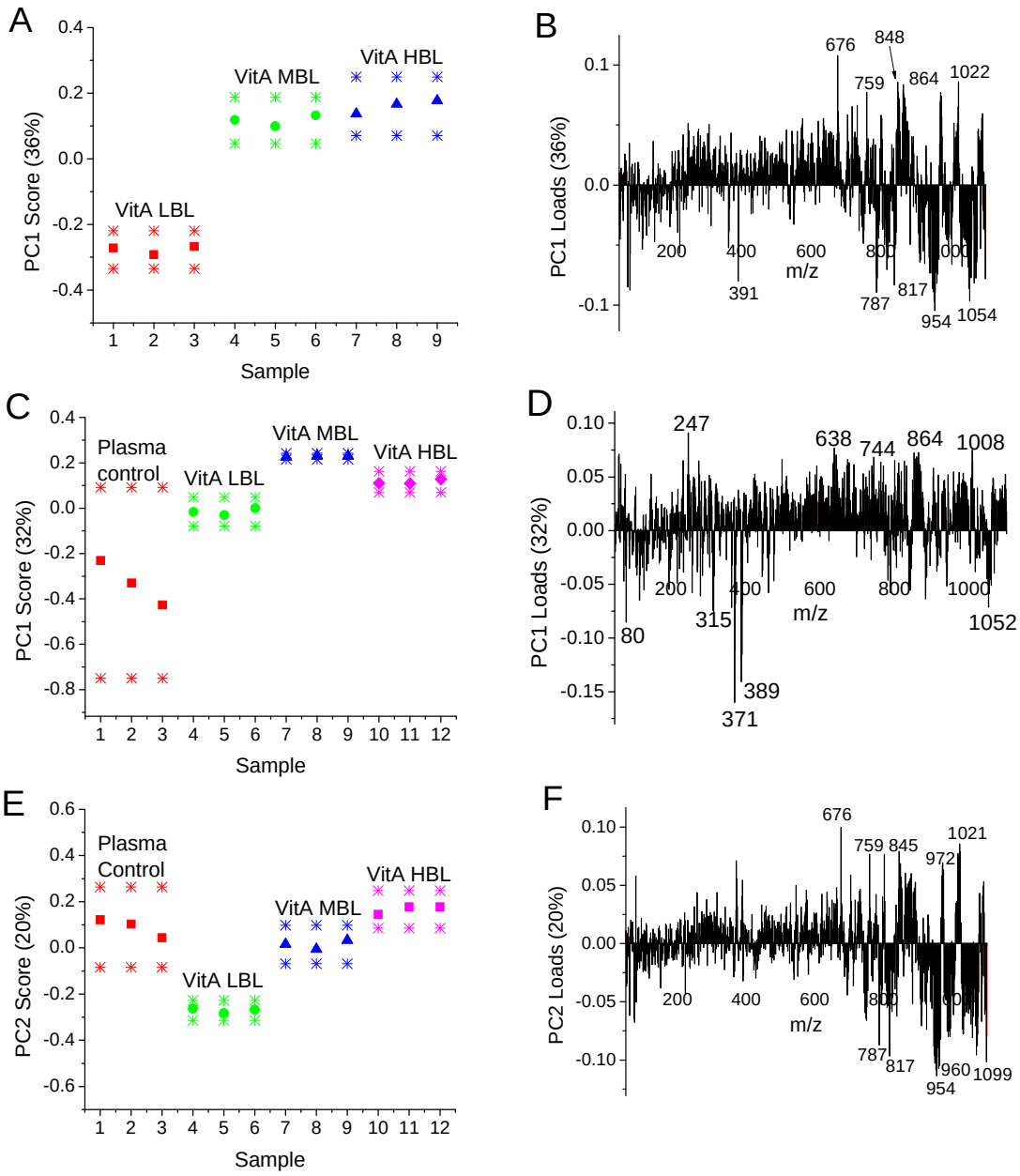

Figure 4-4 PCA on cube root data with and without a porcine plasma control. A, B) PC 1 scores and loadings comparing VitA LBL, MBL and HBL. VitA LBL separates from the MBL and HBL concentration, however, MBL and HBL have completely overlapping data points. C, D) PC 1 scores and loadings comparing a porcine plasma control with VitA LBL, MBL and HBL. The plasma control separated towards the negative loadings while the VitA samples separate towards the positive scores (not to 95% confidence). E, F) PC 2 scores and loadings comparing a porcine plasma control with VitA LBL, MBL and HBL. The three VitA levels separate from each other and show a trend, with score increasing with concentration (not to 95% confidence), however, the plasma control no longer separates from the other samples. Many of the intense loadings from B) overlap with those seen in F), thus, an altered weighting of the loadings allows for separation of the samples. * indicates 95% confidence intervals.

After analysis of data from individual days, combined analysis of multi day data was also performed. Complete data sets taken across different days were compiled and analyzed with PCA, an example utilizing the cube root transformation is shown in Figure 4-5 (A, B). PC 1 of this plot, comparing VitA variations across two separate days, indicates that the data primarily separates based on day, rather than sample content. The samples tested on Day 1 all separate towards the negative scores, and the samples tested on Day 2 towards the positive. This was consistent across both square and cube root analyses. Analysis of normalized spectra between different days showed vast differences in peak expression, even for the same sample types. This is shown in Figure 4-6, with a comparison between porcine plasma spectra collected on separate days. As labeled in the figure, several peaks have marked increased expression in Day 2, such as *m/z* 459, 476 and 533, which appeared due to contamination of the instrument, as discussed in section 4.4.4.

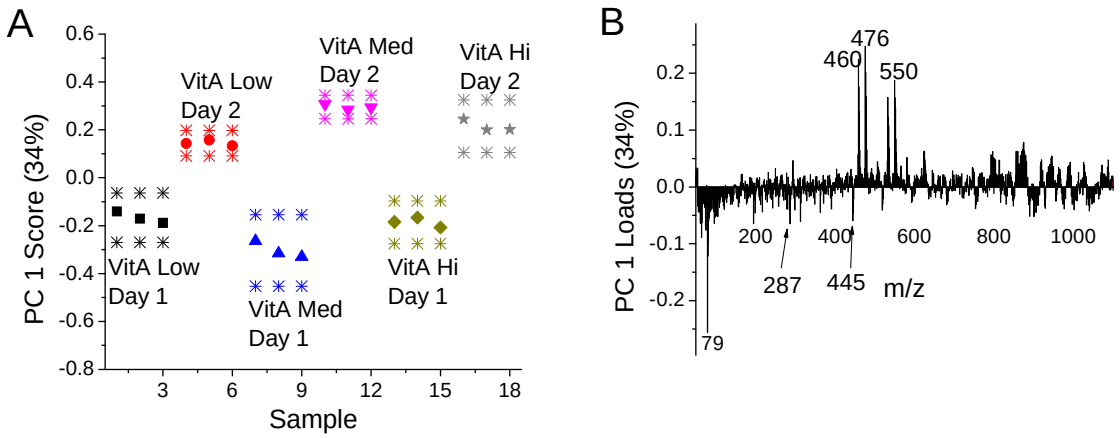

Figure 4-5 PCA on multi-day data comparison. A, B) Data separation of VitA over LBL, MBL and HBL concentrations over two separate days, after cube root transformation. Data taken from day 1 showed negative scores and data taken from day 2 showed positive scores in PC 1. This indicates that the primary separation in the data sets occurred due to differences in the day experiments were completed rather than sample contents. This is likely due to contamination peaks which have high intensities, an example of which is shown in Figure 4-6. * indicates 95% confidence intervals.

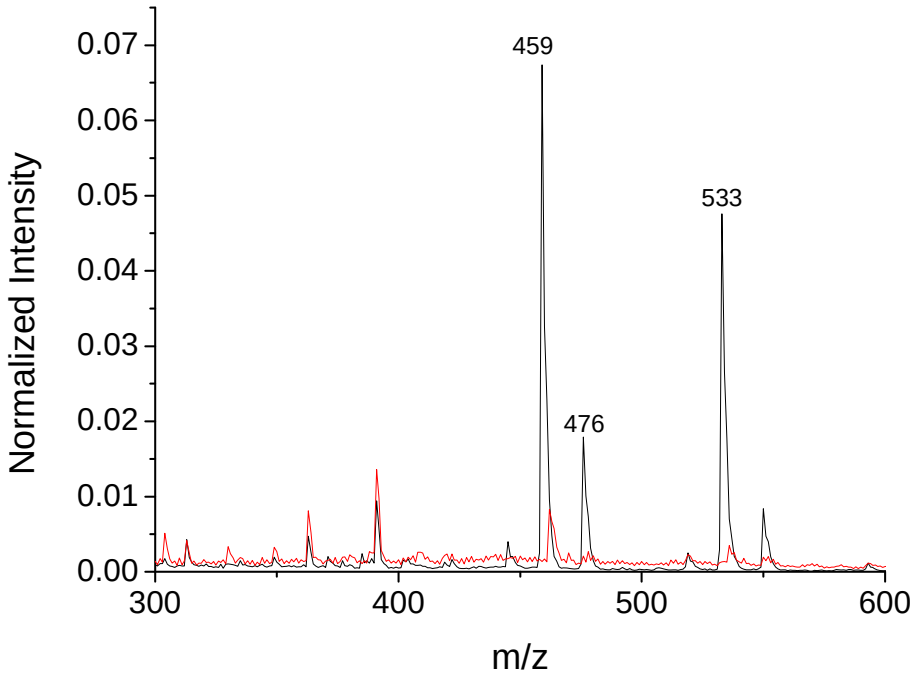

Figure 4-6 Comparison of raw spectra of plasma control samples across different days. The spectra contain many intense peaks that are different from each other. These different peaks likely originate due to contamination on the MS from experiments run by other users. ——: Day 1, ——: Day 2.

4.3.5 Data Binning

To determine if any loss of information would be apparent with binning of the data to 1 amu, a comparison between unbinned and binned data was performed. In general no loss of information was seen, as data separation between binned and unbinned data was equivalent for the analyses. An example of this is shown in Figure 4-7. Here, both unbinned and binned data resulted in the full separation (to 95% confidence) of the different Fe levels in PC 2.

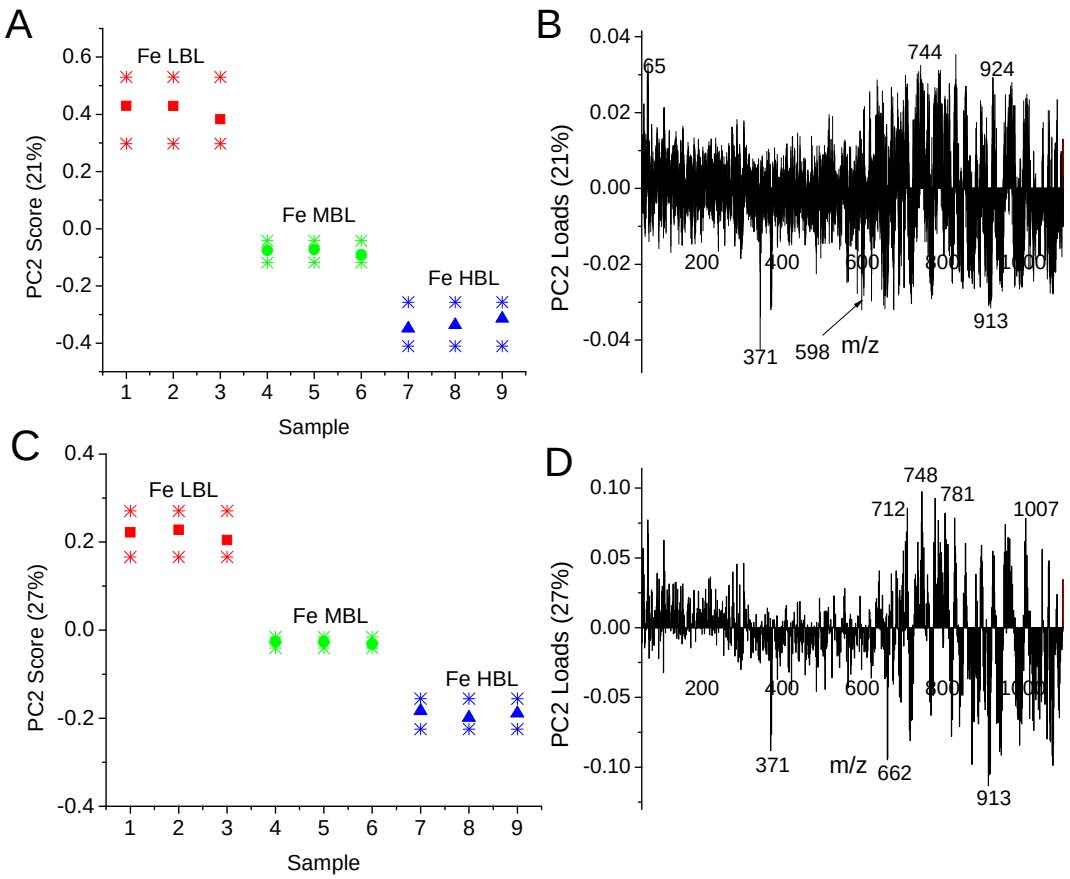

Figure 4-7 Comparison of PCA on unbinned and binned data. A, B) Scores and loadings for unbinned data. Data separates to 95% confidence and shows a trend between different levels of Fe, with Fe concentration increasing as scores decrease. C, D) Scores and loadings for binned data (to 1 amu). Data separation to 95% confidence is maintained after binning. Similar plots between binned and unbinned data were seen for all comparisons. * indicates 95% confidence intervals.

4.3.6 Cationization effect

Additional tests were completed to determine the effect of the availability of cations, and whether or not this effect would be different for the metal nutrients (Fe, Zn) compared to an organic nutrient (VitA). The results from the addition of HCl or NaOH are shown in Figure 4-8 and Figure 4-9. The PC1 scores and loadings plots for Fe are shown in Figure 4-8 (A,B), for Zn in Figure 4-8 (C,D) and for VitA in Figure 4-9. For Fe and Zn, PC 1 separates the data to 95% confidence. Here, the pH 6 samples are separated towards the negative scores, the pH 9 samples towards the positive scores and the pH 7.4 samples in between. For the VitA samples, however, the data did not all separate to 95% confidence. In fact, the pH 6 and pH 7.4 samples completely overlap (Figure 4-9 (A)). While separation between the data points could be seen in PC 2 (Figure 4-9 (C)), this is not to 95% confidence. The separation in PC 2 shows the pH 6 samples

separating towards the negative scores, the pH 7.4 samples separating towards the positive scores, and the pH 9 scores in between. Similar results were obtained in an experiment using acetic acid and ammonium hydroxide to adjust pH (data not shown).

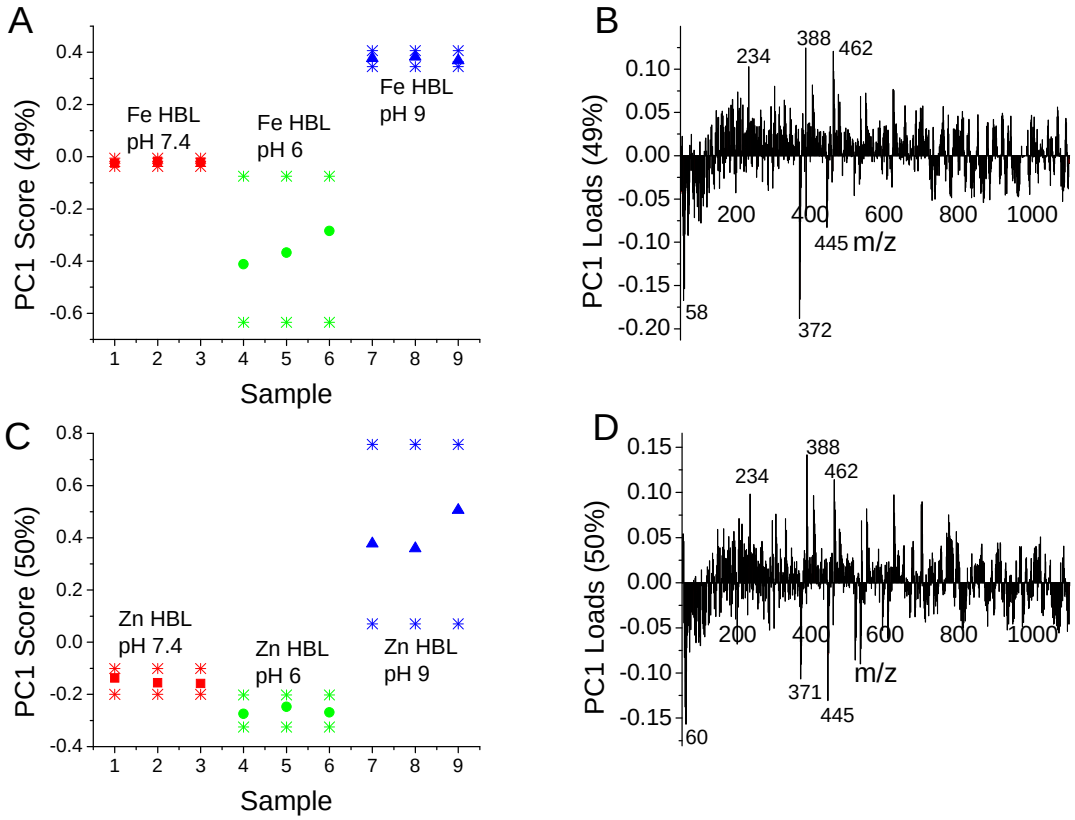

Figure 4-8 Cationization effect on metallic nutrients. A, B) Scores and loadings for a comparison between samples with Fe at the HBL concentration, and the pH varied using HCl and NaOH. The pH 6 samples separate towards the negative loadings, the pH 9 samples separate towards the positive loadings, and the pH 7.4 samples in between. C, D) Scores and loadings for a comparison between samples with Zn at the HBL concentration, and the pH varied using HCl and NaOH. Like Fe, the Zn pH 6 samples separate towards the negative loadings, the pH 9 samples separate towards the positive loadings, and the pH 7.4 samples in between. These separations are expected as the pH 6 and 9 samples most different from each other, and the pH 7.4 sample should be intermediary between the two. All separations are to 95% confidence. * indicates 95% confidence intervals.

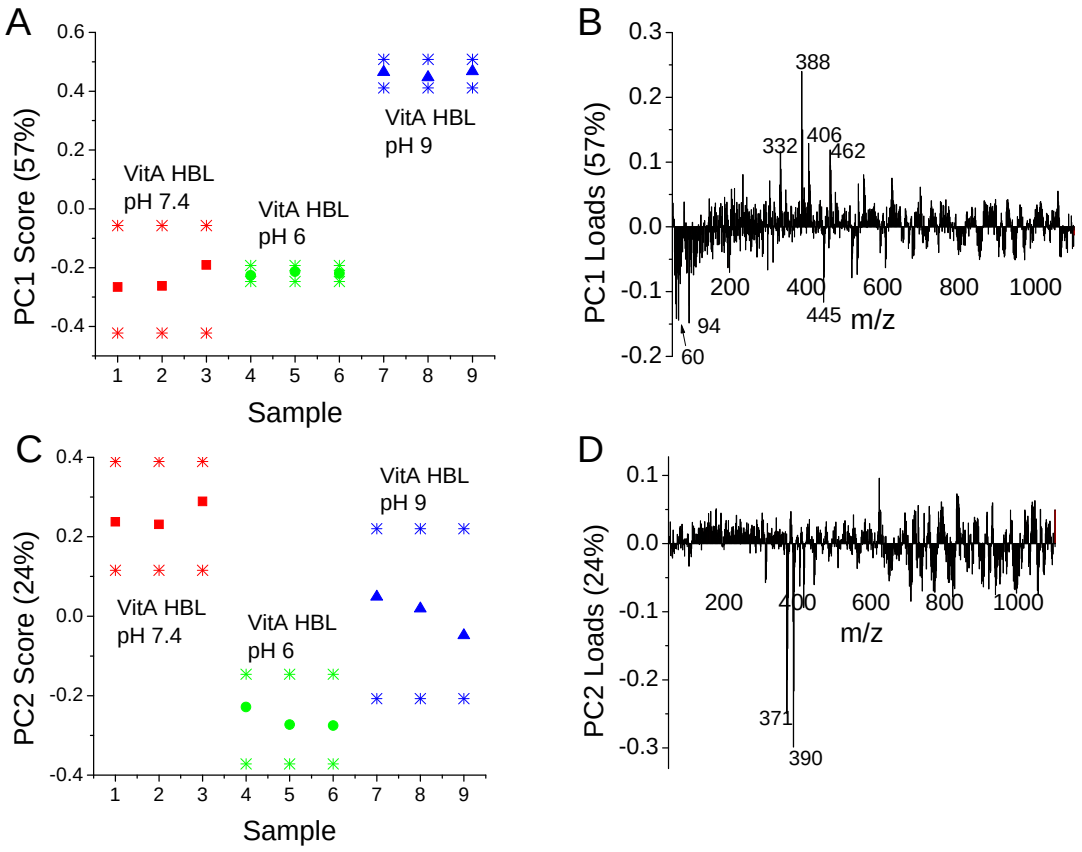

Figure 4-9 Cationization effect on VitA. A,B) PC 1 scores and loadings for a comparison between samples with VitA at the HBL concentration, and the pH varied using HCl and NaOH. The pH 6 samples and pH 7.4 samples are displayed towards the negative loadings and overlap completely with each other, and the pH 9 samples separate towards the positive loadings. C, D) PC 2 Scores and loadings for a comparison between samples with VitA at a high level, and the pH varied using HCl and NaOH. The samples at different pH are separated (not to 95% confidence). However, the separation is not the expected separation, like that seen in Figure 4-8. * indicates 95% confidence intervals.

4.3.7 Orbitrap

To confirm the ionization of the nutrients, a higher mass resolution mass spectrometer was used. Here, we identified several fragments within the spectra that originated from the nutrients. VitA solutions were thoroughly analyzed to find many of the expected peaks. A partial spectrum with highlighted *m/z* values is shown in Figure 4-10 (A). The *m/z* values highlighted in Figure 4-10 (A) along with their identities, expected molecular masses are shown in Figure 4-10 (B). Several fragments of VitA were observed from the tail portion of the molecule. For the structure of the full VitA molecule, see Appendix C. Identified fragments were *m/z* 98.0732 ($C_6H_{11}O^+$), 112.0888 ($C_7H_{13}O^+$), 138.1045 ($C_9H_{15}O^+$) and 152.1201($C_{10}H_{17}O^+$).

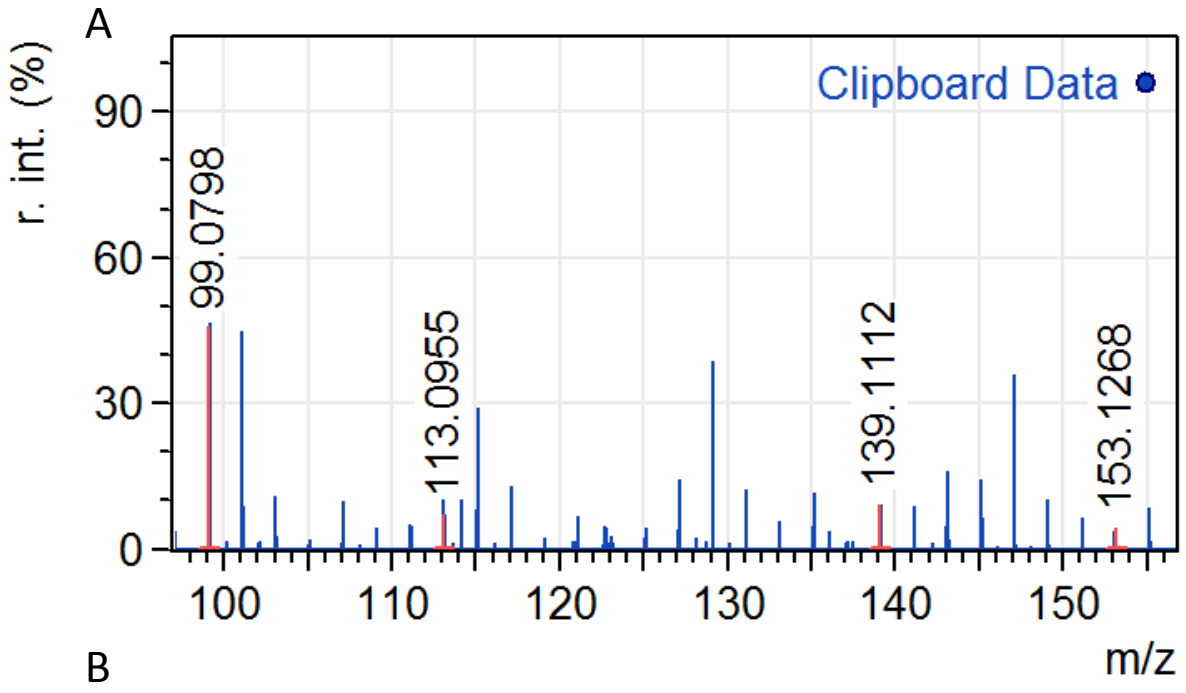

Observed Mass ($M+H^+$)	Expected Mass (M)	Deviation (ppm)	Sketch (Uncharged)
99.0798	98.0732	6.2	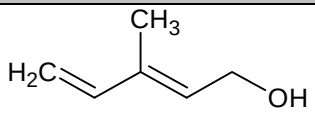
113.0955	112.0888	5.5	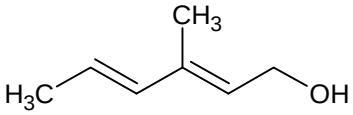
139.1112	138.1045	4.2	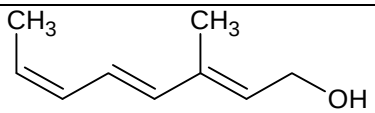
153.1268	152.1201	3.9	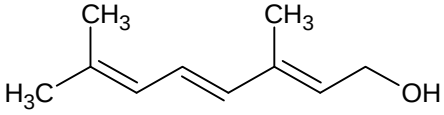

Figure 4-10 Orbitrap nutrient verification. A) Partial spectra observed from a VitA high sample. 4 peaks have been highlighted in red and identified as VitA fragments. B) Identification of the 4 VitA fragments. Each peak was identified to be ~5 ppm from the expected mass. These peaks are all breakdowns from the tail portion of the VitA molecule. The full VitA structure can be viewed in Appendix C.

4.3.8 DPCA

Previous attempts at comparing data obtained across different days did not result in the expected samples to group together, as data separation was observed based on day collected rather than sample contents, as shown in Figure 4-5 (a, b). To try to further improve data grouping, DPCA was applied. In general, the data was seen to separate in a more expected fashion, with samples of the same concentration grouping together. However, while DPCA provided separation between sample types, in general, a consistent trend that matched nutrient level was not seen. For example, as seen in Figure 4-11, while the change in concentration of Thyr results in separation of the spectra to 95% confidence, the MBL concentration separates towards the positive scores, the HBL towards the negative scores and the LBL is in between. In one case with FolA analysis, a trend is seen with a decrease in score as FolA concentration increases. However, that separation was not to 95% confidence.

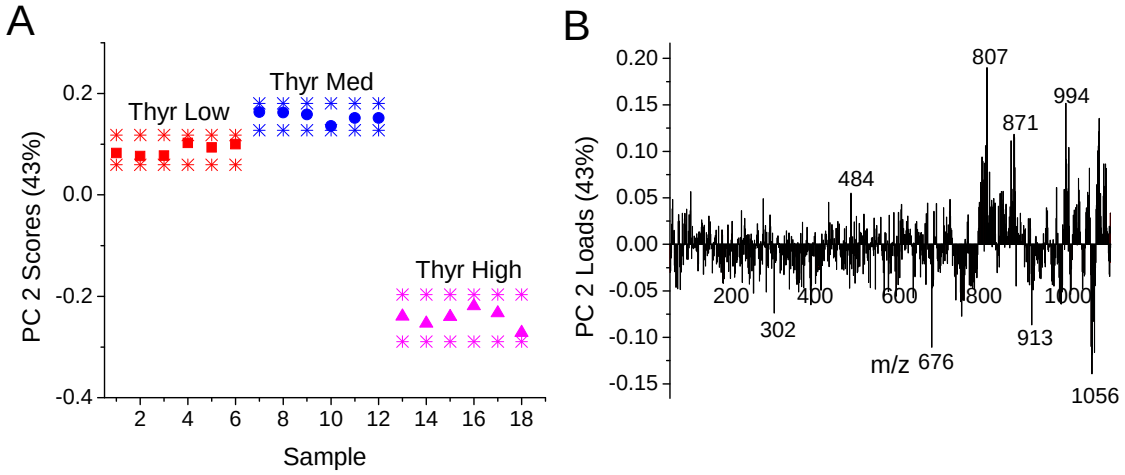

Figure 4-11 DPCA on Thyr variation. A,B) Scores and loadings comparing 2 separate days of Thyr being varied. Day 1 is the first three data points at each concentration level, and day 2 the second three. Each level is separated to 95% confidence (in contrast to the non-separation seen in the PCA comparison of Figure 4-5 (C)). However, this separation was not the expected separation as it does not show a trend based on the Thyr concentration, and thus might not be caused by the changing Thyr concentration. PC1 did not separate the samples. * indicates 95% confidence intervals.

4.3.9 Additional PCA

4.3.9.1 Additional PCA on multi-day comparison

Further analysis was also completed on data collected across multiple days. Here again, as observed in Figure 4-5, data was found to separate based on the day collected, rather than based on concentration, as shown in Figure 4-12 A, B). This separation was largely caused by new contamination peaks, which correspond to the peaks shown in Figure 4-6. After the removal

of these peaks, while the data becomes more comparable, as shown in Figure 4-12 C, D), most of the data overlaps with each other, and no consistent separation is achieved.

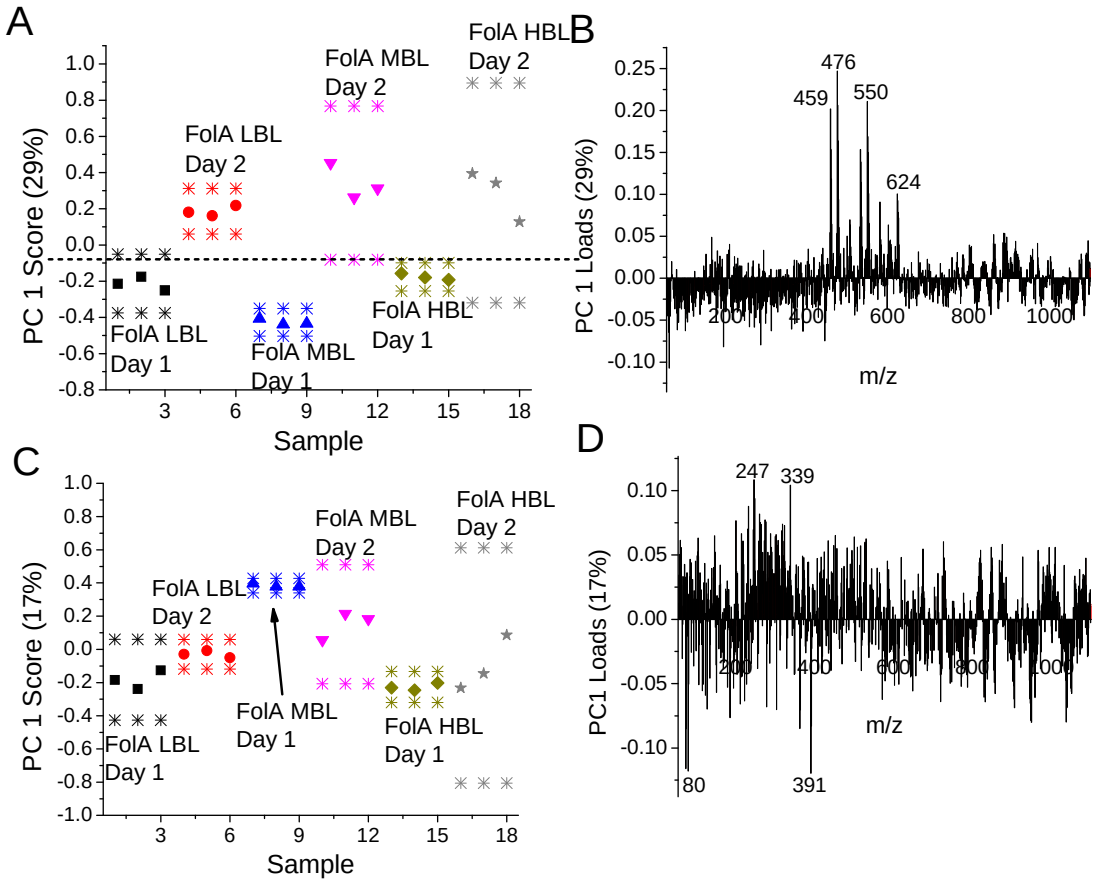

Figure 4-12 PCA on multi day data before and after peak removal. A) In the PC 1 scores, data separates based on day of acquisition, with Day 1 separating towards negative and Day 2 separating towards the positive scores. B) Corresponding loadings plot. As expected from data shown in Figure 4-6, specific peaks (the contaminants with greatly changed expression) seem responsible for the separation. C, D) PC 1 after removal of key contamination peaks. Data no longer separates based on day of acquisition. * indicates 95% confidence intervals.

4.3.9.2 Principal Component 1 Analysis

Separation according to nutrient content within the sample was mainly observed in PC2. Closer inspection of PC1 showed that trends in sample grouping in the scores plot generally occurred based on the order in which the spectra was collected within the experiment. As shown in Figure 4-13, the samples collected later separate most from the samples collected earlier. In this figure, the sample number ("Sample X") indicates the order in which the spectra was collected, where Sample 1 was the first sample group collected and Sample 27 the last. In both the examples shown in Figure 4-13, the LBL concentration was grouped closer to the HBL concentration, but between the MBL and HBL concentrations in the scores plots. In both cases,

the LBL samples were collected just prior to the HBL, and the MBL samples were collected much earlier in the experiment.

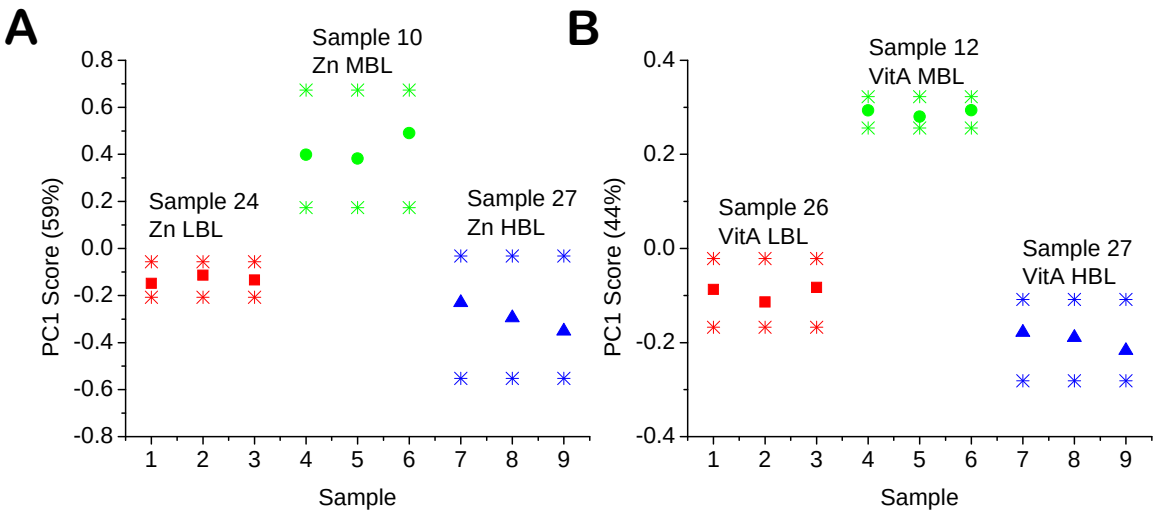

Figure 4-13 PC1 for different nutrients. Sample group number indicates the chronological order in which the sample was analyzed using PPAMS (i.e. Sample 26 was chronologically collected close to Sample 27). A) PC1 for Zn, corresponding to the analysis from Figure 4-1. Sample 10 (Zn MBL) separates away from Sample 24 and Sample 27 (LBL and HBL, respectively). In PC1, separation occurs based on when the sample was analyzed, rather than sample content. B) This phenomena was observed consistently, with another example from VitA analysis.

4.4 Discussion

4.4.1 Raw analysis

PCA was unable to separate data based on analysis without any data transformations. This may be explained by several reasons. First, an assumption when applying PCA is that the data set is linear, which might not be the case, as is known in systems such as ToF-SIMS[77] and other MSs which have uncertainties due to 'counting statistics'.[78] Furthermore, interactions between the nutrients and the porcine plasma, may also cause non-linear changes in the spectra. Thus, further data treatment, such as data transformations, may be required to improve data separation. Second, the presence of high concentrations of other molecules in the sample may confound results. Due to the high amount of the salts and proteins in solution, any fluctuations in their concentrations may mask the changes in nutrient content, as their presence in relatively minor. Thus, if more emphasis is placed on these small, but important peaks separation may be improved. Overall, while the previously inspected peaks did not show the expected trend, this is not unexpected because of new interactions/reactions of the nutrients with the plasma, causing the spectra to change.

4.4.2 Square root transformation

The first data transformation attempted was the square root transformation, which is commonly used in ToF-SIMS analysis to account for counting statistics.[77] Although ion traps do not follow the same Poisson distribution, this commonly applied technique was selected as a starting point, as the large salt and protein peaks may be attenuated to improve analysis. While data separation was improved for many of the nutrients, overall, data separation was still inconsistent, with only half of the analyses showing the expected separation. This may be due to several factors, including the relatively low intensity of the peaks of interest (nutrient peaks), as well as the contamination present in the instrument.

4.4.3 Peak list formation

After limited success with data separation using the square root transformation, peak list formation was attempted. Peak lists were constructed by forming separate peak lists made from individual days, using data from analyses showing trends (like those seen in Figure 4-2). To eliminate peaks that may have displayed a trend due to chance rather than being related to the nutrient, initially, separate peak lists for each nutrient were constructed for each day of analysis. These peak lists were then consolidated to single peak lists for each nutrient by comparing them, and keeping only the repeating peaks. Removal of the low value loadings (<|0.009|) was thought to highlight the key peaks responsible for separation of the different nutrient levels. The results shown in Figure 4-3 highlight that peak list formation may be able to improve data separation, even when initial analysis is unsuccessful. Overall, however, the peak list formation had limited success, thus, alternate peak removal methods and more specific peak removal may be required to improve overall data separation.

4.4.4 Higher order transformations

Due to the limited success of the square root transformation and peak list construction, a literature search was performed to determine other common methods of data transformation to try to improve data separation. Here, we found that two additional methods have been employed, the cube root and logarithmic transformations.[79] We decided on the cube root transformation due to the logarithm's inability of handling zero intensity values. If the logarithm was employed, a small arbitrary factor would be required to be added to all values in order to ensure that no zero *m/z* intensities would appear in the spectra.

The cube root transformation was seen to greatly improve data separation, and caused the data to largely separate in the anticipated manner. After this transformation, more sample analyses showed a trend between the concentration of the nutrient and the score of the samples, as shown in Figure 4-4. This is likely due to the relatively increased importance placed on the low intensity peaks after the cube root transformation while simultaneously making the weighting of the more intense salt and protein peaks attenuated. While many of the most intense loadings are conserved across all transformation types (i.e. *m/z* 62, 121, 217 and 371), after the cube root transformation, many additional peaks in the loadings plot have a significant effect on separation. Surprisingly, Thyr, FolA and VitA had better and more consistent separation when compared to Fe and Zn which are at higher concentrations. This may be due to a combination of factors, such as a potentially increased number of breakdown peaks observable in the organic nutrients or the cationization effect, discussed in sections 4.3.6 and 4.4.6.

Analysis with a fourth sample type included, a porcine plasma control, also slightly improved data separation. In Figure 4-4 (E, F), when the porcine plasma control is added, PC 2 is capable of separating the nutrients. Without the porcine plasma, none of the PCs can separate the data with the expected trend. While many of the peaks between PC 1 without the porcine plasma (Figure 4-4 (a,b)) and PC 2 with the porcine plasma overlap, the separation is vastly improved in the latter. So, with a different emphasis on the peaks, separation of the different nutrient levels is possible. A fourth root transformation was also attempted, however, this did not improve separation, thus, the cube root was selected as the primary analysis method.

Data was expected to separate according to sample contents, however, upon PCA analysis of a multi-day data set, the most significant differentiating factor was found to be the day in which the data was taken. This was seen to be caused by large differences between spectra of the same sample type across different days. These peaks are thought to be from the instrument, rather than the samples. The Bruker ion trap is a heavily used and shared system. Other users have samples that will attach to the instrument, as shown in Figure 4-14. Several peaks, such as those listed in Figure 4-6, are likely ionized particles from previously run experiments. Thus, a direct comparison across data collected from different days did not result in the anticipated grouping. To try and compensate for these highly intense contamination peaks, as well as further improving overall data separation, the contaminant peaks were removed from analysis. This, however, only resulted in the data becoming more comparable, and did not result

in data grouping based on nutrient concentration in the sample. This may be due to the presence of other, less intense contaminant peaks which were not easily found.

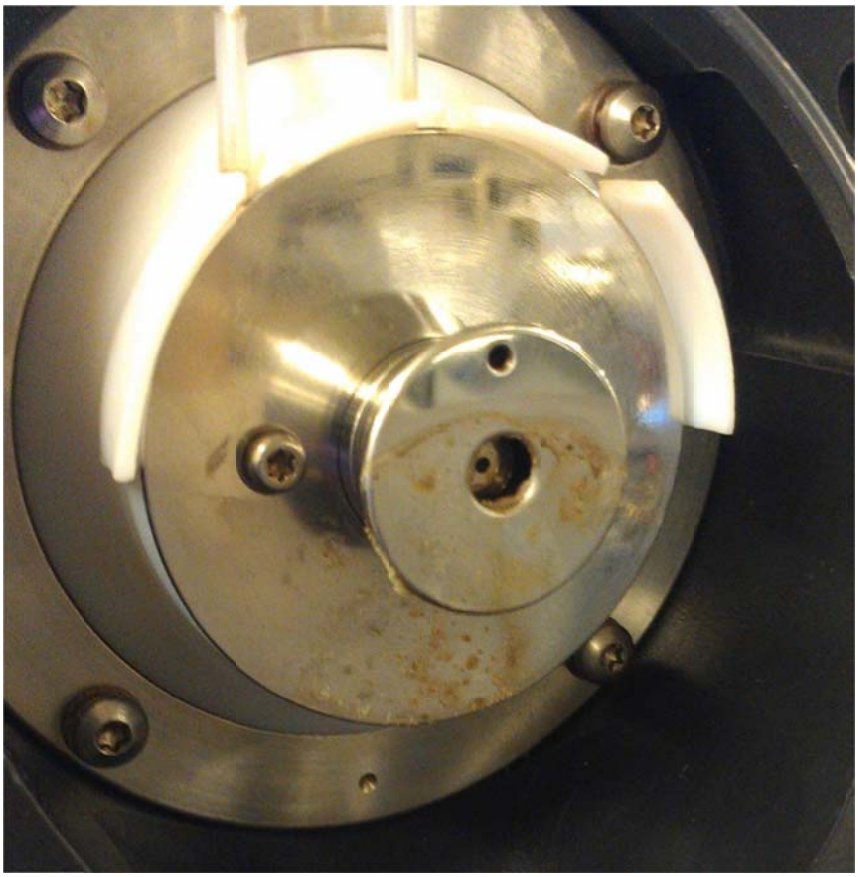

Figure 4-14 Instrument contamination. Contamination present on the mass spectrometer inlet prior to use. The instrument is cleaned using water and isopropyl alcohol, however, this is only a surface cleaning. Residues of past experiments are left on the surface, as well as internal contamination that cannot be reached via this cleaning method.

4.4.5 Data binning

Binned data was able to separate the different nutrient concentrations to the same degree as unbinned data. Data binning was necessary for several reasons. First, the analysis of data using the full peak set is very time consuming. To load the data into MATLAB requires more than 10 hours for an average data set containing 80 samples. This lengthy analysis time would make future work for onsite analysis impractical. Second, this is also important for future work because some of the options for future portable MSs have lower mass resolution, and may effectively only give unit mass information. Thus, the ability to separate data using binned data is key for future applications.

4.4.6 Cationization effect

The metal micronutrients are present in the blood at higher concentrations than the other nutrients, and were thus expected to be detected and separated more easily than the other nutrients. However, even after peak list formation and data transformation, the metal nutrients (Fe and Zn) had more difficulty with separation than anticipated. This was hypothesized to be caused in part by the cationization effect, where a change in the cation concentration can have a great effect on the overall secondary ion yield.[80] This is a common issue with other cations such as sodium.[39] To test the cationization effect, a sample set containing varied pH levels was tested. This was completed to determine the effect of the change in availability of cations on the overall spectra. As anticipated, this change in free ions had a greater effect on the metals, Fe and Zn, than on an organic nutrient, VitA, which is shown in Figure 4-8 and Figure 4-9, respectively. This was seen in the manner in which the data separated. For Fe and Zn, the pH 7.4 sample separated between the pH 6 and pH 9 samples, with all separations to 95% confidence. This was expected as the pH 9 and 6 samples are chemically most different from each other, and the pH 7.4 sample should be intermediary. This was not observed to be the case in the VitA analysis, where separations to 95% confidence did not occur. Furthermore, the separation that was seen showed the pH 9 sample separating between the pH 7.4 and pH 6 samples. This indicates that the differences observed in the VitA samples are not caused by the change in the level of free ions. Thus, quantitation of Fe and Zn may be more challenging than with the other nutrients.

4.4.7 Orbitrap

PCA will find differences in data, regardless of whether that difference is real or artificial, for example, the separation may be a result of spectral noise. Thus far, analysis of grouped data collected across different days has had limited success in providing expected separation. While previous studies identified probable ionized fragments of the nutrients, few of these studies were completed on nutrient samples in complex solutions (based in porcine plasma), and many of these peaks did not overlap. Thus, as an additional confirmation an experiment was performed coupling the plasma ionization device to an orbitrap MS. The orbitrap MS allowed for more information to be collected by having the ability to verify the ionized particles, without requiring MS/MS to be performed on each peak. This is advantageous because collecting MS/MS data can be very time consuming if many peaks are desired, while other important peaks are likely to be missed. With the orbitrap data, a confirmation that the nutrients

of interest are being ionized at detectable levels was obtained. Several peaks originating from VitA were identified at the high concentration to about a 5 ppm deviation. Overall, this data reaffirmed that the PPAMS system is capable of ionizing the nutrients.

4.4.8 DPCA

As expected, DPCA was able to improve the ability to separate data when analyzing data collected from different days. The actual separation, however, was generally not consistent with expectations. Ideally, an increase in nutrient level would result in a visible trend in the scores plot, such as that seen in Figure 4-1 (E). In particular, an increase in nutrient concentration should result in a corresponding increase or decrease in the scores of the sample groups, particularly if the data could be used for quantitative purposes. Thus, while DPCA was able to find similarities in the same sample types across different days, these similarities might not truly be related to the nutrients.

To supplement this analysis, peak list formation was attempted with DPCA. This was completed by performing PCA in parallel to the DPCA. The scores and loadings plots from PCA were studied to determine the cause of sample separation. When the scores indicated that the data was being separated by data collection day, rather than sample contents, the corresponding loadings were studied. Here, loadings with values >|0.009| were removed, to reduce the presence of noise/background peaks. The next round of DPCA and PCA were then performed using the shortened data set. This was continued until the PCA no longer showed the separation as primarily due to data collection day. This additional analysis, however, did not significantly improve data separation in DPCA. By forming groups of data based on sample contents, DPCA will attenuate those peaks that have high intergroup variation – i.e. those new contamination peaks. Thus, the removal of these peaks had little effect on overall data separation. A larger scale peak removal may have a greater effect. Overall, however, DPCA may not currently be the appropriate technique for this study. DPCA is applied, ideally, to data which has only random variance for within-group samples.[47] This, however, is not the case for this system due to changing contaminants in the MS.

4.4.9 Additional PCA

4.4.9.1 Additional PCA on multi-day comparison

As discussed earlier, when comparing data obtained across different days, separation occurred based on the day collected. To achieve any type of quantitative ability, however, data

collected across multiple days must be comparable. Unfortunately, because the Bruker MS is a shared system, new peaks appear in the spectra, as discussed earlier. With the removal of the prominent contaminant peaks, the data becomes more comparable however, separation based on concentration was still not achieved. This may be due to additional, smaller contaminant peaks that were not removed, and would be difficult to identify. This would also cause problems for future, longer term studies as new contaminant peaks would potentially continue to appear in the spectra.

4.4.9.2 Principal Component 1 Analysis

Data separation based on concentration via PCA was consistently observed in PC2, rather than PC1. The compared samples should only differ in nutrient content, thus, the observed differences in spectra are expected to be caused solely by the change in nutrient concentration and should appear in PC1. In practice, however, PC1 was observed to separate the data based on the order in which the sample was collected. Thus, not only is the analysis affected by the presence of new contaminants, but also by the changing conditions in the system, which may be due to molecules desorbing from the inlet capillary walls. This could potentially be remedied by collecting multiple control samples throughout the experiment. By determining how the background spectra is changing over the course of data collection, it may be possible to subtract the noise and/or contaminant peaks from the spectra, even for a shared system.

4.5 Conclusions

Overall, the work in this aim was completed to provide semi-quantitative results by classifying the samples based on concentration. Ideally, by separating known data into distinct nutrient levels, then testing new samples, PCA models could then be applied to future sets to determine the nutrient levels in unknown samples. Initial analyses were unable to provide consistent separation of data based on concentration, however, with the application of a cube root transformation, separation was observed. However, contaminants were observed to effect the intraday analyses, and made inter-day comparisons difficult. While potential solutions to these problems are possible, for example through extensive peak list formation and DPCA, the use of a dedicated mass spectrometer is expected to greatly improve these results.

5 Specific Aim 3a: To acquire a compact mass spectrometer and optimize system settings for Vitamin A detection and demonstrate quantitation using partial least squares analysis

5.1 Background

5.1.1 Motivation

In the previous aims, the PPAMS system has been shown to be capable of ionizing nutrients at microgram per liter levels and determining differences between samples with only minute variations in the nutrients, even in the presence of other molecules at milligram per liter levels. To this point, the experiments have been completed on laboratory scale mass spectrometers which are costly and heavy, making them less than ideal as a deployable solution for low resource settings. In order to move towards a field applicable solution, several system modifications must be made. A more portable, cost effective system would be more feasible for testing and transportation. VitA will first be tested as this was the most studied nutrient in earlier experiments using the Bruker Esquire Ion Trap and showed consistent separation from control samples.

5.1.2 Mass spectrometer selection

The Advion Express**ion** is a single quadrupole mass spectrometer measuring 66 x 28 x 56 cm^3 (excluding pumps). This relatively small size allows the system to be placed inside a hood (chemical or biological), where experiments could be completed on human based samples. Due to safety concerns, such as virus transmission or other blood borne pathogens, human samples cannot currently be tested using the PPAMS system while it is coupled to the larger Bruker Esquire Ion trap, where the entire system is open to the environment. Overall, the manufacturer lists the resolution of this system as *m/z* 0.5-0.7 at *m/z* 1000 (i.e. a resolving power of 1430-2000), which is slightly lower than that of the previously used Bruker Ion Trap. However, as binned data to unit resolution was shown to separate samples in aim 2, the resolving power of the Express**ion** should be sufficient. Other specifications, such as the testable *m/z* range and the accuracy are also similar to the ion trap and should give similar results. This system, is not capable of MS/MS which may be beneficial for verification experiments, however, this function should not be required for the final system.

Several alternatives to the Express**ion** also exist, however, each of these have major drawbacks and will thus not be used. For example, the Griffin 460 from FLIR is a robust system which has been used extensively for military applications. However, this MS is expensive, at approximately $130,000, and furthermore can only detect analytes at the µg level.[81] Another available MS, the Torion Tridion 9 GC-TMS, is a compact system with better detection than the Griffin. In this case, the MS inlet, is a membrane which requires samples to be injected and is incompatible with the LTP. Overall, the inlet would require extensive modification (as well as the addition of a secondary pumping system) to be used for PPAMS. Finally, the 'Mini' series of MS, developed in the Cooks lab at Purdue[82] is another possible alternative. This system has been used in several applications with different ambient ionization sources,[83,84] however, this system has yet to be fully commercialized and is not available for purchase.

5.2 Materials and Methods

5.2.1 Chemicals and Reagents.

All chemicals were purchased from Sigma-Aldrich Chemical Co. (St. Louis, MO) unless otherwise noted. VitA (in the form of retinol) was dissolved methanol (MeOH) at 3.75 mg/mL to form a stock solution. Deionized/distilled water (dH_2O) was obtained from a Barnstead/Thermolyne deionizer unit (Nanopure, 18MΩ·cm resistivity, Dubaque, IA). For the PPAMS experiments, samples were then further diluted in MeOH, dH_2O or porcine plasma (PL26009, Innovative Research, Novi, MI). Porcine plasma samples were diluted to a 10% porcine plasma/90% isotonic citrate-phosphate buffered saline (cPBSz) solution. cPBSz was made using sodium azide (0.01 M sodium citrate, 0.01 M sodium phosphate, 0.12 M sodium chloride, 0.02% (w/v) sodium azide, and was adjusted to a pH 7.4 with sodium hydroxide). For the electrospray ionization (ESI) experiments, stock solutions were diluted in water (Macron Fine Chemicals, Center Valley, PA) or MeOH with 0.1% formic acid (J.T. Baker, Center Valley, PA). When required, a mobile phase B of acetonitrile (Fisher Scientific, Pittsburgh, PA) with 1% acetic acid (Fisher Scientific) was used. Porcine plasma was initially tested by the University of Washington Research Testing Service to determine the baseline level of VitA using the current testing standard, high-pressure liquid chromatography (HPLC).[85]

5.2.2 Plasma Pencil Atmospheric Mass Spectrometry (PPAMS).

Experiments were mainly performed on an Express**ion** quadrupole mass spectrometer (Advion, Ithaca, NY), however, select verification experiments were performed by coupling the

LTP to an LTQ Orbitrap XL (Thermo Scientific, Waltham, MA). For the Express**ion**, spectra were collected over a mass range of *m/z* 10-1200 with a scan time of 1000 ms with Advion's Mass Express software. Initial MS settings were set as: capillary temperature: 50 °C, capillary voltage: 20 V, source voltage: 10 V and source voltage dynamic: 0 V. Spectra was collected for 2 minutes or less per sample, after which data was exported using Advion's Data Express software as a CSV-file, and preprocessed with an in-house Matlab (The MathWorks, Inc., Natick, MA) program. Data preprocessing included rolling-ball baseline correction (radius of 0.75 and sample spacing of 0.5 Da), negative value removal and peak binning to 1 *m/z*. In the standard upright position of the Express**ion**, the MS inlet is vertical. After initial experiments, the MS was rotated on to its side to make the MS inlet horizontal to simplify sample handling.

The LTP ionization source was constructed in-house, as described in section 2.2.3.3.[86-88] In brief, a high voltage electrode (stainless steel, 1.33 mm) was centered in a glass tube (o.d. 8 mm, i.d. 6 mm), with a 2.5 cm strip of copper tape wrapped around the tube as the ground. An adjustable, alternating 6-12 kV square-wave was applied to the high voltage electrode at a frequency of 5-8 kHz by a custom-built power supply. Helium gas was then supplied through the glass tube to generate a low temperature plasma, measured to be 34 °C. Input voltage was set at 11.2 V (corresponding current of 0.39 A). 12.7 mm paper filters (Grade 40, GE Healthcare Life Sciences, Piscataway, NJ) were used as the sample substrate. For the heated experiments, an aluminum block was machined to hold a stainless steel heating element (model CSH-101100, Omega Engineering Inc., Stamford, CT) and thermocouple (model 5TC-TT-E-30-60, Omega). Power for the heating element and thermocouple were supplied by a bench top controller (model CI32, Omega).

A sample enclosure was constructed to house the heated stage, LTP nozzle and sample with several design features. In brief, the heated stage was set on adjustable screws to allow for height control and the distance of the LTP from the MS inlet could be adjusted as well. A filter was placed on the back wall of the enclosure to reduce pressure build up. Set screws were used to secure the enclosure to the MS in the same way the default ionization source (an ESI source) attaches to the instrument. Sample images of the enclosure can be seen in Figure 5-1. After optimization with the enclosure, samples were placed 4 mm away and 4 mm below the MS inlet. The LTP probe was positioned at an angle of 60° from the horizon, and was placed 17 mm away and 5 mm above the inlet.

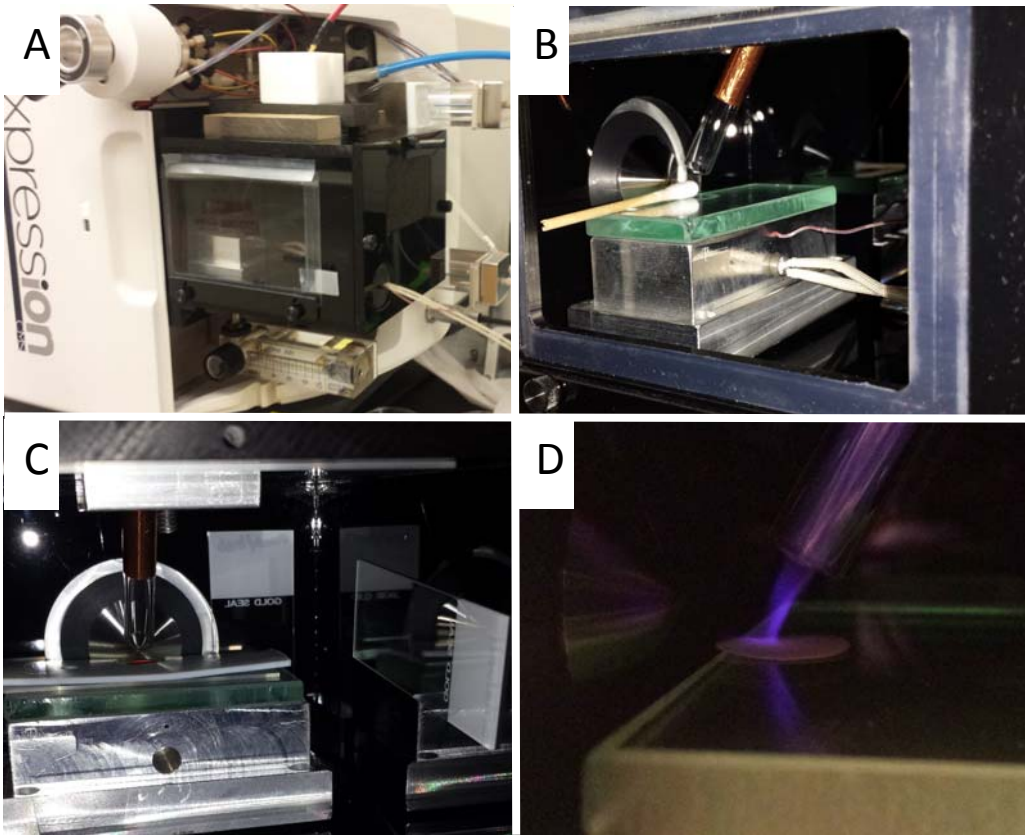

Figure 5-1 Images of the LTP enclosure. An enclosure was constructed to protect the sample and the user. A) External view of the entire enclosure. B) Close up of the internal components of the enclosure. C) View of the enclosure from the rear, with back panel removed. D) View of the active LTP inside the enclosure.

20 µL of sample solution was spotted onto filters for analysis. Sample solutions diluted in MeOH were dried overnight in a desiccator prior to analysis, due to the interference of MeOH in the mass spectra, while samples in water or porcine plasma solution could be analyzed directly after application to the filter paper. Prior to analysis, desiccated samples were re-wet with 20 µL of water, unless otherwise noted. Experiments performed with nitrogen flushing were completed by flowing N_2 into the chamber at 1 LPM. Upon inserting the sample and sealing the chamber, the N_2 was allowed to flush the system for 1 minute, to allow for the removal of oxygen before analysis. Due to the wait time prior to data collection, as well as to eliminate extra oxygen, the samples were analyzed dry. Aqueous solution testing was completed by dissolving VitA in MeOH, or in a 1:99 MeOH:dH_2O mixture. Samples were then desiccated overnight. One set of samples was run dried while another was run re-wet using dH_2O.

5.2.3 ESI-MS and ToF-SIMS

ESI experiments were performed on either an Esquire LC-ion trap MS (Bruker, Billerica, MA), or the LTQ Orbitrap described above. For the Esquire LC-ion trap, most samples were injected via syringe pump (Model 74900, Cole Parmer, Vernon Hills, IL) at 1.5 μL/min and ionized in a standard orthogonal Bruker ionizer. Spectra were collected over a mass range of *m/z* 50-1100. For the LTQ Orbitrap, 10 μL of sample solution was loaded into the system, with a mobile phase B injected at 10.0 μL/min and collected over a mass range of 50-1000 m/z. See section 3.2.2 for details about ToF-SIMS experiments.

5.2.4 Statistical analysis.

Statistical analysis of spectral peaks was completed by performing a two-tailed, paired Student's t-test, included in the Microsoft Excel software.

5.2.5 PCA and PLSr

Refer to section 3.2.5 for a description of PCA. For PLSr, calibration and test data were obtained on VitA samples from porcine plasma using the PPAMS system coupled to the Advion MS. The calibration samples were collected for a fixed 10 seconds and no care was taken to select specific samples for calibration beyond ensuring that the samples received uniform treatment prior to analysis. Data was preprocessed using the rolling ball techniques and removal of chief contaminate peaks as described earlier. PLSr was then performed using the PLS_Toolbox (Eigenvector, Wenatchee, WA). The sample-axis was autoscaled and mean-centered and variable-axis was mean-centered and normalized. Following the application of the PLSr program, the prediction model was exported and used to validate additional spectra. PLSr data was converted from a concentration to a mass of VitA by multiplying by the volume (20 μL).

5.3 Results

5.3.1 Initial nutrient matrix

After the system was purchased and set up, nutrient matrices, similar to those from section 4.2.1, and were studied as dried samples in 10% porcine plasma to better mimic previous experiments. Upon analysis, no separation based on nutrient concentration was observed. PCA was completed using no transformation, square root transformation and cube root transformation, however, no separation between sample types was observed for any nutrients in any of the principal components. A representative example of PCA results can be found in Figure 5-2.

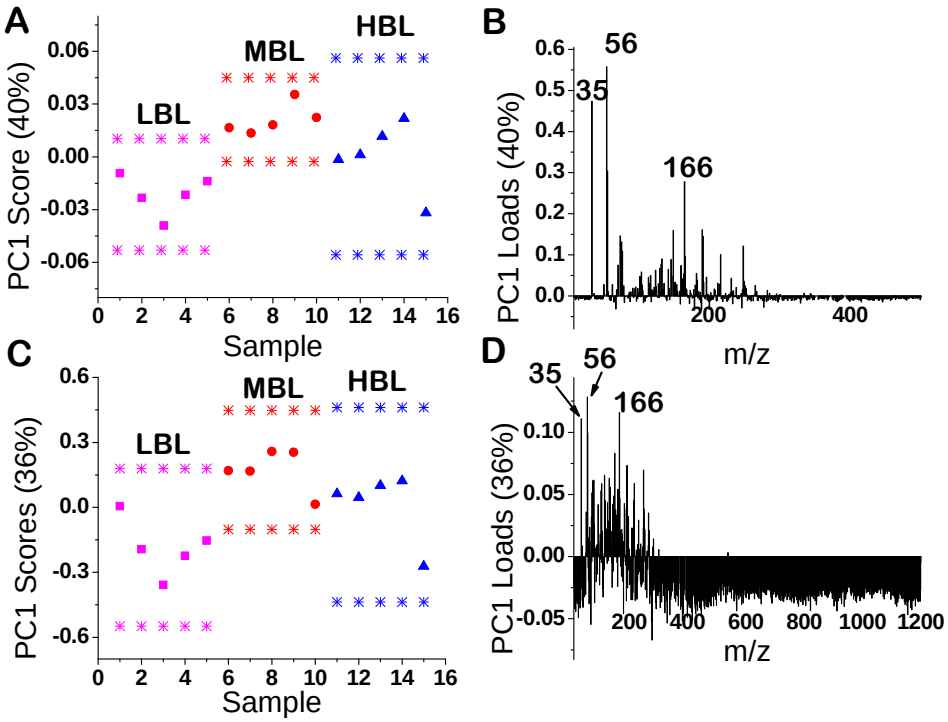

Figure 5-2 Sample PCA on 3^3 matrix. A 3^3 matrix containing Fe/Thyr/VitA was tested. Separation of the data was not achieved for any of the nutrients, in any of the PCs, an example of which is shown here with VitA analysis, while the other nutrients were held at LBL. A, B) Scores and loadings plots for PCA with no transformation applied to the spectra. C, D) Scores and loadings plots for PCA with a square root transformation applied to the spectra. In the scores plots, no separation can be observed between different concentrations for this, or other PCs. In the loadings plots, the key loadings which provide the greatest variance are *m/z* 35, 56 and 166. The raw spectra show that these peaks are high intensity, high variability peaks, which cause the large degree of variance.

5.3.2 Initial VitA detection

Using the original system settings recommended by the manufacturer, as listed in Section 5.2.2, experiments were performed by spotting samples with VitA dissolved in MeOH. Final concentrations tested were 650 µg/L (healthy blood level, HBL) up to 3,750,000 µg/L (labeled as 6000xHBL). Several peaks were found to be related to VitA, two of which are shown in Figure 5-3 (A, B). These peaks at *m/z* 165 and 181 were seen to increase with increasing VitA, however, they were only visible starting at 600x the level expected to be found in a healthy individual. PCA was also performed to determine if data separation could be achieved in the absence of visible peaks at lower concentrations. Overall, while not to 95% confidence, separation via PCA could begin to be seen at the 600 to 6000xHBL concentrations, as shown in Figure 5-3 (C). The chief loadings responsible for the separation are seen at *m/z* 55 and 73. Additional PCA was performed by removing samples with concentrations ≥600xHBL, however, this did not improve separation of lower concentrations.

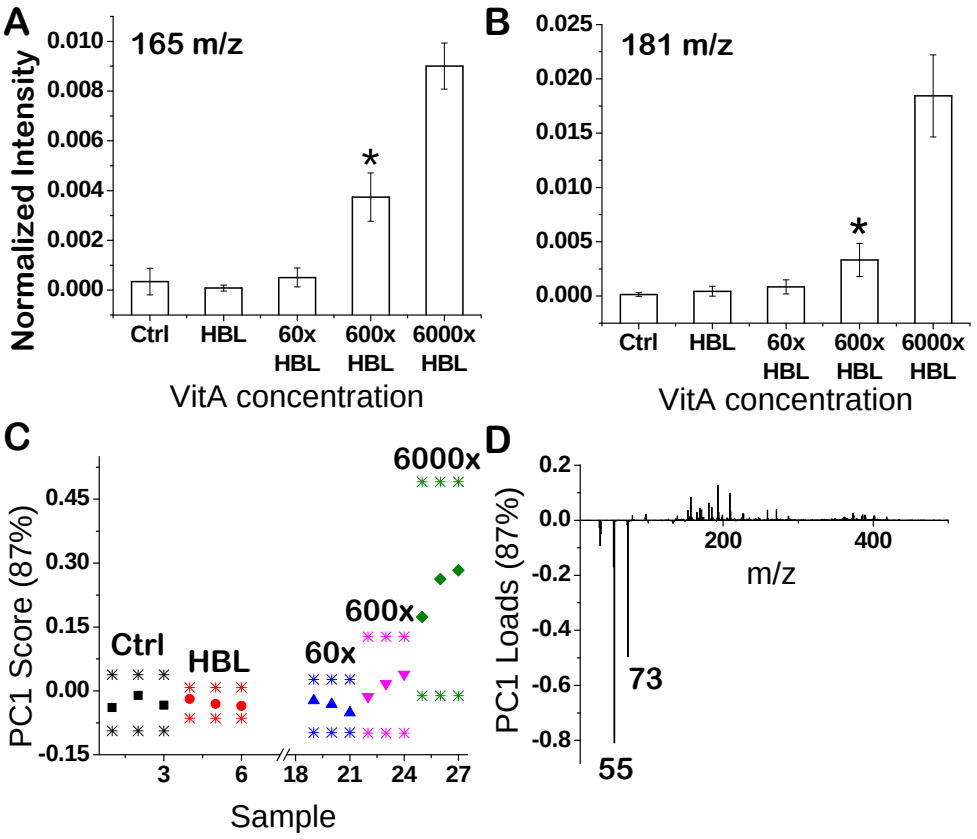

Figure 5-3 VitA detection with original settings. VitA was dissolved in MeOH to concentrations at or above human blood level (HBL = 650 µg/L, samples contained concentrations up to ~6000xHBL=3,750,000 µg/L). Samples were dried overnight, and rewet with 20 µL water prior to analysis. Several peaks were found to increase with increasing concentration of VitA, such as A) *m/z* 165 and B) *m/z* 181.These peaks could be separated from control samples starting at 600xHBL. The spectra were also compared using PCA. Resulting scores and loadings plots can be found in C, D). As with the individual peaks, separation is beginning to occur at 600xHBL and is clearer at 6000xHBL, though neither to 95% confidence. Peaks containing the most variance were found to be *m/z* 55 and 73. In A, B) * indicates the lowest concentration of VitA with a p-value < 0.05 compared to the control. In C), * indicates 95% confidence intervals.

5.3.3 VitA detection optimization

5.3.3.1 Peak removal

Several peaks were removed from the spectra prior to normalization, including the most prominent peaks *m/z* 37, 55, 73, 350-355, 370-375 and 390-395 (please see section 9.5, Appendix E for the full list of removed peaks). Upon peak removal, data from section 5.3.2 was re-analyzed and the detection limits for VitA improved by a factor of 10 for *m/z* 181 to 60xHBL, as shown in Figure 5-4 (A), while the detection of *m/z* 165 remained the same (not shown). With PCA, separation was also improved, with 6000xHBL separating to 95% confidence from the control, and 600xHBL separating more from the control as well (though still not to 95% confidence), both shown in Figure 5-4 B). Chief positive loadings (corresponding to a greater

expression in VitA samples) were *m/z* 181 and 209 while major negative loadings included *m/z* 97 and 191, as shown in Figure 5-4 (C).

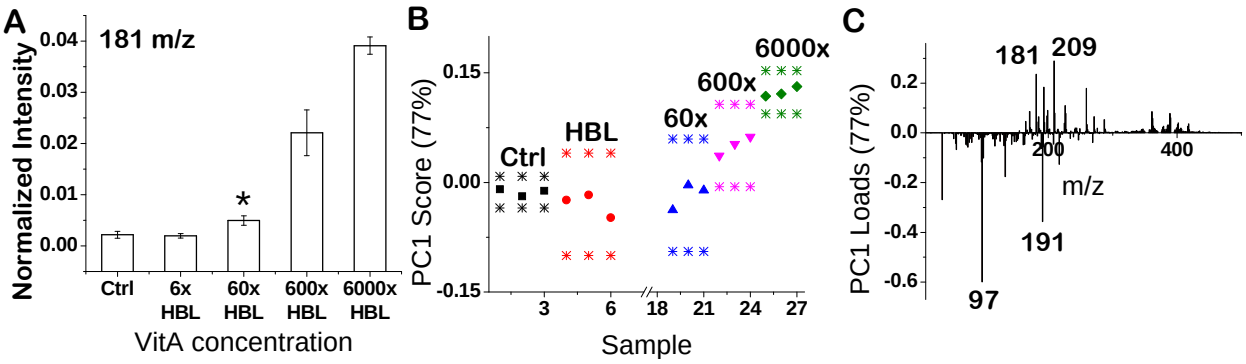

Figure 5-4 VitA analysis after peak removal. VitA was dissolved in MeOH to concentrations at or above human blood level. After studying the spectra, peaks were removed from analysis prior to normalization which were highly variable, and unrelated to nutrient content. Removed peaks can be found in Appendix E. A) Peak removal resulted in improved detection of *m/z* 181, at 60xHBL, compared to 600xHBL without peak removal. B, C) Scores and loadings plots from PCA. The scores plot is improved, with 6000xHBL now separating to 95% confidence, and the data points of 600xHBL separating. The loadings are also improved, with the increased total variance summarized by peaks known to relate to VitA, such as *m/z* 181. In A) * indicates the lowest concentration of VitA with a p-value < 0.05 compared to the control. In B), * indicates 95% confidence intervals.

5.3.3.2 MS settings optimization

To further improve VitA detection, experimental parameters were adjusted. These experiments were performed on samples of VitA doped into a 10% porcine plasma solution to account for interactions that may occur in biological solutions. As previously mentioned, when the original settings were tested, *m/z* 181 was visible above the control at 60xHBL, shown again in Figure 5-5 (A). After testing multiple internal temperature and voltage combinations for the MS, the optimized settings for VitA detection were found to be: capillary temperature: 250 °C, capillary voltage: 150 V, source voltage: 15 V and source voltage dynamic: 30 V. With these settings, the detection of *m/z* 181 was improved by an additional tenfold to 6xHBL, shown in Figure 5-5 (B). These settings modifications not only improved the detection limit of VitA, but also increased the overall signal intensity. The intensity of *m/z* 181 for the 60xHBL sample with the optimized settings is approximately 5x the signal intensity of the original settings (0.024 ± 0.004 vs 0.0050 ± 0.0009 normalized intensity).

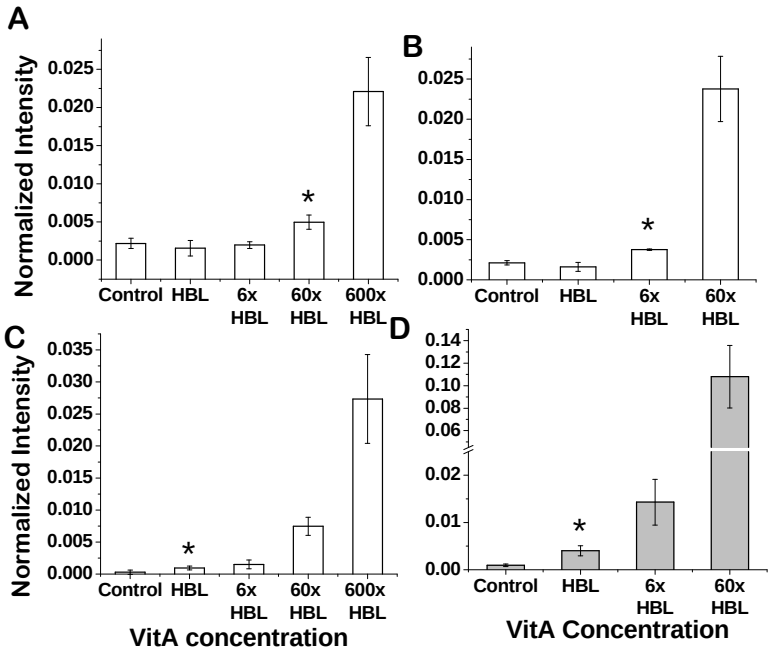

Figure 5-5 MS Settings and heat optimization of VitA detection via *m/z* 181. Samples were prepared in a 10% porcine plasma solution in buffer, and analyzed directly. (HBL = 650 μg/L, samples contained concentrations up to ~600xHBL=375,000 μg/L). A,C) contain up to 600xHBL VitA while B,D) contain up to 60xHBL (37,500 μg/L). A) Original MS settings, room temperature. The *m/z* 181 is detectable above the control at 60x HBL VitA. B) Optimized MS settings, room temperature. With these settings, *m/z* 181can be detected down to 6xHBL at room temperature, a 10-fold improvement over the original settings. C) Original MS settings, heated. Sample was heated to 110 °C. The heat improved detection to the HBL level, however, no difference can be seen between HBL and 6xHBL (3,750 μg/L) samples. D) Optimized MS settings, heated. Again, VitA is detectable to HBL. In this case, however, HBL and 6xHBL can also be separated. Note the intensity for the 60xHBL VitA is more than 10-fold higher than in C). * indicates the lowest concentration of VitA with a p-value < 0.05 compared to the control.

5.3.3.3 Heated sample

To further improve nutrient ionization, desorption and detection, a heated sample stage was constructed and set to 110 °C. This heated stage was used to analyze samples with both the original MS settings (Figure 5-5 (C)), as well as the optimized settings from Section 5.3.3.2 (Figure 5-5 (D)). In both cases, *m/z* 181 could be separated from the control starting at HBL. Additional concentrations of low blood level (LBL, 300 μg/L) and medium blood level (MBL, 475 μg/L) were also tested to span the entire healthy blood range, as shown in Figure 5-6. All blood level samples (LBL, MBL and HBL) could be separated from the control 10% porcine plasma samples containing no additional VitA. Furthermore, LBL and HBL could be differentiated from each other. While MBL could not be separated from other blood levels, the average lay between LBL and HBL.

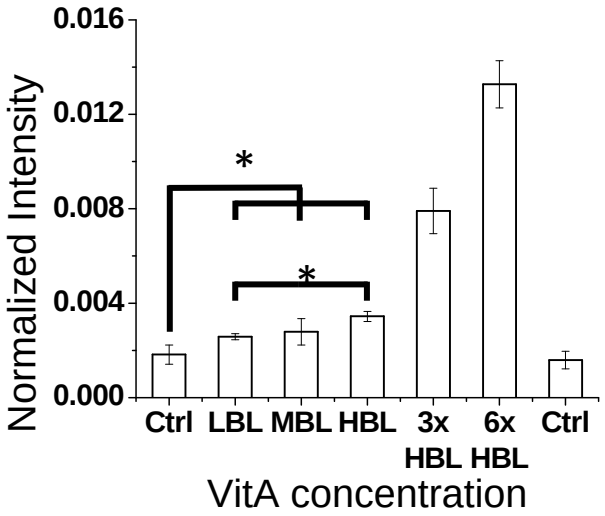

Figure 5-6 *m/z* 181 for extra concentrations of VitA.Extra concentrations of VitA were tested to determine whether or not differences between blood level concentrations could be observed. VitA concentrations tested were LBL= 300, MBL = 475, HBL = 650, 3xHBL=2250, 6xHBL=3750, all in µg/L. All samples, including blood level concentrations (LBL, MBL and HBL), were above the control samples collected at the start and end of the experiment. HBL was also greater than LBL, and while the average for MBL was between LBL and HBL, the difference was not significant, due to a larger standard deviation. * indicates a p-value < 0.05.

5.3.4 Comparison to ToF-SIMS and ESI-MS

A comparison of PPAMS to ToF-SIMS and ESI-MS was performed using 10% porcine plasma based samples, as shown in Figure 5-7. As previously mentioned, PPAMS could detect individual peaks for VitA at blood concentrations. For ToF-SIMS *m/z* 43.0172, the same peak which was previously observed to relate to VitA, could be detected at 6xHBL, while for ESI-MS, no detection was possible. In the ToF-SIMS and ESI-MS cases, no separation could be achieved with PCA.

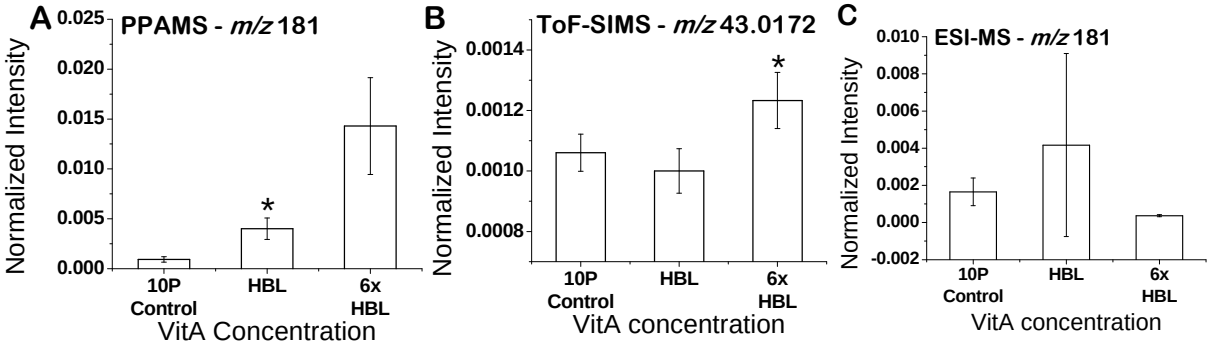

Figure 5-7 Comparison of PPAMS to ToF-SIMS and ESI-MS in 10% porcine plasma. A) PPAMS is able to detect *m/z 181* at HBL. B) ToF-SIMS is able to detect *m/z 43.0171* at 6xHBL. This peak was also previously observed for VitA in Figure 3-4. C) ESI-MS cannot detect *m/z* 181, or any other VitA-related peak at or below 6xHBL. Similar as the PPAMS results, *m/z* 181 was previously observed as the predominant peak relating to VitA for ESI-MS.

5.3.5 Vitamin A peak identification

At raised concentrations (≥60xHBL), several peaks related to VitA were found, the most prominent of which are shown in Figure 5-8. The identities of these peaks were determined by coupling the LTP to an Orbitrap mass spectrometer. Using the more precise masses detected by the Orbitrap, *m/z* 153, 165, 181 and 193 were identified as $C_{10}H_{16}O + H^+$, $C_{11}H_{16}O + H^+$, $C_{11}H_{16}O_2 + H^+$ and $C_{13}H_{20}O + H^+$, respectively, all to within 3 parts per million error. Proposed structures for these molecules can be found inset in Figure 5-8 (A, B, D), except for *m/z* 181 which will be discussed later, while the full structure of VitA can be found in Figure 5-9 (A).

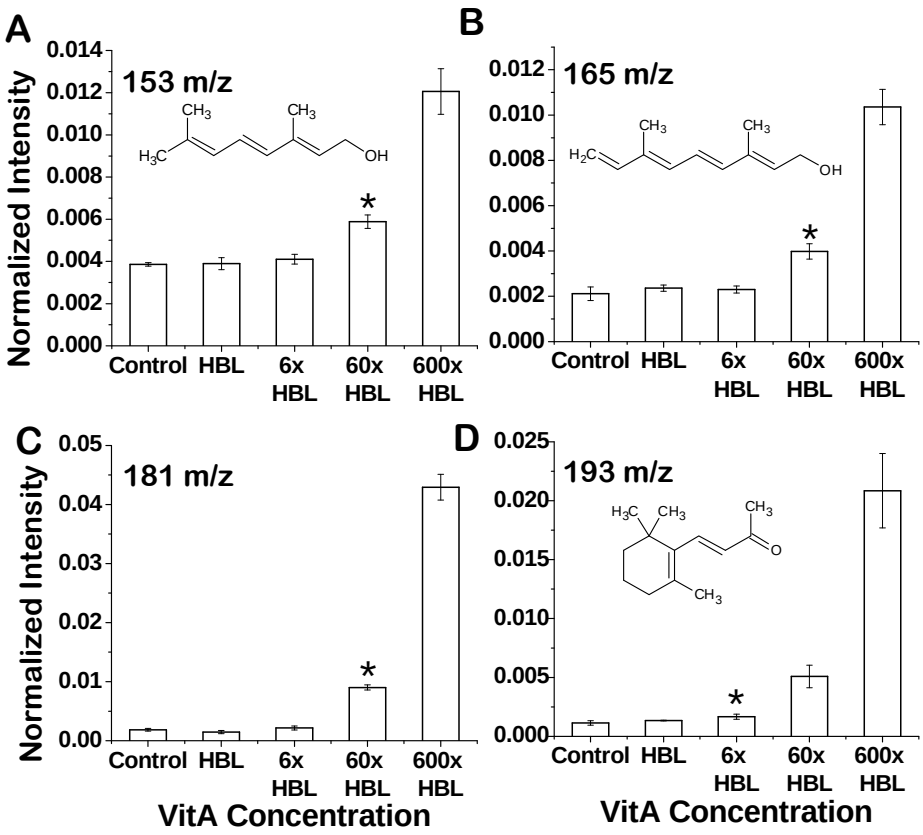

Figure 5-8 PPAMS peaks related to VitA. VitA was dissolved and diluted in MeOH to concentrations at or above healthy blood level (HBL = 650 μg/L, samples contained concentrations up to ~600xHBL=375,000 μg/L). Samples were then hydrated with 20 μL dH_2O prior to analysis. 4 peaks are shown which increase with increasing VitA concentration: A) *m/z* 153 m/z ($C_{10}H_{16}O + H^+$), B) 165 ($C_{11}H_{16}O + H^+$), C) 181 ($C_{11}H_{16}O_2 + H^+$), and D) 193 ($C_{13}H_{20}O + H^+$). Most peaks were visible starting at 60x HBL, with one peak, *m/z* 193, being visible as low as 6x HBL, compared to the 100% methanol control. The structure of *m/z* 181 was not determined until additional experiments were performed. The use of a blood-based solution (10% porcine plasma) in lieu of methanol normally resulted in sensitivity decreasing by at least 10-fold (data not shown). * indicates the lowest concentration of VitA with a p-value < 0.05 compared to the control.

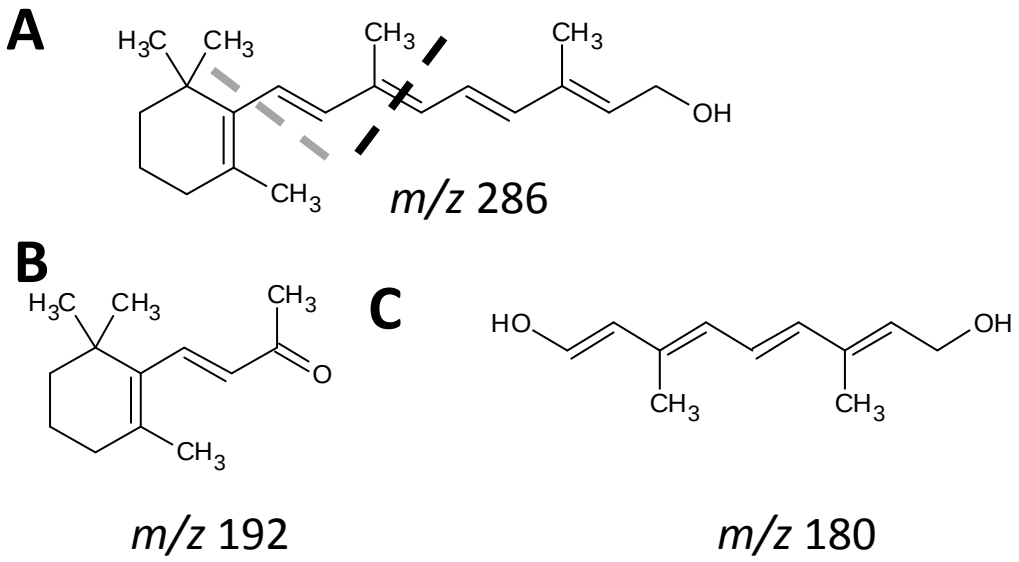

Figure 5-9 Proposed formation mechanisms for *m/z* 192 and 180. A) Full structure of VitA. B) Structure of *m/z* 192 (193 with the addition of an H^+). This molecule is formed through the ozonolysis of VitA, as indicated by the black dashed line, and results in the formation of an aldehyde. The other fragment of ozonolysis was also observed. C) Structure of *m/z* 180 (*m/z* 181 with the addition of an H^+). This structure may be formed through the cleavage of the ring structure from the hydrocarbon chain, and the addition of a hydroxyl group (shown by the gray dashed line). This fragment was originally thought to relate to *m/z* 192, however, other studies, shown in Figure 5-10 and Figure 5-11 indicate this illustrated structure is more likely.

An additional study on *m/z* 181 and 193 was performed by inserting a stream of nitrogen into the sample chamber during data collection. The results show that *m/z* 181 decreases by approximately 44% when the stream of nitrogen is added (Figure 5-10 (A)), and that *m/z* 193 decreases by approximately 75% with the addition of a nitrogen stream (Figure 5-10 (B)).

5.3.6 Aqueous solutions

5.3.6.1 Effect of aqueous solution on spectra and ionization

Two sets of samples were studied using ESI. The first set of samples was based in pure MeOH while the second was prepared in a MeOH/H_2O mixture. *m/z* 269 was clearly visible only in the samples prepared in pure MeOH, while samples with H_2O contained no visible peak. *m/z* 181, on the other hand, was only visible in solutions containing H_2O, shown in Figure 5-11 (A, B). For PPAMS, testing the effect of the aqueous solution was completed by analyzing dried samples, where VitA was dissolved in MeOH or a MeOH/H_2O mixture. The spectra indicate that in samples dissolved in MeOH only, the *m/z* 181 peak is not visible above the control, even at the 60xHBL level. On the other hand, in samples dissolved in a MeOH/H_2O mixture, *m/z* 181 was clearly visible above the control, both of which can be seen in Figure 5-11 (A).

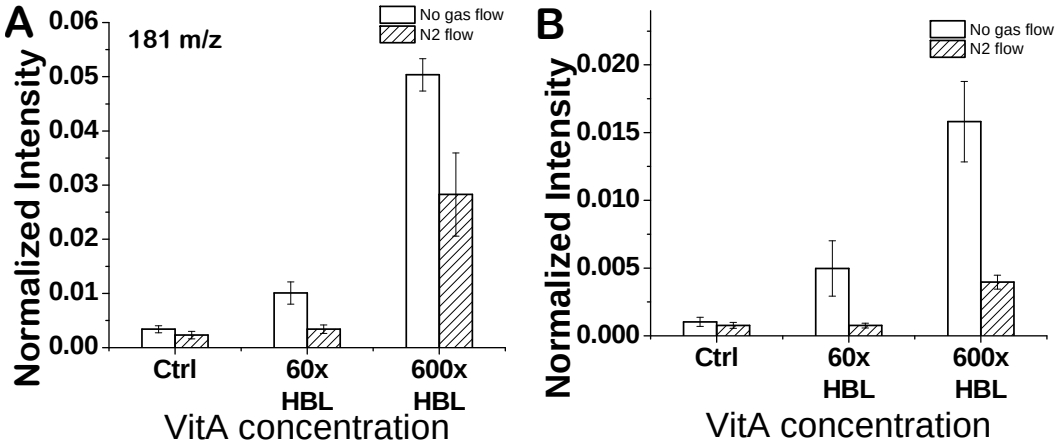

Figure 5-10 Effect of N_2 stream on peak intensities. VitA was dissolved and diluted in MeOH to concentrations of 60xHBL = 37,500 μg/L or 600xHBL=375,000 μg/L). Dry samples were placed in the sample chamber, and a stream of nitrogen was inserted, and allowed to evacuate the oxygen in the chamber for 60 seconds. The LTP was then initiated and the spectra collected. Two peaks were then studied more closely. A) *m/z* 181 decreases by approximately 44% when the stream of nitrogen is added, and B)*m/z* 193 decreases by approximately 75% with the addition of a nitrogen stream. The much greater decrease in signal of *m/z* 193 suggested that *m/z* 181 formation was not solely dependent on ozonolysis.

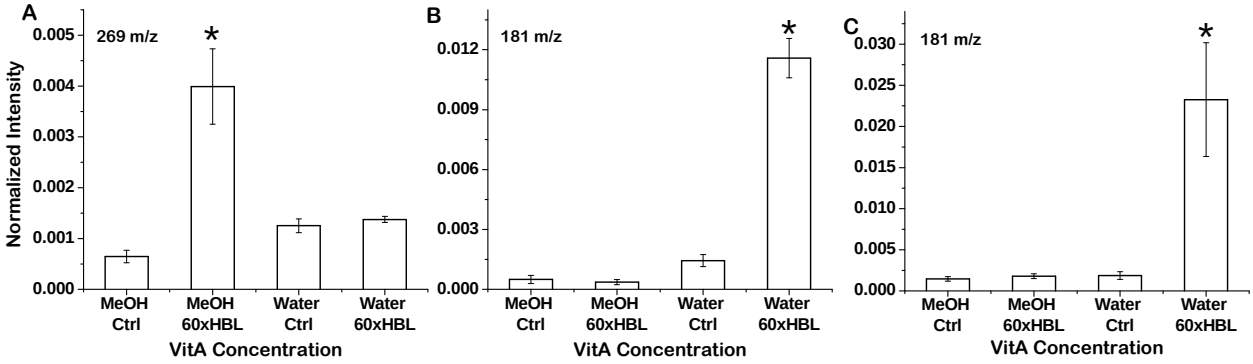

Figure 5-11 Effect of aqueous solution on VitA spectra. When analyzing VitA samples which were prepared or analyzed containing water, the resulting spectra were different than when prepared and analyzed without water. 4 samples types were compared - samples prepared in MeOH without (control) or with VitA added at 60xHBL (37,500 μg/L), and samples prepared in a 99%dH_2O/1%MeOH solution without (control) or with VitA. Samples were then analyzed using ESI-MS (A, B) or PPAMS (C). ESI-MS samples were run as liquid samples while PPAMS samples were spotted on filters, desiccated overnight, and analyzed dry. A) For ESI, when compared to the paired control sample, *m/z* 269 for the 60xHBL VitA in MeOH is greater than the MeOH control, while *m/z* 269 for the 60xHBL VitA in water is the same as the water control. B) For ESI-MS, when compared to the paired control sample, *m/z* 181 for the 60xHBL VitA in MeOH is equal to the MeOH control, while *m/z* 181 for the 60xHBL VitA in water is greater than the water control. C) PPAMS results corroborate the ESI-MS results for *m/z* 181, as the peak is only observed in the 60xHBL VitA in water sample. (60xHBL = 37500 μg/L).

5.3.6.2 Effect of sample drying

Initially, spectra were collected for 2 minutes, and the entire spectrum was used for analysis. After introducing the heated stage several peaks were observed to decrease in intensity over time. In particular, the water related peaks were shown to decrease, as shown for *m/z* 73 in Figure 5-12 (A). *m/z* 181 was also shown to decrease with time, as shown in Figure 5-12 (B).

Peak intensities are shown for 10 second intervals, starting from 0-10 s. By the 20-30 s time point, the signal drops to nearly half the original intensity. *m/z* 181 is no longer visible above the control at the 70-80 s time point. Additional experiments were also run to compare dry samples to re-wet samples, for 6xHBL VitA. Here, *m/z* 73 was much higher in samples which were re-wet, regardless of VitA content (as shown in Figure 5-12 C)). For *m/z* 181, intensity was raised only in the re-wet sample containing added VitA.

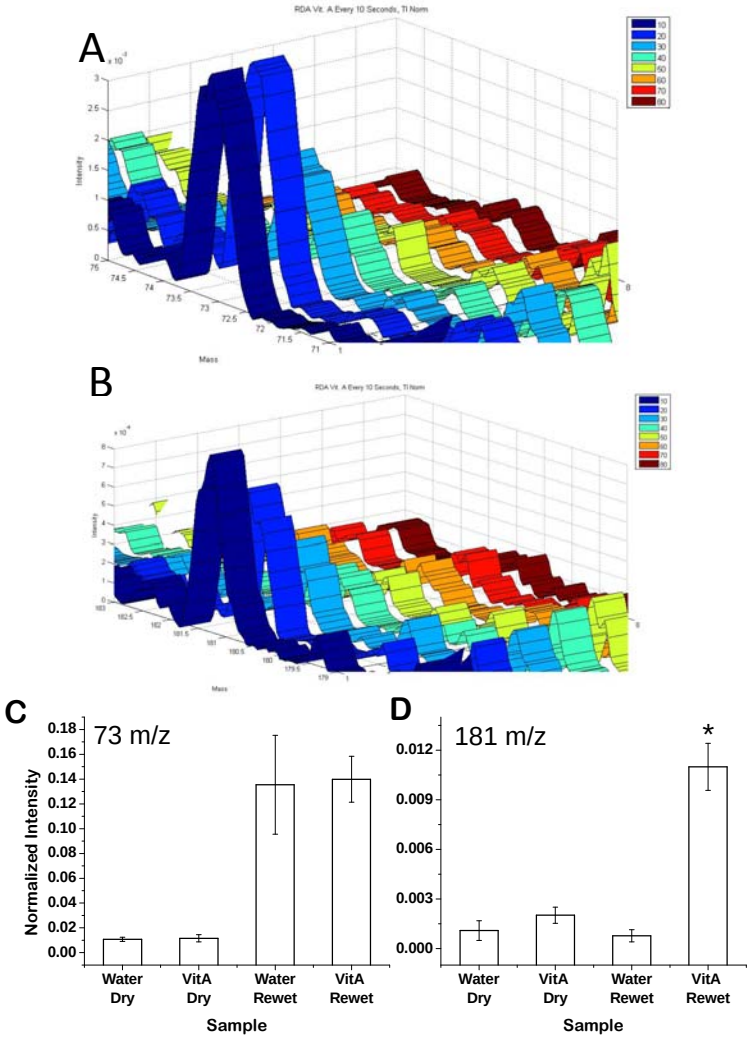

Figure 5-12 Effect of sample drying. A, B) Samples re-wet with 20 µL of water were placed on a heated sample stage and were analyzed immediately. Spectra were collected for 2 minutes to determine the change in spectra as the filter dried over time. Two peaks were then studied more closely in 10 second intervals, with 0-10s shown in dark blue. A) As expected, the water cluster peak, *m/z* 73 decreases with time as the sample dries, and reaches a steady state at approximately 60s. B) *m/z* 181 also decreases as the sample dries, reaching a relatively stable level at 50s. The ionization of *m/z* 181 is believed to be dependent on ionization from water clusters, and thus the intensity closely matches the water content in the sample. C, D) Dried samples were compared to samples re-wet with water, with and without 6xHBL VitA added. A) *m/z* 73 is raised in both re-wet samples. B) *m/z* 181 is raised only in re-wet samples containing VitA. A, B) were provided courtesy of M. Jeanette Stein. In D), * indicates a p-value < 0.05 compared to the paired control.

5.3.7 Additional analyses via PCA and PLS

5.3.7.1 PCA square root transformation

After optimizations, PCA was performed on additional concentrations of VitA, from the data set of Figure 5-6. Initial results show that separation between the control samples and concentrations up to 6xHBL could not be separated via PCA, as shown in Figure 5-13 A), even though *m/z* 181 is shown as highly influential in the corresponding loadings plot (Figure 5-13 (D)). Other *m/z* peaks 45, 77, and 209 appear strongly in the negative loadings. Additional PCs were also studied, however separation was still not achieved.

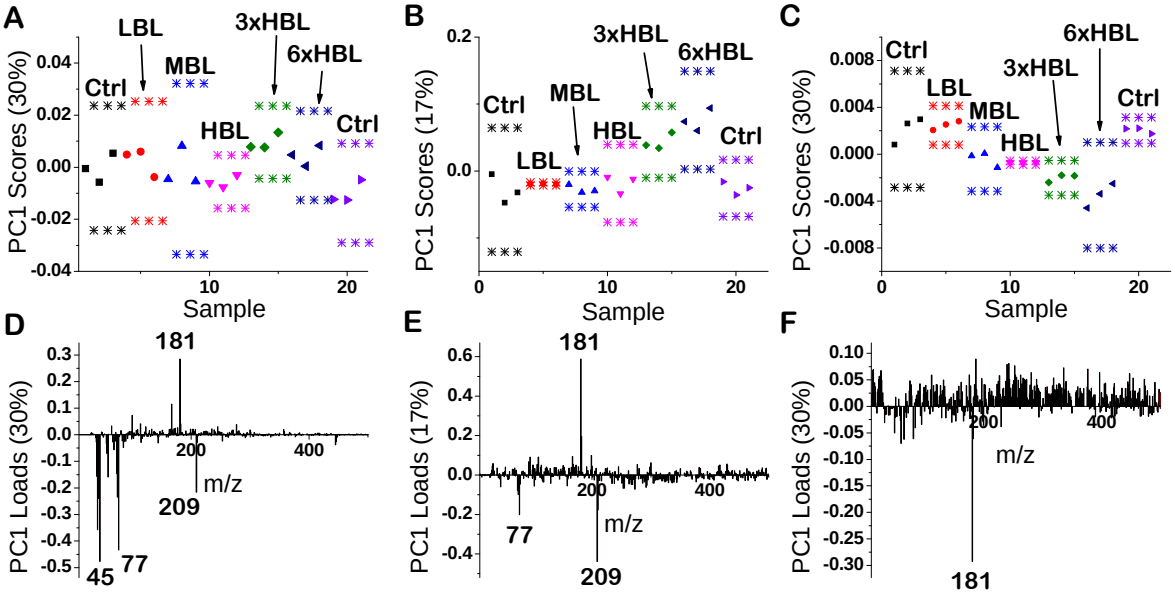

Figure 5-13 PCA on additional VitA concentrations. Upon detection of *m/z* 181 in the blood range, additional PCA was performed. Scores and loadings plots for 3 different analyses are shown: Scores plots for A) No transformation, B) square root transformation and C) discriminant PCA. Corresponding loadings plots shown in D-F), respectively. A, D) Upon initial analyses, when no transformation was performed, separation between samples containing different concentrations of VitA was not visible. Several peaks which did not seem to be related to VitA are shown to contain much of the variance. B, E) After a square root transformation, separation from the control samples is beginning to show at 3xHBL, though not to 95% confidence. Several peaks (in the *m/z* <50 range) are no longer present in the loadings plot, while *m/z* 181 has an increased influence. C, F) After DPCA was performed, the separation improved again, with a clear trend visible in the scores plot, even in the blood level range. In this case, *m/z* 181 is the only peak that has a loading value >0.1, due to a relatively small variance in the peak. This data corresponds to the spectra found in Figure 5-6. * Indicates 95% confidence intervals.

Further analysis using a square root transformation showed the 3x and 6xHBL concentrations starting to separate from the other samples, as shown in Figure 5-13 B), though not to 95% confidence. With the square root transformation, *m/z* 181 is an even more weighted positive loading, as shown in Figure 5-13 E). With this transformation, the number of prominent negative loadings were reduced to only include *m/z* 77 and 209. DPCA was then performed and

started to show separation at blood levels, in particular, the data points for MBL and HBL concentrations began to separate from controls, as shown in Figure 5-13 C), though again not to 95% confidence. In this analysis, *m/z* 181 is the sole peak with a loading >0.1, as shown in Figure 5-13 F). A cube root transformation was also performed but did not result in improved separation over the square root.

5.3.7.2 PLSr

Three sets of VitA varying from 9.7 µg/L (0.19 ng, ultralow blood level) up to 3757 µg/L (75.2 ng, 6x HBL concentration) were prepared in a 10% porcine plasma solution over three different days. One subset was assigned to be the calibration set and the remaining two were utilized as test sets. The results are shown in Figure 5-14, where most predicted concentrations are at or near to within error. The overall root mean squared error of prediction (RMSEP) was 2-3 ng when using PLSr at blood level concentrations.

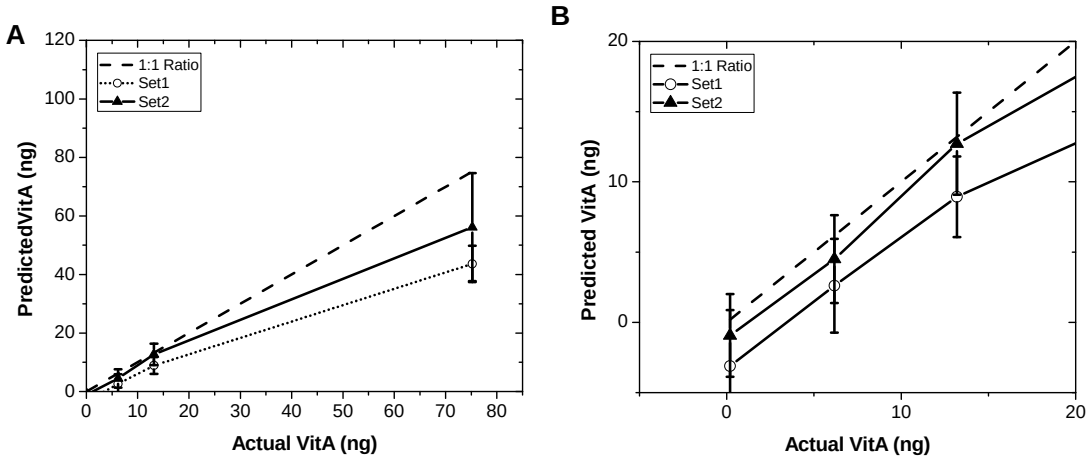

Figure 5-14 PLSr on VitA. A calibration set of samples was used to construct the model, which was then applied to two independent data sets. The model for VitA prediction was built using samples containing 0-75 ng of VitA (up to 6xHBL concentration, converted to mass). A) At greater than blood levels (75 ng), the predicted values (triangle and open circle) do not match the perfect prediction, shown by the 1:1 ratio dashed line. B) At lower concentrations, in the blood range, predicted concentrations match much more closely to the perfect prediction. Predictions were generally within error to the actual VitA present in the samples. The root-mean squared error of prediction was found to be 2-3 ng for the blood range values shown in B).

5.4 Discussion

5.4.1 Initial nutrient matrix

Originally, the results for analysis with the new MS from Advion was expected to produce similar, or better results, when compared to that of the Bruker Iontrap. The Bruker was often found heavily contaminated with samples from other users, and spectral analysis revealed

that although we cleaned the surface of the instrument, the spectra changed through time as collection progressed. Since the Advion was purchased new, the resulting spectra were anticipated to be cleaner, and thus, have improved separation with PCA. Improved analytical ability, however, was not observed, and in fact, data separation could no longer be achieved when the new instrument was used. Most of the variance in these initial spectra was contained in *m/z* 35, 56 and 166, however, upon closer inspection of the spectra, these peaks were intense (up to 10% of the total intensity of the spectra) and highly variable (standard deviation up to 30% of the peak intensity), and did not give information about nutrient status. To improve this technique, studies on individual nutrients were performed, which will be discussed throughout this chapter for VitA, and the next chapter for other nutrients.

5.4.2 Initial VitA detection

Upon failure of 10% porcine plasma samples to separate at blood levels via PCA with data from the Advion instrument, increased concentrations of VitA were studied in clean samples dissolved in MeOH, in addition to porcine plasma based samples. In contrast to earlier experiments in section 5.3.1, samples were run re-wet with water. This was found to increase *m/z* intensities for VitA-related peaks, and will be further discussed in section 5.4.6. Overall, while several peaks were visibly related to VitA, these were not visible until concentrations much higher than those found in blood, even in these cleaner samples prepared in MeOH rather than a porcine plasma solution. While peaks could not be visualized until 600xHBL, additional analyses was performed using PCA to see if separation could occur at lower concentrations even with this lack of visible peaks. Previous results from Aim 2 suggested that individual peaks may not be necessary for separation based on nutrient concentration, thus PCA was seen as a promising method. This analysis, however, resulted in similar detection ability as the individual peaks, with a very slight separation starting at 600xHBL and a larger separation at 6000xHBL. While the identified VitA-related peaks are separating towards the positive loadings (which aligns with 600 and 6000xHBL VitA separating towards the positive scores), the major contributors to the separation were seen to be *m/z* 55 and 73. These peaks were the largest in the spectra (up to 40% of the total spectra, when binned to unit mass), and were thought to be water clusters in the form of $(H_2O)_n+H^+$ where n=2-4 and not VitA. While high concentrations of VitA (at or above the 600xHBL levels) had some effect on peak intensity, this was inconsistent, as water content in the sample had a greater effect.

5.4.3 Vitamin A detection optimization

5.4.3.1 Peak removal

The removed *m/z* peaks were seen to be highly variable, and unrelated to nutrient content in data collected over multiple experiments and were thus removed from analysis. The most prominent peaks removed that had the greatest effect on analysis were related to water (*m/z* 37, 55, 73), the effect of which will be further discussed in section 5.4.6. Upon further refinement of the peak removal list after repeated experiments, several more peaks were removed, such as silicon based contaminates (*m/z* 350-355, 370-375 and 390-395). Overall, this improved the detection limit of VitA, and in particular *m/z* 181 by tenfold. The removal of these peaks had a significant effect on overall analysis largely due to the intensity of the peaks. Any shift in their expression had a great effect on the normalization of the spectra that might not have reflected on the actual nutrient content. This was confirmed by the more consistent intensities of the VitA-related peaks after contaminant removal.

5.4.3.2 MS settings optimization

Adjusting the internal MS settings affects the transport of ions to the detector and thus can change the relative peak intensities in the spectra. We hypothesized that by optimizing the detection in the *m/z* 100-200 range, the detection of VitA could be enhanced, as the majority of the observed VitA peaks lay within that range. Overall, the combination of removing high intensity, unrelated peaks with the settings optimization resulted in a 100x improvement in the detectability of *m/z* 181 over the control samples, down to 6xHBL.

5.4.3.3 Heated sample

Garcia-Reyes et. al. have previously shown that sample heating can improve limits-of-detection for this ionization method,[89] thus a heated sample stage was constructed and set to 110 ± 10 °C. Sample heating had significant effect on the detection of VitA, and is likely caused by an increased desorption of VitA molecules, as this technique is believed to rely on thermal desoprtion.[90] Comparing the original settings at room temperature vs. 110 °C, heat improved the detection of VitA by 100 fold, down to blood level. However, while the HBL VitA could be separated from the control sample, the HBL and 6xHBL samples completely overlapped. In order to build a quantitative model, separation must also be achieved between concentrations near blood levels, thus a combination of all optimizations was tested, which allowed for separation of data even within the blood range. This series of optimizations was capable of

significantly improving VitA detection. Thus, different nutrients may require optimization as well to achieve blood level detection.

5.4.4 Comparison to ToF-SIMS and ESI

In Chapter 3, initial comparisons of PPAMS to ToF-SIMS and ESI were completed. These comparisons, however, featured samples that differed from each other, with PPAMS samples being based in porcine plasma, Tof-SIMS in BSA solution and ESI in MeOH. Specific sample types were utilized which were expected to be amenable for each analysis method. Here, a more direct comparison of samples was completed with the same sample solvent, 10% porcine plasma. As expected, ToF-SIMS and ESI-MS were greatly affected by the high salt content of the samples. In both cases, VitA detection is worse than in earlier experiments using cleaner sample matrices. In comparison, PPAMS was capable of detecting VitA at LBL, an order of magnitude more sensitive than Tof-SIMS for the same sample. This result shows that for these minimally prepared samples, PPAMS can perform better than other highly sensitive systems, at a fraction of the cost.

5.4.5 Vitamin A peak identification

After identifying the chemical formulae for the nutrient related peaks, the VitA molecule was studied to determine their likely structures. *m/z* 153 and 165 likely originate from the hydrocarbon chain region of the VitA molecule (Figure 5-8 A-B), respectively). *m/z* 193 was identified to originate from the ozonolysis of one of the carbon double bonds to form an aldehyde, as shown in Figure 5-9 B). The other product from this ozonolysis reaction ($C_7H_{10}O_2$) was also observed, though with a much smaller intensity (data not shown). This fragmentation/ionization pathway was previously observed using this ionization method on a study of fatty acids.[91]

Originally, *m/z* 181 was thought to relate to the *m/z* 193 peak, however, upon further studies, this was found to likely not be the case. To test the ozonolysis, a stream of nitrogen was inserted into the sample chamber to remove as much oxygen as possible. By reducing the free oxygen, the formation of ozone would be attenuated, and thus, the effect of ozonolysis would be minimized. The results showed a very large drop in the signal intensity of *m/z* 193, consistent with a reduction in ozonolysis, while the decrease in *m/z* 181 was much smaller. This decrease in *m/z* 181 was likely caused by other factors, such as the increased gas flow within the chamber which may reduce the number of ions entering the MS. An alternate formation mechanism of *m/z*

181 was proposed, as shown Figure 5-9 (C), and was further verified in proceeding experiments, shown in section 5.3.6.1 and discussed in section 5.4.6.1. This fragment was likely formed through the cleavage of the ring structure and the addition of a hydroxyl group to the hydrocarbon chain.

5.4.6 Aqueous solutions with VitA

5.4.6.1 Effect of water on spectra

PPAMS is known to be a relatively gentle technique that causes limited fragmentation,[88] thus, the extensive fragmentation of VitA was surprising. Upon closer study, we found that when no water was used during sample preparation, the spectra would display very different peaks. To determine the effect of aqueous solution on the spectra, solutions containing MeOH only, or an MeOH/H_2O mixture were used. In ESI experiments, when dissolved in a MeOH only solution, the peak at *m/z* 269 is the most prominent peak above the control. In other literature, this is the expected peak for VitA and corresponds to [M-H_2O+H^+].[92,93] *m/z* 269, however, was not visible in the ESI experiment where an H_2O solution was used. In this case, *m/z* 181 was the most prominent peak, much like that observed in earlier PPAMS experiments. This proves that *m/z* 181 was not related to ozonolysis, as ozonolysis does not occur with ESI. Furthermore, due to the known gentle nature of ESI, *m/z* 181 likely forms through hydrolysis of the chain from the ring, caused by the H_2O solution prior to analysis and ionization.

In the PPAMS experiments, MeOH samples could not be run with the MeOH freshly spotted due to the volatility of MeOH which causes signal saturation from MeOH related peaks. To keep the experiment consistent, and to isolate the effect of H_2O on VitA fragmentation, the samples were run dry. As expected from the ESI experiment, *m/z* 181 was only visible over the control when VitA was dissolved in an H_2O solution. This effect can also be observed in other aqueous solutions, such as the porcine plasma solutions in Figure 5-5. Overall, while water had a very significant effect when used as part of the solvent, this effect was exacerbated when the samples were run wet, the reason for which is explained in section 5.4.6.2. This can be observed by comparing the signal intensity for *m/z* 181 when analyzed dry (Figure 5-11 C)) vs when wet (Figure 5-5 D)), where the signal is nearly 5x higher. The effect of the aqueous solution is beneficial for the samples of interest in this project, due to the high water content in biological solutions.

5.4.6.2 Effect of sample drying and ionization mechanism

The decreasing *m/z* 73 peak over time was caused by the evaporation of water. This effect was not as prevalent in the samples run without heating, as the samples remained wet through the entire analysis (though some evaporation occurred from the gas flow). The decrease in *m/z* 181, however, was unexplained (Figure 5-12 B)), though consistent with previous results as the intensity of *m/z* 181 was decreased in dry samples compared to rewet samples, as mentioned in section 5.4.6.1. The decrease in *m/z* 181 aligned with the evaporation of water, indicating that water or water ions may have played a key role in sample ionization. Other studies have found that for LTP and other atmospheric ionization methods using helium, the main mode of ionization occurs through a multi-step process where the high-energy, metastable helium in the plasma ionize water clusters which then ionize the molecules of interest, shown in *Equation 5-1*.[76,94] This is further corroborated by Figure 5-12 C, D), where VitA ionization is improved in the presence of water. While *m/z* 73 is also a common silicon contamination peak, the absence of related peaks at *m/z* 147 and 207,[95] indicate that *m/z* 73 is more likely water-based. Furthermore, other studies have also noted the presence of water peaks for $(H_2O)_n+H^+$ for n=2-4.[96]

Equation 5-1 [76]

1. $He^m + H_2O \rightarrow He + H_2O^+ + e^-$
2. $H_2O^+ + H_2O \rightarrow H_3O^+ + OH$
3. $H_3O^+ + (n-1)H_2O \rightarrow (H_2O)_nH^+$
4. $(H_2O)_nH^+ + M \rightarrow n\,H_2O + MH^+$

Where He^m is He at a high energy, metastable level.

5.4.7 Additional analyses via PCA and PLSr

5.4.7.1 PCA square root transformation

Although *m/z* 181 was detectable at blood levels, PCA was unable to detect consistent differences between samples, even up to the 6xHBL level. Additional analyses were performed using the square root transformation, which improved overall separation. This improvement stems from the increased influence of the known VitA peak, *m/z* 181 on PC1. As expected, *m/z* 181 corresponds to the same direction as the VitA scores separation – both towards the positive side. While *m/z* 77 and 209 were also prominent as negative loadings, these did not appear consistently in other VitA studies and were thus not likely caused by VitA.

Due to the nature of a quadrupole MS as an ion-current measurement system, the variance in the signal intensity is expected to be dependent on Poisson statistics,[97] and thus, the square root transformation is expected to improve analysis. While the overall separation was improved, upon closer analysis, the variance in peak intensities was found not to be Poisson limited. The standard deviation was expected to increase with the square root of the peak intensity, but this was not observed. This can be clearly visualized in Figure 5-6 where the standard deviations for the control and MBL samples are greater than that of the HBL sample. This is likely due to the presence of other sources of error, such as inconsistencies in data collection start time (i.e. the sample may dry a different amount from sample to sample), sample spotting, gas flow rate to the plasma or plasma production from the HV source, which may cause more noise than the optics within the MS.

DPCA was also performed, and provided the best separation. Here, *m/z* 181 was the only peak that separates from the background for the loadings plot. Interestingly, while these results indicate a similar trend as analyzing the individual *m/z* 181 peak, the separation with DPCA is not as clear. In the spectra, the LBL concentration can be separated from the control, while in DPCA scores plot, the data points for the LBL completely overlap with both controls. In fact, the separation for each of the VitA concentrations is slightly less clear in the scores plot, compared to *m/z* 181 alone. This is due to the other peaks in the spectra which also slightly influence the data separation, as shown in the corresponding loadings plot (Figure 5-13 F)).

5.4.7.2 PLSr

PLSr on VitA data was successful. While the predicted 6xHBL VitA deviate further from the actual VitA added, concentrations at and below the blood range matched well. The higher concentration, however, was still required to construct the model. This is likely due to the increased weight placed on the VitA-related peaks, such as *m/z* 181, by the model when the higher concentrations are included. This is similar to the effect observed in Figure 5-13, where improved separation of the data coincided with an increased importance of *m/z* 181 in the loadings. Overall, with the experimental optimizations completed, quantitation of unknown samples was achieved.

5.5 Conclusions

VitA can be detected and quantified at blood level concentrations. Initially, detection of VitA could only occur starting at 600x the blood level concentration. To improve these results, a

series of optimizations were completed. Specifically, the first improvement was the elimination of high intensity peaks not related to VitA, the second was the optimization of internal settings for the compact MS, and the third was the addition of a heated sample stage. Each of these modifications resulted in a 10-fold or greater improvement in detection, and when combined, allowed for the detection of VitA at blood level, and could even differentiate between samples at LBL and HBL. Detection was found to be heavily dependent on aqueous solutions – both for fragmentation/formation of *m/z* 181 and for the desorption/ionization as well. For quantitation, PCA could be improved to begin showing classification trends for VitA based on concentration, starting at MBL. These trends, however, were not to 95% confidence. Further quantitative work was completed by building a PLSr model, which gave excellent predictive ability for VitA concentration in the blood range, with 2-3 ng error (<120 μg/L).

6 Specific Aim 3b: To utilize the compact mass spectrometer and improve detection of Iron, Zinc, Folic Acid and Thyroxine

6.1 Background

The PPAMS system, coupled to a compact mass spectrometer, has been shown to be capable of detecting micronutrients in porcine plasma. In particular, previous work showed that a PLSr model could be constructed for VitA to predict concentration at blood levels in independent samples. Other nutrients, however, may also need to be optimized to achieve detection. In this continuation of Aim 3, the remaining nutrients, Fe, Zn, FolA and Thyr will be tested. Overall, the goal of this system is to be capable of measuring multiple nutrients, thus, initial studies on multi-nutrient solutions will also be performed.

6.2 Materials and Methods

6.2.1 Chemicals and Reagents.

See Chapters 4 and 5 for a description of the common reagents.

6.2.2 Plasma Pencil Atmospheric Mass Spectrometry (PPAMS).

See Chapter 5 for a full description of the instrument set up. 20 µL of sample solution was spotted onto filters for analysis. Sample solutions diluted in MeOH were dried overnight in a desiccator prior to analysis, due to the interference of MeOH in the mass spectra. Other samples, prepared in water or porcine plasma solution, could normally be analyzed directly after application to the filter paper. All solutions were spotted at a volume of 20 µL unless otherwise noted.

6.2.2.1 Iron

Iron (II) chloride was dissolved in either water, 10% or 100% porcine plasma. All concentrations tested can be found in Table 6-1. Concentrations were based on levels expected to be found in human blood, however, studies completed in 10% and 100% porcine plasma had offset concentrations, which will be discussed in section 6.4.1.3. Fe concentrations in 10% porcine plasma studies correspond to water concentrations +135 µg/L while 100P concentrations correspond to water concentrations +1350 µg/L, as shown in Table 6-1. Initial samples (in section 6.3.1.1) were spotted on quartz filters (QM-A, GE Lifesciences), however, all later experiments were performed on paper filters.

Table 6-1: Fe concentrations tested.

Solvent	Label	Concentration
Water	Control	0 µg/L
	HBL Fe	1,550 µg/L
	5xHBL Fe	7,500 µg/L
	50x HBL Fe	75,000 µg/L
	500x HBL Fe	750,000 µg/L
	5000x HBL Fe	7,500,000 µg/L
10% Porcine Plasma	10P Control	135 µg/L
	10P HBL Fe	1,685 µg/L
	10P 5xHBL Fe	7,635 µg/L
	10P 50xHBL Fe	75,135 µg/L
	10P 500x HBL Fe	750,135 µg/L
100% Porcine Plasma	100P Control	1,350 µg/L
	100P HBL Fe	3,035 µg/L
	100P 5xHBL Fe	76,350 µg/L
	100P 50x HBL Fe	751,350 µg/L

6.2.2.2 Zinc

Zinc (Zn) was dissolved in 10%, 20% or 100% plasma at concentrations ranging from 0.2xMBL up to 4000xHBL, as described in Table 6-2. For analysis, some data points were combined by averaging. For these experiments, 12 replicates were collected for each concentration level. Using the random number generator in Microsoft Excel, values were assigned randomly to each of the 12 samples within the same concentration and rearranged in ascending order. Keeping this order, each group of 4 samples were then averaged together to give 3 independent data points from the original 12 samples.

6.2.2.3 Folic Acid

Folic acid (FolA) was dissolved in water, 10% or 100% porcine plasma, at concentrations listed in Table 6-3. In most cases, samples were run directly after spotting solutions on filter papers. For the acid re-wetting experiments, samples were dried, then rewet with water containing 1% acetic acid (Fisher) or 0.1M hycrochloric acid (Fisher) just prior to analysis. For sinapic acid experiments, sinapic acid was dissolved in a 50:50 acetonitrile:dH_2O mixture and

pre-spotted on filter paper. The filter paper was allowed to dry overnight, after which the FolA solution was spotted just prior to analysis. Silver samples were initially spotted with 1 M silver nitrate and allowed to dry, then covered with 1 M glucose dissolved in water adjusted to pH 10 using ammonium hydroxide and allowed to dry again. Following reduction from silver nitrate to silver, FolA solution was spotted prior to analysis.

Several FolA analogues present in the blood were also tested. 5-methyl tetrahydrofolic acid, tetrahydrofolic acid, dihydrofolic acid, dihydrofolic acid dihydrate and folinic acid salt were all purchased from Santa Cruz Biotech (Dallas, TX), and were prepared at the same concentrations as FolA in 10% porcine plasma. An alternative indicator of FolA levels, homocysteine (Hcyst), was also tested. These concentrations are also listed in Table 6-3. For the UV experiments, samples were spotted with FolA and desiccated overnight. Samples were then irradiated for 1 hour at a distance of 25 cm using a 450 W Hg lamp (PC 451050, Hanovia Specialty Lighting, Fairfield, NJ). After exposure, samples were re-wet with water just prior to analysis.

6.2.2.4 Thyroxine

As previously mentioned, Thyr was dissolved in 4M NH_4OH in MeOH and then further diluted. Initial studies were performed only in NH_4OH solution. Later studies were diluted in 10% porcine plasma, with the NH_4OH concentration held constant. After spotting, samples were dried and were re-wet with either water or acetic acid (CH_3COOH) prior to analysis. Additional studies were performed on Thyr mixed directly in 10% porcine plasma as a suspension. Solutions were agitated using a vortex prior to sample spotting. Finally, for the increased power experiment, the LTP input power was increased to 15.9 V (with a current of 0.58 A). To collect data with this setting, the sample and LTP glass tube were moved an additional 3 mm away from the MS inlet. All tested concentrations can be found in Table 6-4.

6.2.2.5 Data analysis

Data analysis was performed using various techniques, such as PCA and PLSr. A description of the techniques utilized in this section can be found in Chapters 3 through 5.

Table 6-2 Zn concentrations tested

Label	Concentration
Control – 10% Porcine Plasma	0 µg/L
Control – 20% Porcine Plasma	158 µg/L
Control – 100% Porcine Plasma	1580 µg/L
0.2xMBL	180 µg/L
0.2xHBL	240 µg/L
0.5xMBL	450 µg/L
LBL	600 µg/L
MBL	900 µg/L
HBL	1,200 µg/L
40xHBL	45,800 µg/L
400xHBL	458,000 µg/L
4000xHBL	4,580,000 µg/L

Table 6-3 FolA related concentrations tested

Analyte	Label	Concentration
Folic Acid	Control – 10% Porcine Plasma	0.4 µg/L
	Control – 100% Porcine Plasma	4.1 µg/L
	LBL	5 µg/L
	MBL	27.5 µg/L
	HBL	50 µg/L
	35xHBL	1,700 µg/L
	350xHBL	17,000 µg/L
	3500xHBL	170,000 µg/L
	35000xHBL	1,700,000 µg/L
Homocysteine	Control	Unknown (not tested)
	LBL	620 µg/L
	HBL	2,020 µg/L
	10xHBL	20,200 µg/L
	100xHBL	202,000 µg/L
	10000xHBL	20,200,000 µg/L

Table 6-4 Thyr concentrations tested

Label	Concentration
NH_4OH Control	0 µg/L
10P Control	6.5 µg/L
LBL Thyr	49 µg/L
MBL Thyr	78 µg/L
HBL Thyr	108 µg/L
6xHBL Thyr	625 µg/L
60xHBL Thyr	6,250 µg/L
600xHBL Thyr	62,500 µg/L
3,000xHBL or 3E3xHBL Thyr	367,000 µg/L
6,000xHBL or 6E3xHBL Thyr	625,000 µg/L
30,000xHBL or 3E4xHBL Thyr	3,670,000 µg/L
60,000xHBL or 6E4xHBL Thyr	6,250,000 µg/L

6.3 Results

6.3.1 Iron

6.3.1.1 Water vs. porcine plasma testing

Initial experiments were performed on iron (II) chloride dissolved in H_2O or 10% porcine plasma. Iron in H_2O did not display any trends in PCA, nor any individual peaks that varied with Fe concentration, even at the 5000xHBL (7.5×10^6 µg/L). When iron was dissolved directly in 10% porcine plasma, *m/z* 70 was seen to trend with concentration of Fe, starting at 50xHBL. This can be seen in Figure 6-1, labeled as 10P 50xHBL (50xHBL concentration of Fe in 10% porcine plasma).

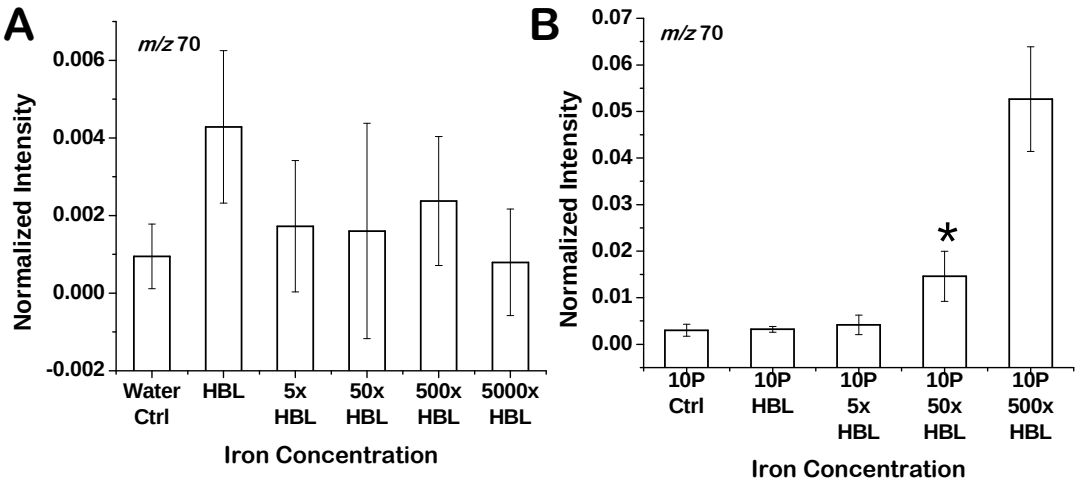

Figure 6-1 Iron in water or 10% porcine plasma. Iron was dissolved at concentrations listed in Table 6-1, and spotted on to quartz filter paper. A) Water was used to dissolve Fe and was analyzed using PPAMS. *m/z* 70 showed no trend based on the concentration of Fe, even at 5000xHBL. No other peaks showed any trend, either. B) 10% porcine plasma was used to dissolve Fe and was analyzed using PPAMS. *m/z* 70 was shown to be related to Fe concentration, and increases starting at 50xHBL. * indicates the lowest concentration where $p < 0.05$ compared to the control.

6.3.1.2 Instrument settings optimization

A series of 50 MS settings were tested to improve nutrient detection. For many settings, no difference was visible for *m/z* 70 between the control and the sample containing Fe at 10P 50xHBL. The results from a subset of 4 tested settings are shown in Figure 6-2. In each case, the average of the Fe containing sample is higher than the control, however, the difference is significant only in the second and third settings. Overall, the third setting was selected for future experiments, which corresponded to instrument values of: capillary temperature: 150 °C, capillary voltage: 100 V, source voltage: 20 V and source voltage dynamic: 20 V. After MS settings optimization, the position of the LTP was also optimized, leading to an increased intensity of *m/z* 70 at the 50xHBL concentration, as shown in Figure 6-3 A).

6.3.1.3 10 vs. 100% porcine plasma

100% porcine plasma was also tested and compared to the results from a 10% porcine plasma solution, as shown in Figure 6-3. As before, in the 10% porcine plasma solution, *m/z* 70 is detectable at the 50xHBL concentration. This detection limit was improved to 5xHBL when 100% porcine plasma was used. Overall, the signal intensity for *m/z* 70 increased nearly 10-fold in 100% porcine plasma, for the 5xHBL and 50xHBL concentration. A 4-fold increased expression of *m/z* 70 was also observed when comparing controls, which may be due to the higher concentration of Fe in 100% porcine plasma, compared to 10%.

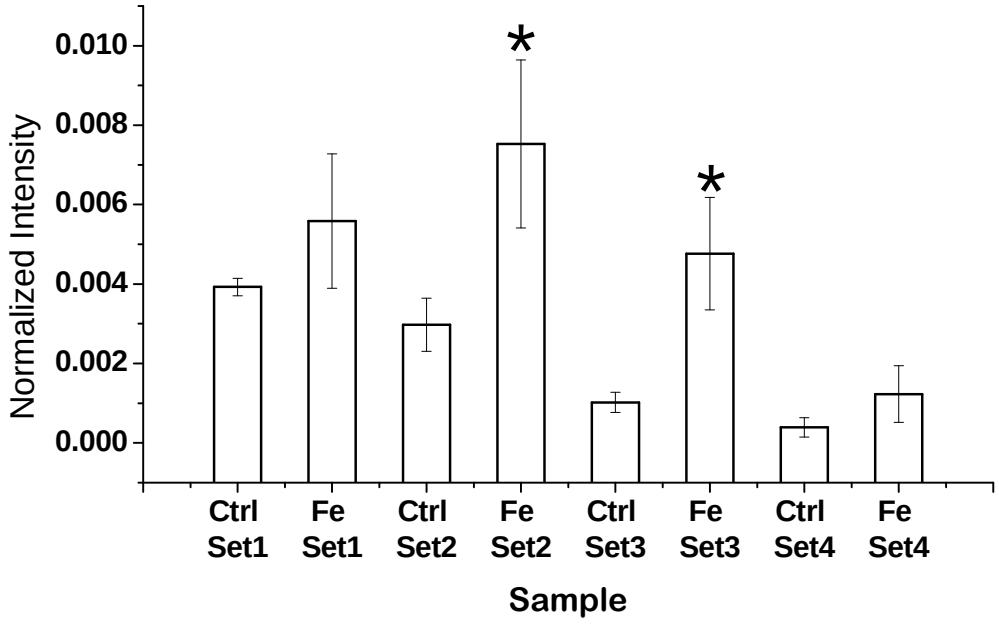

Figure 6-2 Iron settings optimization. A set of 50 system settings were tested to improve Fe detection, 4 of which are displayed here. 10P 50xHBL Fe was dissolved in 10% porcine plasma and was compared to controls containing no additional Fe for *m/z* 70. Different settings are indicated by Set'X' where X=1-4. In this subset of settings, Set1 and Set4 could not differentiate between the control and the sample containing Fe. In Set2 and Set3, the Fe containing samples had greater intensity than the controls. Overall, Set3 was selected as the optimized setting, using the method described in section 6.4.1.2. * indicates $p < 0.05$ compared to the control, for the specific setting.

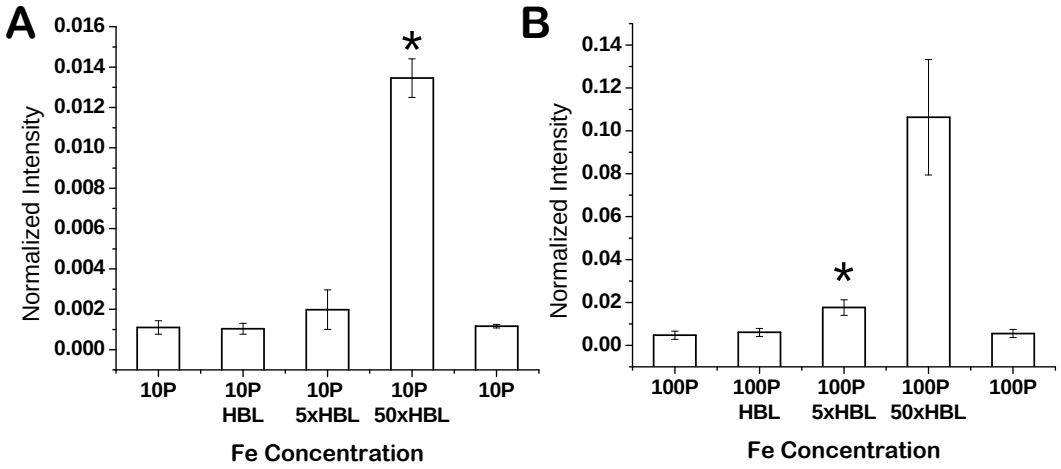

Figure 6-3 Fe detection for 10% vs 100% porcine plasma. A) Fe dissolved in 10% plasma. In this solvent, Fe is visible above the control for *m/z* 70 at 10P 50xHBL. B) Fe dissolved in 100% plasma. In this solvent, Fe is visible above the control for *m/z* 70 at 100P 5xHBL. Along with a ~10x improvement in the detection limit, *m/z* 70 is also ~10x more intense for the 100P solution. Upon analysis with an Orbitrap MS, *m/z* 70 was identified as C_4H_7N. * indicates the lowest concentration where $p < 0.05$ compared to the control.

6.3.1.4 Peak identification

To determine the identity of *m/z* 70, an Orbitrap MS was used. The exact mass was determined to be *m/z* 70.0653 and was identified as C_4H_7N, to 1.9 ppm error. Peaks related to atomic iron, i.e. Fe^+, FeH^+, etc., were not observed.

6.3.1.5 PCA and PLSr

PCA was performed on the square-root transformed Fe data, and was found to separate the data points of the 100P 5xHBL and 100P 50xHBL samples from the control samples, as shown in Figure 6-4. Neither, however separated to 95% confidence from the control, with the 100P 50xHBL concentration confidence intervals overlapping slightly. For the loadings, *m/z* 70 is by far the most dominant loading in PC1.

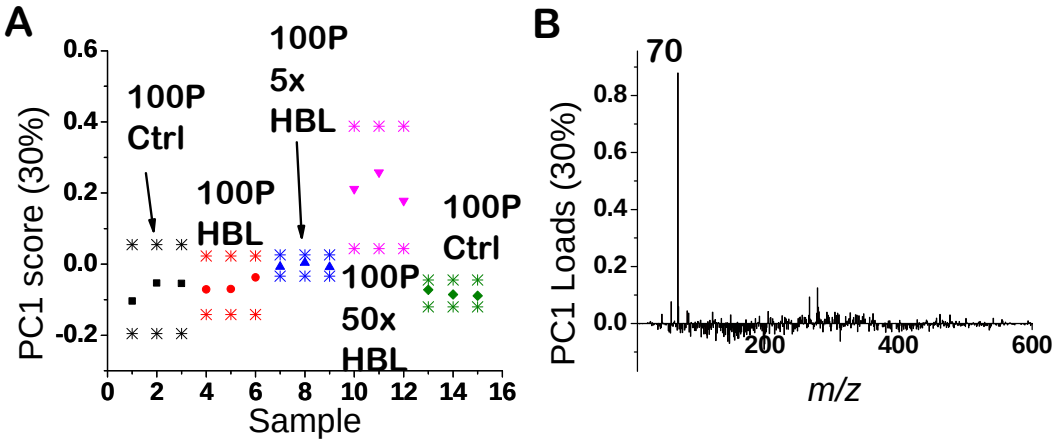

Figure 6-4 PCA on Iron spectra. Scores and loadings plots for iron analysis with PPAMS. A) At 100P 50xHBL, the data points separate from the other concentrations very well, however, a slight overlap of the 95% confidence intervals. 100P 5xHBL data points also separate from the samples containing lower concentrations of Fe, however, the data points are completely encompassed by the confidence intervals of the lower concentrations. B) *m/z* 70 was found to be the most heavily weighted source of variance. All samples prepared in 100% porcine plasma. Concentrations can be found under the 100% plasma labels of Table 6-1. * indicates 95% confidence intervals.

PLSr was also performed on Fe data, and was unable to quantitate an independent set of Fe data. Predictions were inaccurate, and resulted in a wide discrepancy between the predicted value and the actual Fe content. As in the VitA prediction plot shown before, predictions should lie on or near the 1:1 ratio line, however, this was not observed, as shown in Figure 6-5. RMSEP for Fe prediction was approximately 2300 µg/L.

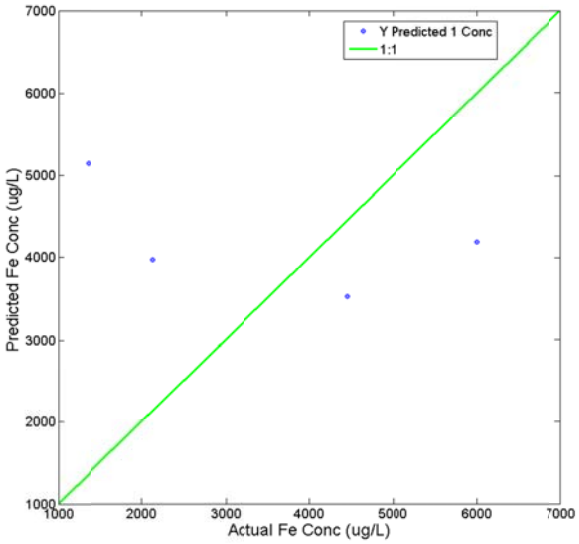

Figure 6-5 Iron prediction via PLSr. The PLSr model for Fe was unable to predict Fe content for an independent group of samples. Although Fe was detectable at levels between 100P 2-5xHBL Fe above controls in the raw spectra, this did not translate in to prediction ability. The 1:1 ratio line (green) indicates the ideal model where the prediction perfectly overlaps the actual concentration. Overall RMSEP was approximately 2300 µg/L.

6.3.2 Zinc

6.3.2.1 100%, 10% and 20% porcine plasma

Using the settings optimized for Fe detection, initially, Zn was tested in 100% porcine plasma. Several peaks were identified as potentially indicating trends in concentration. For example, *m/z* 57 and 69 seemed to increase in intensity with concentration, and drop when control samples were tested, as shown in

Figure 6-6 A, B). These differences, however, were not significant when compared to controls taken at the end of the experiment, even at 4000xHBL. Repeated experiments did not give improved results. When Zn was instead dissolved in 10% plasma, the results improved, as peaks at *m/z* 69 and 89, and to a lesser extent 115 and 145 showed a trend with concentration. *m/z* 69 and 89 were both significantly above the controls at blood level, and seemed to increase with increasing concentration. Differences between LBL, MBL and HBL, however, were not significant as shown in

Figure 6-6 C, D). Additional analysis was performed on Zn in 20% porcine plasma, and resulted in detection of Zn above the control down to 0.2xMBL. For concentrations tested

between 0.2xMBL and HBL, the Zn-related peaks increase, on average, with concentration (though some increases were not significant), which is shown in Figure 6-7 A, B).

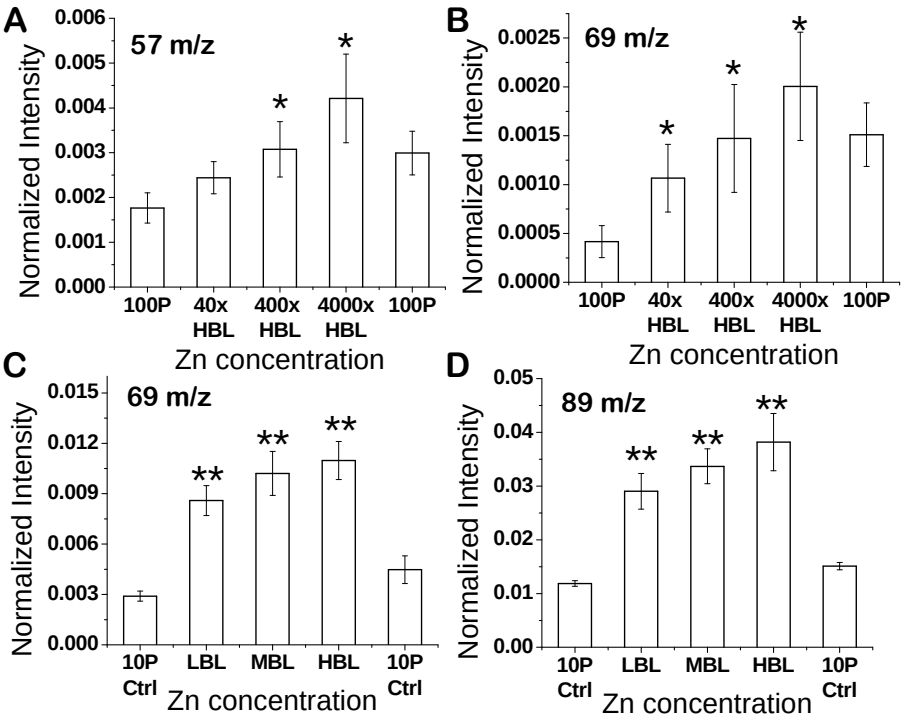

Figure 6-6 Zn in 100% or 10% porcine plasma. A, B) In 100% porcine plasma, *m/z* 57 and 69 show a slight trend with concentration, starting as low as 40xHBL. However, the control analyzed at the end of the experiment also had increased expression. C, D) In 10% porcine plasma, *m/z* 69 and 89 show a slight trend in concentration. In this case, samples with Zn have greater expression than both analyzed controls, even in the blood concentration region. Overall, detection was much improved in 10% porcine plasma. * Indicates p-value <0.05 compared to the first control, but not the second control. ** Indicates p-value <0.05 compared to the first and second controls.

6.3.2.2 Peak identification

As with Fe, Zn samples were tested using the Orbitrap to determine peak identifications. The exact masses relating to Zn were determined as *m/z* 69.071 and 89.0601, which were identified as C_5H_8 and $C_4H_8O_2$ to within 5 ppm error. *m/z* 115.0762 and 145.1235 were also observed as Zn related peaks, and were identified as $C_6H_{10}O_2$ and $C_8H_{16}O_2$, to within 10 ppm. Peaks related to atomic zinc, i.e Zn^+, ZnH^+, etc., were not observed.

6.3.2.3 Sample combining and PCA

As mentioned in section 6.2.2.2, 12 samples were studied for each concentration of Zn. Upon averaging samples into groups of 4, the standard deviation became noticeably smaller, which can be observed by comparing Figure 6-7 A, B) to C, D). Particularly, in Figure 6-7 D), LBL, MBL and HBL can all be separated from to 95% confidence. These averaged samples were

then analyzed using PCA. The resulting scores and loadings plots (shown in Figure 6-8) show that sample scores increase with Zn concentration. This separation is to 95% confidence between the LBL and HBL concentrations. The MBL data points are separated between the LBL and HBL samples, however, this difference is not to 95% confidence. For the loadings plots, peaks at *m/z* 69, 89 and 115 are the more intense loadings, which correspond to the peaks identified as Zn-related.

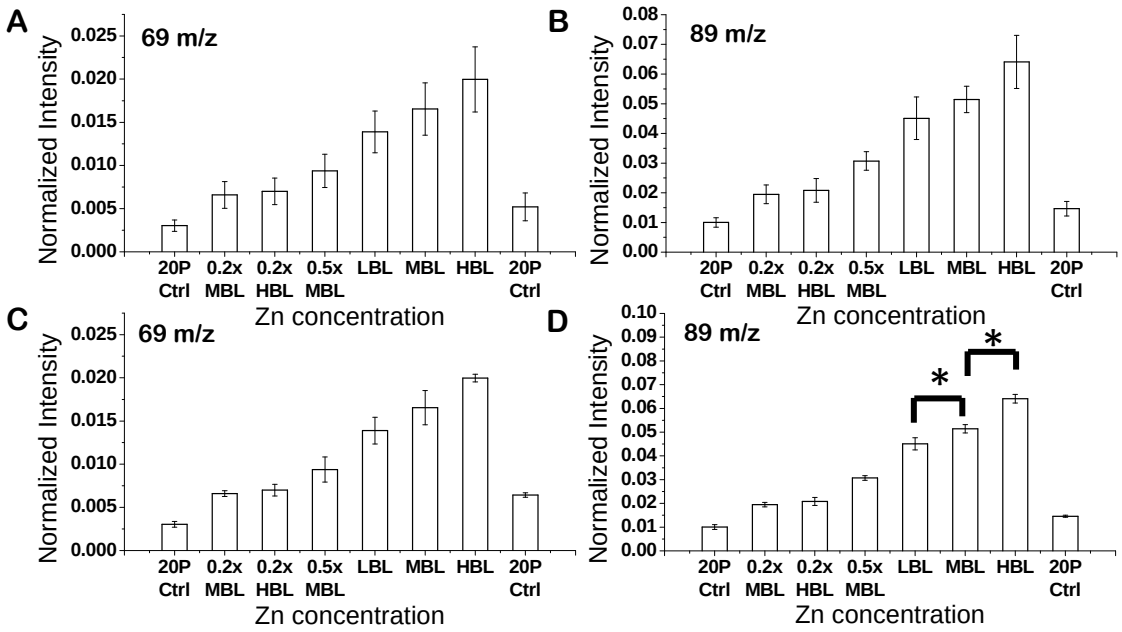

Figure 6-7 Zn in 20% porcine plasma. A, B) Samples containing Zn were dissolved in 20% porcine plasma and were analyzed with n=12. An increasing trend can be seen for both *m/z* 69 and 89 as Zn concentration is increased. C, D) Samples within single concentrations were grouped randomly into sets of 4, effectively reducing the number of unique data points to 3. After grouping, the standard deviations decreased and resulted in an improved separation of the data and Zn could be separated for all blood level concentrations. Note that in all 4 graphs, the samples containing additional Zn are significantly different than the control samples, labeled as 20P Ctrl.

6.3.2.4 PLSr on Zn

PLSr was completed on Zn data in 20% porcine plasma. The model was created, then applied to an independent data set and was able to predict most concentrations of Zn within error. While two concentrations were predicted incorrectly (0.2xMBL and 0.2xHBL), the rest of the concentrations, including all concentrations in the blood range (600-1200 µg/L), were correctly predicted. The root mean squared error of prediction was found to be approximately 110 µg/L. These results are shown in Figure 6-9.

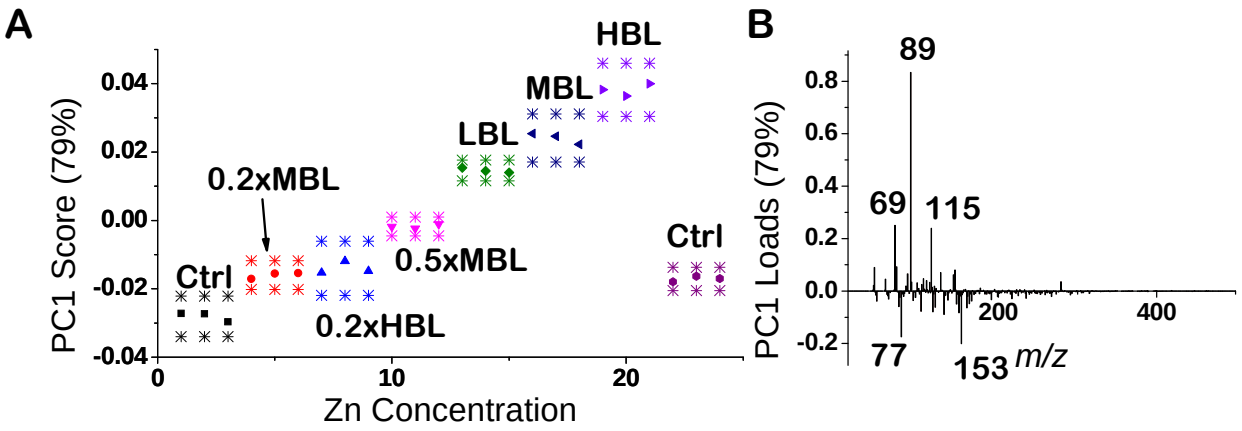

Figure 6-8 PCA on grouped Zn samples. A) PC1 scores plot. While most sample sets have an overlap in confidence intervals with the adjacent concentrations, a clear trend can be observed with the PC1 score increasing as the concentration of Zn is increased. B) Chief loadings align with the expected Zn-related peaks at *m/z* 69, 89, 115 and 145. * indicates 95% confidence intervals.

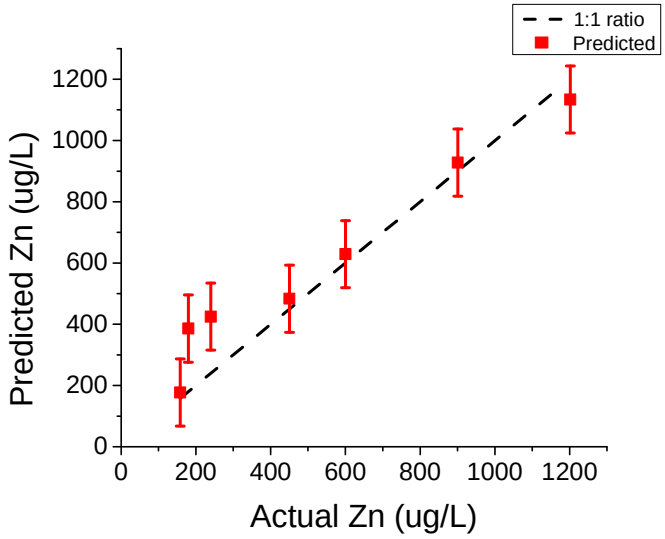

Figure 6-9 PLSr on Zn. The PLSr model for Zn was capable of predicting Zn concentrations in an independent sample set. Although samples below the blood range (~200-300 µg/L) were predicted incorrectly, the samples within the blood range (600-1200 µg/L) were within error. The 1:1 ratio line (red) indicates the ideal model where the prediction perfectly overlaps the actual concentration.

6.3.3 Folic Acid

6.3.3.1 Initial studies

Folic acid was studied in various solutions, in water, 10% and 100% plasma. With these solutions, no *m/z* peaks were consistently visible above the control samples, and no separation was observed in PCA even at the 1000xHBL concentration. Additionally, 5 different MS settings were tested, however, again, no information regarding FolA concentration was found.

6.3.3.2 Acid re-wetting

Rather than rewetting with dH_2O, acetic acid was used. After rewetting with acetic acid, no major changes in the spectra were observed. As with the initial studies, no individual *m/z* peaks, nor any separation via PCA was observed. A strong acid, hydrochloric acid, was used as well and did not result in improvements in spectra or PCA, either.

6.3.3.3 Sinapic acid and silver

Sinapic acid and silver were both pre-spotted on filters. In this case again, neither compound showed any increase in individual *m/z* peaks, nor any separation via PCA.

6.3.3.4 FolA derivatives

5 FolA derivatives were studied using the PPAMS. No compounds showed any increase in individual *m/z* peaks, nor any separation via PCA.

6.3.3.5 FolA alternative – homocysteine

Homocysteine (Hcyst) was studied using the standard PPAMS system, as well as the LTP coupled to an Orbitrap MS. Using PPAMS (with the Advion system), no peaks were detected and no separation with PCA was achieved, even at 10,000xHBL. With the Orbitrap, a single peak at *m/z* 118.0315 was visible above the background, as shown in Figure 6-10. This was identified as $C_4H_7NOS + H^+$, or, $[Hcyst\text{-}H_2O+H^+]$ to within 5 ppm.

6.3.3.6 UV treatment/peak identification

FolA samples exposed to UV displayed a peak at *m/z* 94 which consistently appeared above the control samples. This peak showed an increasing trend compared to the controls starting at 35xHBL, but was not significantly above the controls until 3500xHBL, as shown in Figure 6-11 A). UV samples were also studied using the Orbitrap MS. Here, the exact mass was found to be 94.0644 and was identified as C_6H_7N.

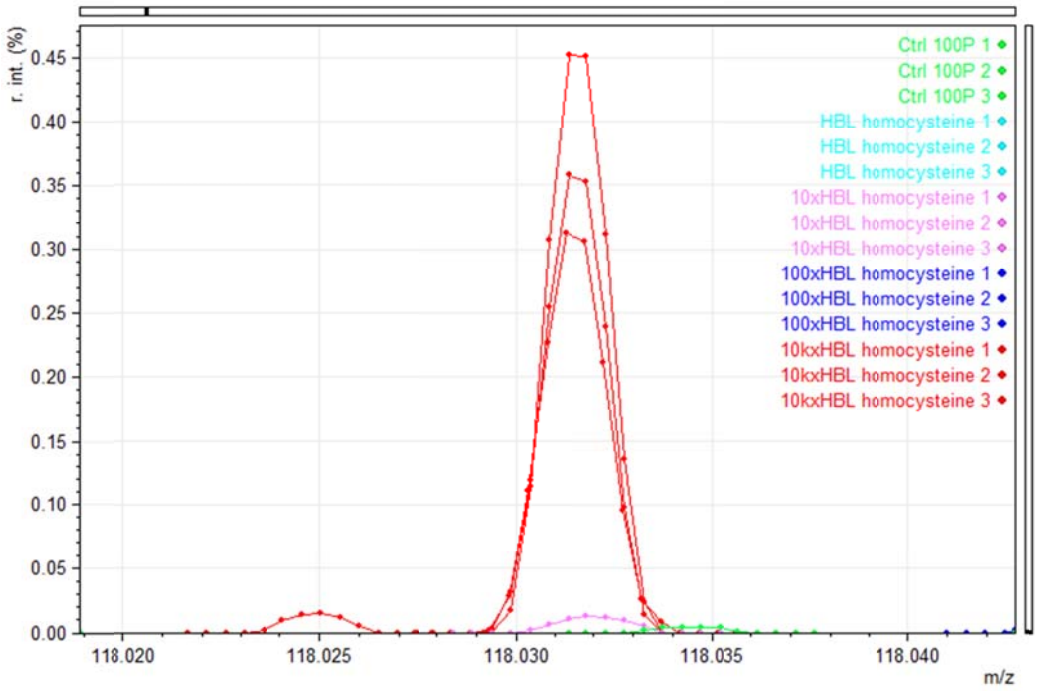

Figure 6-10 Homocysteine detection with LTP and Orbitrap. Hcyst could be detected using the Orbitrap at 10,000xHBL (red). Other concentrations do not shown any consistent signal above the control. Intensities were normalized to the largest peak in the spectra.

6.3.3.7 PCA

PCA was performed on the UV treated samples, however, no separation was observed. *m/z* 94, the identified FolA-related peak, was not identified as a chief loading. Other *m/z* peaks, such as 84, 70, 77 and 43, were weighted much more heavily. The PCA plots are shown in Figure 6-11 B, C) and spectral intensity for *m/z* 84, is shown in Figure 6-11 D).

6.3.4 Thyroxine

6.3.4.1 Initial studies

Initial studies on Thyr were performed on samples prepared directly in 4M NH_4OH, desiccated, then rewet with water. No consistent peaks were observed to indicate a trend with Thyr concentration, and no information was apparent in PCA even up to 60,000xHBL. Additional experiments utilized CH_3COOH as the rewetting solution, here, again, no information regarding Thyr content was observed, as shown in Figure 6-12 A, B).

6.3.4.2 Thyr in porcine plasma

Thyr was then dissolved in 4M NH_4OH and diluted in 10% porcine plasma. Concentrations up to 60xHBL were compared and no trend was observed. Later, Thyr added

directly to porcine plasma and was tested up to 60,000xHBL. Again, no information regarding Thyr content was observed, as shown in Figure 6-12 C, D).

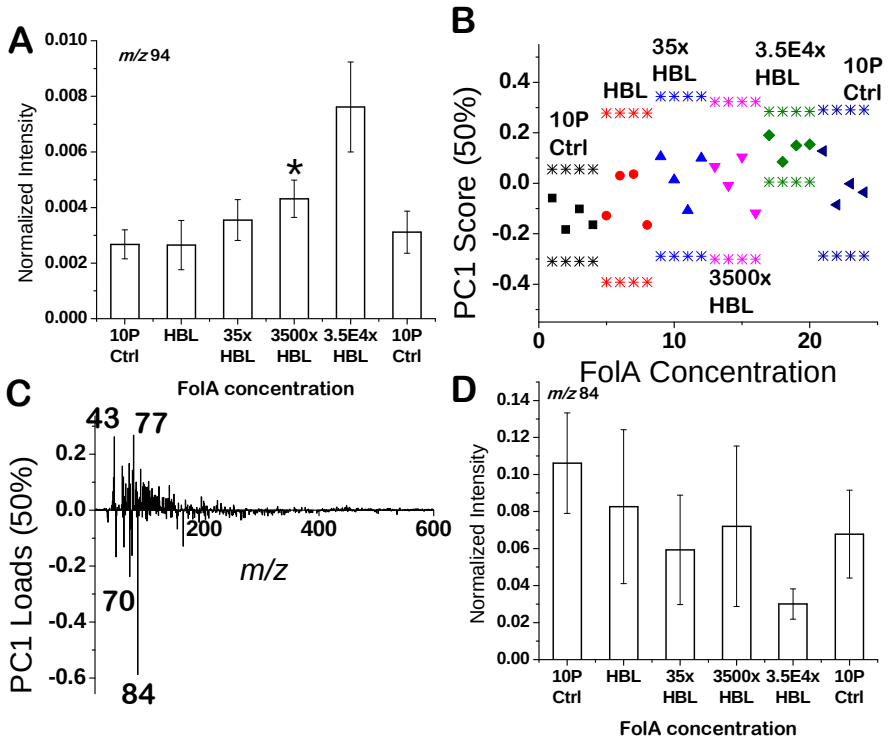

Figure 6-11 FolA after UV exposure. A) After UV treatment, FolA displays a trend in intensity at *m/z* 94, starting at 3500xHBL. B, C) Scores and loadings plots for FolA after UV exposure. The scores plot does not show any separation of the data. The chief loadings are shown to be *m/z* 43, 70, 77 and 84. These peaks, however, were observed to be high intensity, high variance peaks, as demonstrated in D). In A) * Indicates the lowest concentration where p-value <0.05 compared to the first and second controls. In C) * indicates 95% confidence intervals.

6.3.4.3 LTP power adjustment

After adjusting the HV box power settings, Thyr was added directly into 10% porcine plasma at concentrations from HBL to 6000xHBL. Upon analysis of the spectra, no peaks relating to Thyr were observed, and no information regarding Thyr concentration was present in PCA plots. Much like the earlier results, the PCA plots showed no separation of any of the data.

6.3.5 Multi-nutrient samples

Multi-nutrient samples were also analyzed by creating a matrix of solutions with VitA and Zn at various levels surrounding the blood concentration range. Similar to the individual VitA and Zn models, PLSr was used to attempt quantitation on an independent data set. In this mixed nutrient sample, however, no predictive ability was observed. This is shown in Figure 6-13.

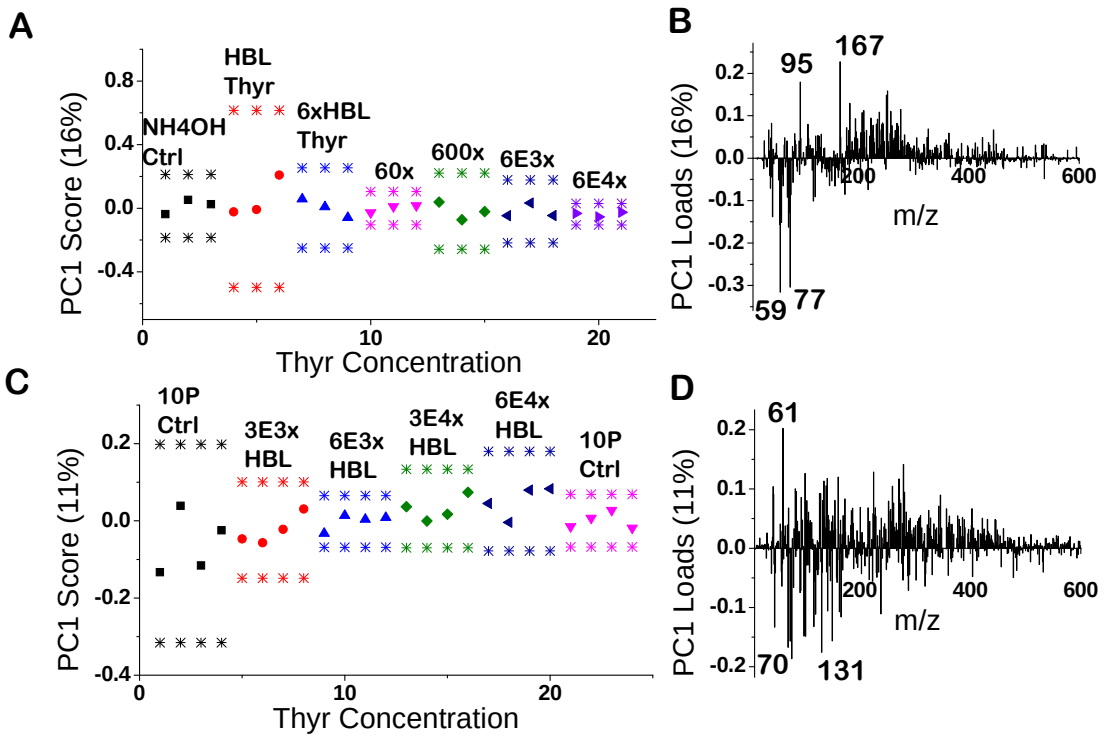

Figure 6-12 PCA on Thyr data. A, B) Thyr was dissolved in NH_4OH and desiccated overnight. Prior to analysis, samples were rewet with acetic acid. A) Scores do not show any separation between any of the sample types. B) The chief loadings occur at *m/z* peaks such as 59, 77, 95 and 167, however, as in Figure 6-11, these were high intensity, high variability peaks. C, D) Thyr was added directly into 10% porcine plasma, and was analyzed with a stronger (higher voltage) LTP. Again, no information regarding Thyr concentration was observed.

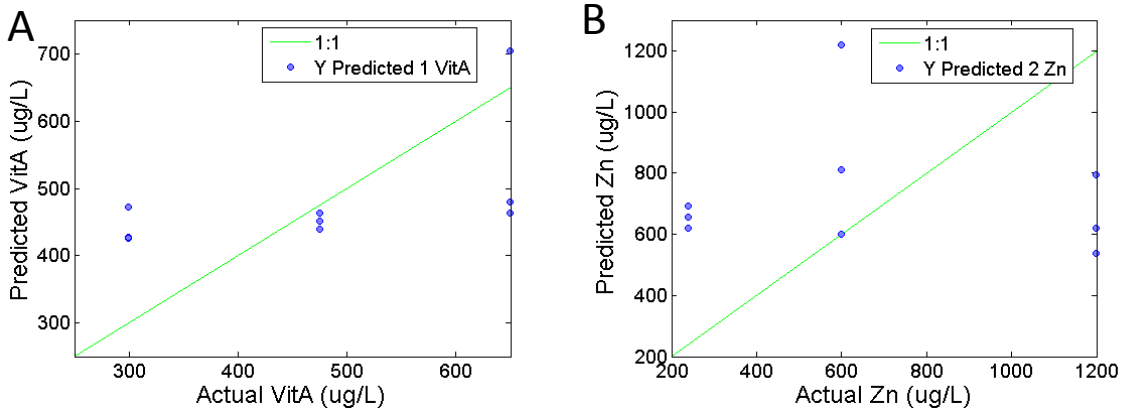

Figure 6-13 PLSr on multi-nutrient samples A sample matrix containing VitA and Zn at various concentrations was analyzed and used to build a PLSr model. The model was then applied to an independent data set to quantify the results. The plot for VitA quantitation is shown in A) and Zn quantitation is shown in B). Neither model was capable of accurately predicting nutrient content, likely due to interactions between the VitA and Zn. The 1:1 ratio lines (green) indicates the ideal model where the prediction perfectly overlaps the actual concentration.

6.4 Discussion

6.4.1 Iron

6.4.1.1 Water vs. Plasma testing

Surprisingly, in the relatively clean samples of iron (II) chloride dissolved in water no peaks were visible which trended with iron concentration, while samples in the relatively complex matrix of 10% porcine plasma showed a clear trend at *m/z* 70. This was the only peak visible and no isotopic signature was observed. However, since ^{54}Fe only encompasses <6% of all Fe, the lack of detectable isotopic pattern is not surprising, given that for 10P 50xHBL, the peak at *m/z* 70 is approximately 1% of the spectra. Upon closer examination, for *m/z* 70 to be directly related to Fe, the adduct formed would require the addition of a species with *m/z* of either 13 or 14, depending on the mode of ionization. Through Penning ionization, which has been observed with this ionization method,[88] theoretically, the Fe (II) could combine with CH_2 and form an excited state molecule $FeCH_2$ which does not require an additional proton. However, based on observations with our system, and in literature, for the LTP, Penning ionization seems to mainly occur in aromatic, multi-ring compounds that likely have more stable excited states. Overall, a more likely scenario is that Fe was affecting another molecule, since adding *m/z* 13 seems unlikely. This hypothesis was later confirmed and will be discussed further in section 6.4.1.4.

6.4.1.2 Instrument settings optimization

Due to the significant effect of the settings adjustment on VitA detection additional settings were tested to improve Fe detection. Several instrument settings resulted in a separation between the controls and the Fe-containing samples, two of which are shown in Figure 6-2. In order to select the best setting, the ratio of the intensity of the Fe-containing sample divided by the control was maximized, as shown in Equation 6-1.

Equation 6-1

$$Ratio_{Fe} = \frac{I_{Fe}}{I_{ctrl}}$$

Where *I* is the signal intensity for a given setting. The repeatability in the signal was also taken into account by determining the overall error, shown in Equation 6-2.

Equation 6-2

$$\Delta(Ratio_{Fe}) = \ (Ratio_{Fe})\sqrt{\left(\frac{\Delta I_{Fe}}{I_{Fe}}\right)^2 + \left(\frac{\Delta I_{ctrl}}{I_{ctrl}}\right)^2}$$

The overall optimized setting was then selected by dividing Equation 6-1 by Equation 6-2, as shown in Equation 6-3.

Equation 6-3

$$Optimized\ setting = \max\left(\frac{Ratio_{Fe}}{\Delta(Ratio_{Fe})}\right)$$

Resulting in the selection of "Setting 3" as the optimized setting. Initial experiments from section 6.3.1.1 were performed on quartz based filters, and overall, gave better optimized settings results, however, due to the difficulty in handling the quartz filters, they were replaced by paper filters in future experiments. Much like the VitA MS optimizations, these settings adjustments seemed to increase the relative expression of the Fe-related peak.

6.4.1.3 10 vs. 100% porcine plasma

Fe concentrations varied in difference solutions. Originally, when the porcine plasma was tested at the UW Research Testing service, the Fe was not detectable. This was caused by a combination of their colorimetric testing method, and the presence of EDTA in the porcine plasma. EDTA is a metal chelator and binds the Fe in solution, which interferes with the colorimetric test which also requires Fe binding. Later, the porcine plasma samples were re-analyzed using Inductively-Coupled Plasma MS, which was able to detect elemental composition, regardless of the presence of the chelator. Thus, the original intended Fe content in the samples was miscalculated, resulting in different concentrations in the water, 10% and 100% porcine plasma samples. Actual tested concentrations are listed in Table 6-1.

Due to the results from section 6.3.1.1, where no peak was observed relating to Fe in plain water, the Fe was suspected to be interacting with another molecule present in the porcine plasma. Thus, an increase in porcine plasma content to 100% was hypothesized to further improve detection. Overall, this increased porcine plasma content matched very well with the increase in signal intensity. Thus, the increased biological components in the more concentrated plasma allowed for better detection of Fe. When additional concentrations were tested (between 100P HBL and 100P 5xHBL), the detection limit was found to be approximately 100P 2xHBL.

In select experiments, 100P HBL could be separated from the 100P control, however, this was inconsistent and thus, not reported.

6.4.1.4 Peak identification

As suspected, *m/z* 70 was not directly related to Fe, but was another molecule, pyrroline (C_4H_7N) whose ionization was affected by Fe. Pyrroline is related to pyrrole (through the hydrogenation of one double bond), and are both used to form porphyrin rings.[98] Thus, the Fe seems likely to be able to interact with and influence pyrroline. This means, however, that in real world, human blood samples, the amount of pyrroline may also affect the detection of iron. Further studies using samples gathered from real patients would be required to verify the validity of this peak.

6.4.1.5 PCA and PLSr

As with the results seen previously with VitA, the PCA performed similar to, but slightly worse than studying the individual nutrient-related peak, in this case, *m/z* 70. Again, while the separation via PCA begins to occur at 100P 5xHBL, where the peak is visible above the control in the spectra, this separation is worse than when studying the individual peak. This result indicates that additional information from the chemical signature was not found in the spectra using PCA which could allow lower concentrations of Fe to be separated.

For PLSr, the results were less encouraging than for PCA. Here, not only were the predictions inaccurate, but no trend following Fe concentration was observed. Although quantitation in the blood region was not expected, due to the lack of individual peak detection in that range, the model was expected to at a minimum indicate the increasing Fe content in the samples above the blood range. This lack of a trend is likely due to the low relative intensity of the Fe peak (at *m/z* 70) and the high standard deviation (relative to the peak intensity). Further developments of the PPAMS system may be able to improve future quantification efforts, as discussed in section 7.2.1.

6.4.2 Zinc

6.4.2.1 10, 20 and 100% porcine plasma

Zn was first tested in 100% porcine plasma due to the optimized conditions obtained during Fe analysis. Zn was expected to ionize similarly to Fe, thus, 100% porcine plasma was expected to be ideal. This however, was not the case, as Zn was not easily detectable in 100% porcine plasma. In this solution, 2 peaks, *m/z* 57 and 69, showed an increased expression

compared to initial controls, but not controls examined at the end of the experiment. This may indicate that their expression was increasing with time, and not only due to the increased Zn content.

When 10% porcine plasma was used as the solvent instead, detection was markedly improved, with the ability to separate samples containing Zn from controls down to at least the LBL concentration. To make the samples more physiologically relevant, concentrations as low as 0.2xMBL and 0.2xHBL were tested in 20% porcine plasma. These concentrations were intended to mimic potential real-world solutions which could be diluted with buffer. While concentrations at 0.2x blood level of Zn were not separable from each other, they were able to be separated from the control samples. Differences between the 0.2x blood levels were likely undetectable due to the closeness of the concentrations, with a difference of only 60 μg/L, or 1.2 ng of Zn on the filter. Overall, of all porcine plasma concentrations, 20% showed the most consistent trend in Zn-peak intensity, as Zn concentration was changed.

6.4.2.2 Peak identification

With the chemical formulas, several potential identities of the peaks were still possible. C_5H_8 may be isoprene, a common organic compound found in plants and animals.[99] The most intense Zn-related peak, $C_4H_8O_2$, may be butanoic acid, while $C_8H_{16}O_2$ may be octanoic acid, both of which are found in blood. While no apparent interaction can be found, these molecules are both acids and are not expected to ionize as readily in the positive spectra. Thus, Zn seems to be interacting with these acids, and making them more ionizable. The compound for $C_6H_{10}O_2$ was not identified, but may also be a carboxylic acid and experience a similar effect as butanoic and octanoic acid.

6.4.2.3 Sample combining and PCA

Assuming the theoretical intensity of any given *m/z* peak should be the same for samples of the same concentration, we would expect the observed intensity to follow a normal distribution around the theoretical value. By combining samples, we expect that the averaged samples will be a better approximation of the theoretical intensity. According to the Central Limit Theorem in mathematics, the standard deviation should decrease by the square root of the number of combined samples. Thus, to reduce the variability of individual data points, 4 samples of the same concentration were combined randomly and taken as an average, and, as expected, the averaging resulted in a reduced standard deviation.

After averaging the samples, PCA was performed. In this case, no square root transformation was completed, however, the results were very similar when the square root transformation was performed. Overall, much like earlier results with VitA and Fe, the results were promising, with results largely reflecting the information observed from the Zn-related peaks in the spectra. Again, however, the separation was slightly worse than when looking at individual peaks, for example, *m/z* 89, where separation between all blood level concentrations was significant. Overall, the results have shown that for the compact MS, when individual peaks are visible, the results are reflected in PCA.

6.4.2.4 PLSr on Zn

PLSr on Zn was promising for the analysis of samples with varied Zn content. For the prediction, analysis was completed by averaging the *m/z* intensities for 6 samples and loading the data into Eigenvector's PLS_Toolbox. While the blood level predictions were accurate, lower concentrations of Zn (20% of the blood level concentration) were not estimated to within error. In the current state of the PPAMS technology, this could potentially cause errors in prediction, as individuals with Zn deficiency may obtain false high readings. With the relatively poor predictive ability at these low concentrations, currently, this dilution might not be a feasible method to aid with Zn quantification. Future work to improve separation at lower concentrations, by performing more optimizations such as those found in section 7.2.1, are expected to improve this quantitative ability.

6.4.3 Folic Acid

6.4.3.1 Initial studies

Although some *m/z* peaks seemed to vary with FolA concentration on occasion, this was not observed consistently, and thus, was not shown, and could not be used for FolA characterization. Due to the larger molecular weight of FolA compared to the previous analytes, different system settings were tested to try optimizing the detection of higher masses. Even with the additional settings, however, no detection was observed. One challenge was that in previous optimizations, single peaks were present which could be maximized, as discussed in section 6.4.1.2. However, because no individual *m/z* peaks seemed to describe FolA, this was not possible and thus optimization of FolA could not be completed actively during data collection. For optimization purposes, a smaller subset of MS settings were tested but did not result in improved detection or separation with PCA or with individual *m/z* peaks. Overall, in previous

FolA experiments using the Bruker MS, PCA resulted in separation of the samples based on concentration. The inability of the current system to separate samples based on concentration was not well understood, thus, several other experiment modifications were tested to try to improve detection.

6.4.3.2 Acid re-wetting

FolA has two carboxylic acids and in physiological solutions, naturally has a charge of -2. This naturally negative charge may make FolA difficult to ionize in the positive spectra (though the negative spectra showed no information, either). Either acetic acid (at 1%) or hydrochloric acid (at 0.1 M) was added to the sample prior to analysis to decrease the pH of the solution, and thus increase the presence of neutral folic acid. Acetic acid was initially used as a relatively safe acid for field use and was hoped to provide a sufficient shift in pH. As a weak acid, however, it may not have induced as much of the desired effect of neutralizing FolA, thus, when the results did not improve, hydrochloric acid was used instead. In both cases, with an increase in neutral FolA, as well as an abundance of free protons from the additional acid, more FolA was expected to ionize. This, however, was not reflected in the collected spectra.

6.4.3.3 Sinapic acid and silver

Studies using other MS methods, particularly matrix assisted laser-desorption/ionization (MALDI) based systems, have shown that using sinapic acid or silver as a matrix/substrate can improve ionization of FolA.[100,101] In other studies, matrices have been shown to be effective in enhancing ionization of larger molecules in other techniques as well, such as in ToF-SIMS,[102] thus, sinapic acid was used to try to enhance the ionization of FolA. In MALDI, the matrix is used to absorb the energy from the laser (and prevent the analyte from fragmenting), which causes the sample and matrix to ablate/desorb, and are subsequently ionized in the gaseous plume.[103] Overall, this matrix may not have aided in ionization in this system due to the relatively low energy of the LTP. Silver was expected to aid ionization through a different mechanism. Specifically, the FolA was expected to interact with silver, to form an $[M + Ag]^+$ molecule, and perhaps, with a pre-ionized molecule, be more detectable. This however, was again not the case. Overall, the $[M+Ag]^+$ molecule was not detected, which may again be due to differences in the desorption and ionization mechanisms between MALDI and PPAMS. One potential reason for the lack of detection is due to the large size of the $[M+Ag]^+$ ion, which may

be more difficult to ionize with the LTP. Due to the difficulty in detecting the FolA molecule, FolA derivatives also present in blood were tested as FolA status indicators.

6.4.3.4 FolA derivatives

Several analogues of FolA were also tested to determine whether small changes in chemistry may result in differences in ionization for PPAMS. This system was capable of detecting individual *m/z* peaks for the organic molecule VitA, as well as other organics, such as cyclic molecules like fluorene (data not shown). Thus, other derivatives were tested to try to determine the reason for the lack of FolA detection. This, however, still did not result in any detection through individual peaks or separation with PCA. Potential reasons for the difficulty in detecting FolA are further discussed in section 6.4.6. Overall, with all the optimizations and derivatives, FolA was still not detectable using this system, thus, an alternate marker for FolA was tested.

6.4.3.5 FolA alternative - Homocysteine

Hcyst was selected as an ideal alternative marker for FolA in these tests, because Hcyst has been shown to be elevated in individuals with FolA deficiencies.[104] After searching through literature, the maximum Hcyst found in unhealthy individuals is approximately 130 μM,[105] or just under 10xHBL. Detection with the LTP, however, was limited to a much higher concentration of 10,000xHBL and required the Orbitrap. Due to the small intensity, in the case of the Advion, the Hcyst peak is likely masked by surrounding peaks, due to the relatively low mass resolution of the system. The molecular weight of Hcyst is in the *m/z* 100-200 range, and thus, optimizations via adjusted MS settings were deemed unlikely to aid in detection. Overall, due to the poor detection, this alternative to FolA was not pursued further.

6.4.3.6 UV treatment/peak identification

Previous experiments using this system were unable to detect FolA when the whole molecule was analyzed in solution. FolA is known to be sensitive to UV,[106] thus, we anticipated that by degrading the FolA, perhaps the lower mass components would ionize more efficiently and be detectable. Upon UV exposure, the resulting spectra showed a single peak which trended with FolA concentration. Identified as C_6H_7N, this peak corresponds to a benzene ring with an NH_2 attached, which can be found in the middle of the FolA molecule (the full molecule can be found in Appendix B). Previous studies on the UV degradation of FolA have indicated that the process results in the formation of 6-formylpterin and p-aminobenzoyl-L-glutamic acid.[107] The

observed aniline (C_6H_7N) may be formed from the further breakdown of p-aminobenzoyl-L-glutamic acid. The other product of this breakdown, $C_6H_7NO_5$, was not observed. While the appearance of a peak relating to FolA is promising, this peak might not uniquely identify FolA, as aniline may be present in other molecules in the body as well.

6.4.3.7 PCA

As mentioned previously, PCA was performed on each of the FolA experiments in section 6.3.3, however, no separation was observed. With the appearance of a FolA-related peak, separation through PCA was expected to improve after UV treatment, however, separation was still not achieved. This may be caused by the relatively small intensity of *m/z* 94, compared to other peaks in the spectra. The peaks contributing most to the variance in the data set were large peaks with large standard deviations, such as *m/z* 84, as shown in Figure 6-11 D) and are unlikely to relate to nutrient status. Interestingly, after UV exposure, *m/z* 70 (the peak found to relate to Fe status) became much more intense and like *m/z* 84 was highly variable. This would likely negatively affect Fe detection and thus, may not be an ideal solution for future analyses.

6.4.4 Thyroxine

6.4.4.1 Initial studies

NH_4OH was required to dissolve thyroxine, and was thus initially used as the only solvent. In the absence of biological solution (i.e. porcine plasma), the detection of Thyr was expected to be more efficient. This, however, was not the case. Due to the basicity of NH_4OH, this may make the ionization of other analytes more difficult as free protons (H^+ molecules) are less abundant, and was reflected by the relatively low total ion intensity (sum of all peaks in the spectra). To improve upon this, acetic acid was used to neutralize the solution. Upon addition of the acid, the total ion intensity increased by approximately 6 fold, however, Thyr was still not detectable. To determine the effect of biological solutions (such as interactions between Thyr and other molecules in blood), Thyr was tested in porcine plasma as well.

6.4.4.2 Thyr in porcine plasma

To ensure comparable results, NH_4OH content was kept constant for all concentrations of Thyr tested. For this reason, the samples dissolved in NH_4OH and diluted in porcine plasma were kept to relatively low concentrations, up to 60xHBL, to maintain the NH_4OH level at 0.1%. In order to test higher concentrations in porcine plasma, a separate set of Thyr samples, with Thyr added directly to porcine plasma as a suspension, was used. For suspensions with concentrations

at blood level, Thyr was soluble, however, above blood level, samples were well-mixed immediately before analysis. While the lack of detection of Thyr may be caused by internal instrument settings, previous settings adjustments were only capable of improving results where some baseline detection was possible. In the case of Thyr, no peaks were seen even at very high concentrations, thus, detection was unlikely to be improved through extensive MS settings adjustments. To try better mimic previous settings, when detection was possible on the Bruker MS, the LTP power was increased.

6.4.4.3 LTP power adjustment

Due to the previous PCA results from Chapters 3 and 4 where separation based on Thyr concentration could be observed with the Bruker ion trap, the new Advion system was expected to work for Thyr detection as well. However, because the analysis had thus far not resulted in any detection, the LTP settings were adjusted to better match previous experiments. During the initial system set up, the sample and LTP positions were set to match previous experiments. This, however, necessitated a decreased LTP power, due to the helium plasma arcing to the MS inlet. In this experiment, rather than matching the position, an alternate strategy was used by matching the input power for the LTP. To use this increased power, the sample and LTP probe horizontally 3 mm further away from the MS inlet – the closest position which eliminated the arcing of the LTP. This, however, still did not result in Thyr detection. Additional potential sources of difficulties for FolA and Thyr detection are discussed in section 6.4.6.

6.4.5 Multi-nutrient samples

In this experiment, a two-nutrient matrix was constructed, similar to previous 3-nutrient matrices analyzed in Chapter 4. In this case, VitA and Zn were analyzed at 3 concentrations each, for a total of 9 sample types. Due to the previous successes in predicting VitA and Zn individually, the multi-nutrient analysis was also expected to be successful. This, however, was not observed as predictive capabilities were not achieved. The predictions indicate that the modelling of individual nutrients is affected by the concentration of other nutrients. This may be caused by the nutrients interacting with each other (or in the case of VitA, interactions may be occurring with Zn-indicators such as C_5H_8 and $C_4H_8O_2$), or, through competitive matrix effects, where the analytes are competing for ionization, which has been observed for LTP in another study.[108] For different MS methods, matrix effects can be reduced or eliminated by performing

separations, such as through column chromatography,[109] however, for PPAMS, this would not be ideal.

Other groups have utilized different optimized internal MS settings to improve detection of individual compounds.[110] While this is normally completed on LC-MS instrumentation where optimized settings will be used in different elution windows, changing the instrument settings may be possible for PPAMS as well. In this work, PPAMS has been shown to provide significantly different capabilities for different MS settings, thus, optimized settings may also alter the observation of matrix effects. In order to utilize this method, however, different instrument modifications may be required. For example, as previously mentioned, sample drying is a significant issue for analysis, and the nutrient ionization drops significantly, even after only 10-20 s. In order to collect spectra on a single sample with multiple settings, a longer analysis time would be beneficial to allow for instrument stopping and starting with different settings loaded. This may be possible by having a system which can continuously hydrate the sample with water to maintain the nutrient ionization. If this is not possible, multiple samples would need to be analyzed per individual, as sample re-wetting after analysis has proven to be difficult, due to the samples becoming highly hydrophobic after analysis with PPAMS.

6.4.6 Additional FolA and Thyr detection notes

PLSr was also used to attempt quantitation of FolA and Thyr (data not shown). These analyses, however, did not result in any useful predictive capability. Much like the Fe and the Zn/VitA matrix results, no trends in FolA or Thyr content were observed using the Advion system. Previously, when FolA and Thyr were analyzed using the Bruker MS, individual peaks were not visible, however, advanced analysis could produce consistent separation in the data at blood level concentrations. This separation was achieved through the combination of many peaks, rather than individual peaks displaying trend information. The inability of the Advion MS to demonstrate any classification ability for FolA and Thyr samples may be due to the system's relatively low signal to noise ratio (S/N). The manufacture documents a S/N of 100 for clean solutions with 20 μg/L reserpine, which is close to the blood concentrations of FolA and Thyr. Quadrupole MS systems routinely have S/N more than an order of magnitude lower than ion trap MS systems.[111] Thus, with the quadrupole, peaks relating to these nutrients might not be detected to any degree above the background due to other large peaks in the spectra, such as the water-related peaks, which could lead to the inability to quantify the data. One potential solution for

this is to run additional samples and to combine results, such as in section 6.3.2.3 which may improve the S/N. For these nutrients which may ionize poorly, however, running sufficient samples to improve the S/N may not be feasible for field applications.

Aside from this potential difference between MS's, differences in the ionization may also be affecting detection. First, the PPAMS system has displayed some aging effects. Over the years of use, when holding the input voltage constant, a shift (decrease) in the input current was observed. This indicates that a change within the HV box was occurring, which resulted in an increased internal resistance. This change was also apparent through monitoring the frequency and voltage applied to the HV electrodes. From initial construction to an oscilloscope measurement 4 years later, the frequency and voltage both nearly doubled from initial settings (which can be seen in the parameters listed in sections 2.2.3.3 and 5.2.2). Furthermore, this design of the HV box has the output frequency and voltage linked. With the aged HV box, we cannot utilize the exact original settings, even though the parameters are adjustable. Future designs should include independently controlled settings to give more control over the LTP, and commercial grade/higher quality components to reduce system aging. Another major difference is that with the Advion system, a sample enclosure is used. This semi-sealed chamber likely changes the ion optics of the system. While the position of the LTP and sample became more consistent and controllable, changes in gas flow patterns and electric fields likely occurred. These changes may have resulted in different ions or different amounts of ions entering the MS, which will change the observed results.

Finally, the samples being analyzed are also different from earlier experiments. In the experiments from Chapter 4, samples were generally analyzed as bulk liquids in Petri dishes. The design of the Advion system, however, has the MS inlet oriented vertically, which prevents the analysis of a pure liquid sample. Largely due to the early success of the analysis of sample solutions deposited on filter paper, when the MS was rotated to have a horizontal inlet, the filter papers were still used. While the early successful results influenced the use of the filter papers, three additional factors also played a key role. The first factor is that the use of filters only requires 20 μL of fluid, compared to the 1 ml utilized in the pure liquid experiments. The second contributing factor was the increased safety through the handling of the filters vs. the handling of bulk liquid. Finally, the third factor was the reduction in medical waste produced by having dried filters (after analysis) for disposal vs. the remaining bulk liquid.

6.5 Conclusions

In this section of Aim 3, although the Thyr was unable to be detected, the detection of the remaining nutrients, Fe, FolA and Zn, were all improved. Fe was best characterized by studying the intensity of *m/z* 70. This was discovered to be an interaction of Fe with biological components in the porcine plasma, as the peak was not observed in water solutions. The detection of Fe was first improved by adjusting internal MS settings, which improved detection to approximately 50xHBL. Interestingly, the detection of Fe was further improved to 5xHBL upon switching the solvent from 10% porcine plasma to 100% porcine plasma. This improvement with more concentrated porcine plasma was not observed with any other nutrients. Detection, however, could not be improved to blood levels, and concentrations could not be predicted using PLSr. For FolA, initially, no detection could be achieved. Much like for Thyr, this may have been due to a low level of ionization coupled with the poor S/N of the Advion MS. To improve this, the FolA was irradiated with UV, due to its light sensitivity. With this, FolA-related peaks could be detected at 3500xHBL, but could not be improved to blood level. Overall, in this chapter, Zn detection was the best characterized. Detection of Zn above the background occurred at levels as low as $1/5^{th}$ of that found in health individuals. Furthermore, precise quantitation was achieved in the blood concentration range with a PLSr model.

7 Conclusions and future studies

7.1 Conclusions

Overall, this work demonstrates a novel method to detect and measure multiple micronutrients at biological levels in blood based solutions. The system operates under atmospheric conditions and can analyze samples with minimal sample preparation, both of which help to decrease total analysis time. In fact, after the sample is collected into a centrifuge tube, total experimental time was reduced to less than 1 minute, including 10 seconds of spectra collection, to achieve quantitative abilities.

In Aims 1 and 2, the PPAMS system was coupled to a laboratory scale MS, a Bruker Esquire Ion trap, and was demonstrated to have a potential equal to or better than other well established techniques, such as ToF-SIMS and ESI for minimally prepared biological samples (i.e. no de-salting or columns). Samples with varying levels of nutrients across the blood range were compared, and were classified based on concentration using PCA. These experiments did not, however, result in the discovery of any individual peaks that showed trend information about nutrient content. To improve the classification ability, different transformations were applied to the spectra, which resulted in the discovery that a cube root transformation of the data greatly improved the data separation. Analysis, however, could not be compared for sample data collected on different days due to the appearance of new contamination peaks, caused by using shared equipment.

In Aim 3, to further advance the work, a new compact mass spectrometer, the Advion Express**ion** was purchased. Initial results showed a decreased sensitivity for nutrient content compared to initial experiments on the Bruker instrument. Several optimizations were required in order to improve detection to blood levels, including the removal of several high intensity peaks that were unrelated to nutrient content, the addition of a heated stage and the adjustment of internal MS settings and the positions of the sample and LTP probe. With these optimizations, individual peaks directly proportional to nutrient content were discovered for VitA, Fe and Zn. Using these results, models were constructed which could quantitatively predict individual nutrient content for VitA and Zn in controlled samples at blood levels. The remaining nutrients, Fe, FolA and Thyr, however, could not be accurately quantified. Furthermore, multi-nutrient samples containing VitA and Zn could not be accurately quantified, either. Thus, future work is

still required to expand this modeling capability for the other nutrients, as well as multi-nutrient and whole blood samples.

7.2 Future work

7.2.1 PPAMS system development

Although this technique has shown significant promise, improvements are still necessary for this to be field deployable and readily usable to detect all desired micronutrients. To accomplish this, both the MS and the LTP can be improved.

7.2.1.1 MS development

One method to improve detection is by using the Selected Ion Monitoring (SIM) mode on the current Advion MS. Advion advertises a 10x improvement in the limit of detection while maintaining a S/N of 100 (2 µg/L vs 20 µg/L for full scan mode). Using Fe with SIM on *m/z* 70, this was shown to improve overall results, as shown in Figure 7-1. Here, detection occurred at HBL Fe, which only contains 15% more Fe than the control (concentrations listed in Figure 7-1). This method seems feasible for nutrients in which identified peaks have been discovered, and thus would not yet be suitable for FolA and Thyr. Furthermore, having the entire spectra may be useful for future retrospective studies, if other information is contained in the data.

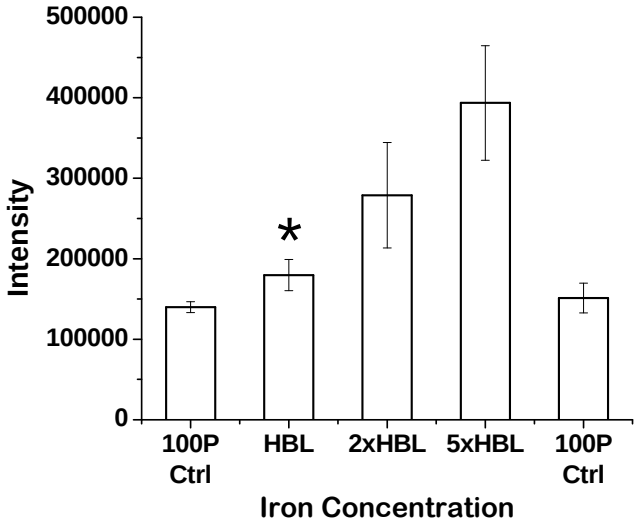

Label	Concentration
100P Ctrl	1,352 µg/L
HBL Fe	1,550 µg/L
2xHBL Fe	3,110 µg/L
5xHBL Fe	7,500 µg/L

Figure 7-1 Fe detection in selected ion monitoring (SIM) mode. Detection is improved to HBL for Iron in SIM mode, compared to ~ 5xHBL in full scan mode. * indicates the lowest concentration where $p < 0.05$ compared to the controls.

To maintain the collection of the full spectra while improving results, a new MS may need to be purchased. MS development continues to produce smaller and more sensitive systems. The Advion MS was one of the first commercially available compact systems which could be easily utilized (i.e. with minor system modifications) for this application. Several research groups, however, have been involved with the development of even smaller portable mass spectrometers,[82,112] some of which have been used for analysis with ambient techniques.[90] With the continued development of these systems, smaller MS with improved sensitivity will become commercially available, and when combined to the ionization device, should provide improved results with a smaller footprint compared to the current generation PPAMS.

7.2.1.2 Ionization development

Some analytes may be optimized by different ionization parameters. One method to accomplish this could be a multiplexed approach. While a previous study has used an array of LTP probes to enhance the analyzable surface area,[113] this strategy could also be used to ionize the sample with varied LTP voltages. A previous study has shown that by adjusting the physical position of the plasma, a different emission spectra can be observed and that adjusting the distance between the positive and ground electrodes can adjust the strength of the plasma.[114] While a short study completed in Aim 3 with an increased LTP strength was unsuccessful with improved Thyr detection, others have observed that the increased LTP strength results in more analyte fragmentation,[86] which may result in improved detection of both Thyr and FolA. Overall, this strategy is likely unsuitable for the current system, as the sensitivity may decrease due to an increased number and variety of produced ions. Ideally, this could be completed in conjunction with advances in MS technology and may be more suitable for use with an ion trap MS.

7.2.2 Additional nutrient testing

Further developments of the PPAMS system should also result in improved ability for detection in single and multi-nutrient solutions, particularly for FolA and Thyr. With these developments in place, further studies should first be completed to characterize the presence of FolA and Thyr in controlled samples, as single nutrients. With the improved MS and ionization source, this is expected to improve on the classification ability observed in Aim 2.

After improving single nutrient testing, further studies on multi-nutrient samples must also be completed. Matrices of nutrients will be constructed to sufficiently populate a nutrient model using PLSr. By varying all nutrients, a model which will take in to account matrix effects

should be achievable. This again should be completed on controlled solutions to ensure a complete model.

7.2.3 Whole blood

Beyond controlled porcine plasma samples, experiments must transition to human whole blood to be more applicable. Due to the large heterogeneity in blood, the samples must be homogenized prior to analysis. Two potential methods to accomplish this are lysing the blood, or separating out the plasma. Ideally, this will be achievable with a stable filter to maintain minimal sample preparation by the end user.

7.2.3.1 Blood Lysis

Blood lysis for homogenization was achieved by pre-spotting filters with Triton-X-100 (Sigma). Whole blood was obtained from Innovative Research. Prior to addition of blood, 12.7 mm paper filters were prepared by the addition of 15 μL of 10% Triton X-100 and allowed to desiccate overnight. 20 μL bovine blood solution (100% or 20% in PBS) was then added to prepared or plain filters and allowed to settle for 5 minutes at RT. Samples were then prepared for scanning electron microscopy (SEM) imaging following work completed by Marikovsky et. al.[115] Fixation solution was prepared by diluting 50% gluteraldehyde (Electron Microscopy Sciences, Hatfield, PA) to 2% gluteraldehyde in PBS. Filters were then covered with 500 μL of 2% gluteraldehyde for 30 minutes at RT in a laminar flow hood. Filters were then gently rinsed 5 times with distilled, deionized water to remove excess gluteraldehyde and salt, and desiccated overnight. Samples were then moved to a lyophilizer until imaging. SEM was performed using an FEI Sirion scanning electron microscope at the University of Washington NanoTech User Facility.

Cells were observed when deposited on plain filter paper, but were not present when deposited on filter paper containing Triton X-100, shown in Figure 7-2. In Figure 7-2 A) a plain filter with 10% whole blood solution was tested. Here, we were able to find groups of cells whereas cells were not found on the filter containing Triton X-100 (Figure 7-2 B)). Figure 7-2 C) shows a 100% whole blood solution on plain filter paper. Here, cells were found across the filter, covering almost the entire surface. Again, the paired sample using a Triton x-100 filter showed no cells (Figure 7-2 D)).

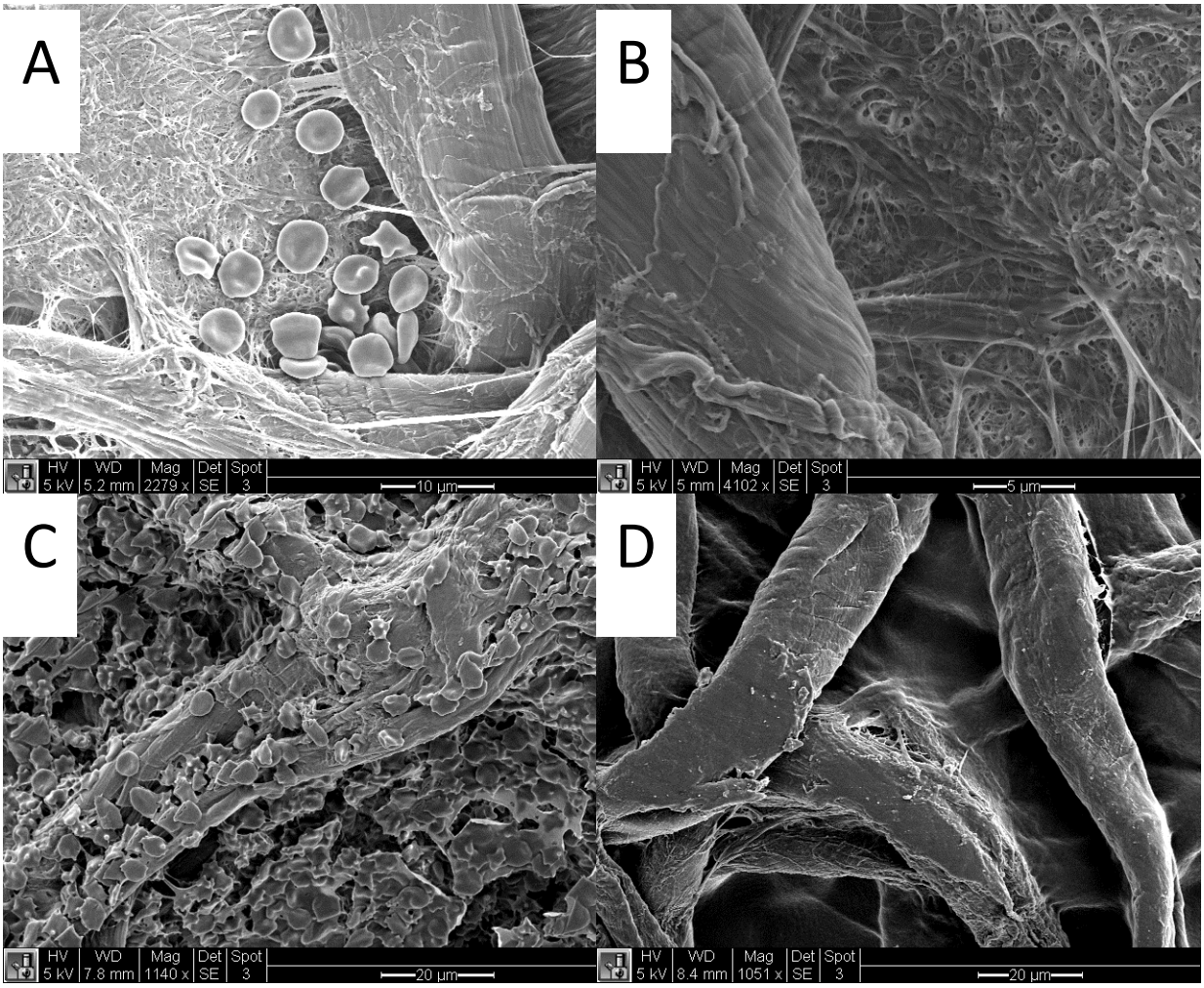

Figure 7-2 Scanning electron microscopy of fixed cells. a) 10% whole blood deposited on a plain filter, then fixed. b) 10% whole blood deposited on a filter with 10% triton x-100, then fixed. c) 100% whole blood deposited on a plain filter, then fixed. b) 100% whole blood deposited on a filter with 10% triton x-100, then fixed.

For field purposes, homogenization of the samples may be useful to ensure variations in other factors, such as amount of cell lysis or protein orientation do not contribute to sample differences during analysis. To maintain a minimal level of sample preparation, the pre-lysing of cells is desirable. Here, a pre-spotting method was employed where a detergent, Triton X-100, was first deposited on the filter. This was meant to lyse the cells and denature the proteins and mimic an affordable pre-packaged sample substrate for field use. Overall, however, this lysis may affect other nutrients due to the contents of red blood cells (RBCs). Specifically, RBCs contain high amounts of Fe and FolA and thus may have a much larger physiological concentration range after lysis, and may eliminate the test's ability to determine nutrient deficiencies.

7.2.3.2 Blood separation

An alternative to blood lysis is to separate the solid and liquid components of blood. This will better mimic previous studies, as we can isolate the blood plasma for analysis. Initially, normal filter paper was used to attempt blood separation by simply spotting the blood on one side of the filter, and flipping the filter over. This, however, was unsuccessful as cells could be found on the bottom of the filter with SEM imaging. Upon closer study, the filters used (Whatman Grade 40) were found to have a particle retention of 8 μm – roughly the size of an RBC. Further studies were then completed on Grade 50 filters with a manufacturer advertised particle retention of 2.7 μm. However, even with these filters, RBCs were still visible on the bottom of the filter with SEM. Additional filters can be tested, however, more expensive solutions, such as commercially available blood filtration paper from Pall Corporation (Port Washington, NY, model T9EXPPA0200S00A), may be required.

7.2.3.3 Real blood analysis

After a suitable blood sample homogenization method, and controlled sample quantitation are achieved, real blood samples will need to be analyzed. A large cache of samples will be required to properly account for both the variability in nutrient content and the variability in other components in blood. After obtaining blood from a suitable source (either a blood bank, or recruitment through an in-house study), nutrient content in samples can be established by current gold standards by submitting samples to a facility like the UW Research Testing Service. Samples will then be analyzed using the PPAMS, and data will be split in to test and verification groups. The test group will be used to build the PLSr model and can be checked with the verification group.

8 References

1 Organization, W. H. Preventing and controlling micronutrient deficiencies in populations affected by an emergency. *Geneva, Switzerland: World Health Organization* (2007).

2 Black, R. Micronutrient deficiency-an underlying cause of morbidity and mortality. *BULLETIN-WORLD HEALTH ORGANIZATION* **81**, 79-79 (2003).

3 Müller, O. & Krawinkel, M. Malnutrition and health in developing countries. *Canadian Medical Association Journal* **173**, 279-286 (2005).

4 Lynch, S. Improving the assessment of iron status. *The American journal of clinical nutrition* **93**, 1188-1189 (2011).

5 Friel, J. K. *et al.* A double-masked, randomized control trial of iron supplementation in early infancy in healthy term breast-fed infants. *The Journal of pediatrics* **143**, 582-586 (2003).

6 Grantham-McGregor, S. & Ani, C. A review of studies on the effect of iron deficiency on cognitive development in children. *The Journal of Nutrition* **131**, 649S-668S (2001).

7 Barceloux, D. Zinc.(1999). *Journal of Toxicology, Clinical Toxicology* **37**, 279-292.

8 Prasad, A. S. Discovery of human zinc deficiency and studies in an experimental human model. *The American journal of clinical nutrition* **53**, 403-412 (1991).

9 Prasad, A. S. 3 Clinical, endocrinological and biochemical effects of zinc deficiency. *Clinics in endocrinology and metabolism* **14**, 567-589 (1985).

10 Ames, B. N. DNA damage from micronutrient deficiencies is likely to be a major cause of cancer. *Mutation research* **475**, 7 (2001).

11 Girodon, F. *et al.* Effect of micronutrient supplementation on infection in institutionalized elderly subjects: a controlled trial. *Annals of nutrition and metabolism* **41**, 98-107 (1997).

12 Dasgupta, P. K., Liu, Y. & Dyke, J. V. Iodine nutrition: iodine content of iodized salt in the United States. *Environmental science & technology* **42**, 1315-1323 (2008).

13 Jacques, P. F., Selhub, J., Bostom, A. G., Wilson, P. W. F. & Rosenberg, I. H. The effect of folic acid fortification on plasma folate and total homocysteine concentrations. *New England Journal of Medicine* **340**, 1449-1454 (1999).

14 Honein, M. A., Paulozzi, L. J., Mathews, T., Erickson, J. D. & Wong, L. Y. C. Impact of folic acid fortification of the US food supply on the occurrence of neural tube defects. *JAMA: the journal of the American Medical Association* **285**, 2981-2986 (2001).

15 De Wals, P. *et al.* Reduction in neural-tube defects after folic acid fortification in Canada. *New England Journal of Medicine* **357**, 135-142 (2007).

16 Allen, L. H. Interventions for micronutrient deficiency control in developing countries: past, present and future. *The Journal of nutrition* **133**, 3875S-3878S (2003).

17 Bürgi, H. Iodine excess. *Best Practice & Research Clinical Endocrinology & Metabolism* **24**, 107-115 (2010).

18 Lee, K., Bradley, R., Dwyer, J. & Lee, S. L. Too much versus too little: the implications of current iodine intake in the United States. *Nutrition reviews* **57**, 177-181 (1999).

19 de Benoist, B., McLean, E., Andersson, M. & Rogers, L. Iodine deficiency in 2007: global progress since 2003. *Food Nutr Bull* **29**, 195-202 (2008).

20 Kitwa, K. E. *et al.* Evaluation of iodine content in table salt consumed in Democratic Republic of Congo. *Food & Nutrition Bulletin* **33**, 217-223 (2012).

21 Charlton, K. & Skeaff, S. Iodine fortification: why, when, what, how, and who? *Current opinion in clinical nutrition and metabolic care* **14**, 618-624, doi:10.1097/MCO.0b013e32834b2b30 (2011).

22 Ashwood, E. R. *Tietz textbook of clinical chemistry*. (WB Saunders, 1999).

23 *UW Laboratory Medicine: Zinc*, <http://menu.labmed.washington.edu/oltg/display?mnemonic=ZN&search_cross_reference=yes&search_as_component=yes&search_text=zinc&search_type=text> (2011).
24 *UW Laboratory Medicine: Vitamin A*, <http://menu.labmed.washington.edu/oltg/display?mnemonic=VITA&search_cross_reference=yes&search_as_component=yes&search_text=vitamin%20a&search_type=text> (2012).
25 Organization, W. H. Serum retinol concentrations for determining the prevalence of vitamin A deficiency in populations. (2011).
26 Low, J. W. *et al.* A food-based approach introducing orange-fleshed sweet potatoes increased vitamin A intake and serum retinol concentrations in young children in rural Mozambique. *J Nutr* **137**, 1320-1327 (2007).
27 Mahmood, K. *et al.* Serum retinol binding protein as an indicator of vitamin A status in cirrhotic patients with night blindness. *Saudi journal of gastroenterology : official journal of the Saudi Gastroenterology Association* **14**, 7-11, doi:10.4103/1319-3767.37794 (2008).
28 Baeten, J. M. *et al.* Use of serum retinol-binding protein for prediction of vitamin A deficiency: effects of HIV-1 infection, protein malnutrition, and the acute phase response. *Am J Clin Nutr* **79**, 218-225 (2004).
29 de Pee, S. & Dary, O. Biochemical indicators of vitamin A deficiency: serum retinol and serum retinol binding protein. *J Nutr* **132**, 2895S-2901S (2002).
30 Balagopal, P. *et al.* Reduction of elevated serum retinol binding protein in obese children by lifestyle intervention: association with subclinical inflammation. *The Journal of clinical endocrinology and metabolism* **92**, 1971-1974, doi:10.1210/jc.2006-2712 (2007).
31 McDade, T. W. & Shell-Duncan, B. Whole blood collected on filter paper provides a minimally invasive method for assessing human transferrin receptor level. *The Journal of nutrition* **132**, 3760-3763 (2002).
32 Nakamoto, K., Kurita, R., Sekioka, N. & Niwa, O. Simultaneous on-chip surface plasmon resonance measurement of disease marker protein and small metabolite combined with immuno-and enzymatic reactions. *Chemistry Letters* **37**, 698-699 (2008).
33 Hix, J. *et al.* Development of a rapid enzyme immunoassay for the detection of retinol-binding protein. *The American journal of clinical nutrition* **79**, 93-98 (2004).
34 Weibel, D. *et al.* A C60 primary ion beam system for time of flight secondary ion mass spectrometry: its development and secondary ion yield characteristics. *Anal Chem* **75**, 1754-1764 (2003).
35 Trauger, S. A. *et al.* High sensitivity and analyte capture with desorption/ionization mass spectrometry on silylated porous silicon. *Analytical chemistry* **76**, 4484-4489 (2004).
36 Yinon, J. Field detection and monitoring of explosives. *TrAC Trends in Analytical Chemistry* **21**, 292-301 (2002).
37 Ewing, R. G., Atkinson, D. A., Eiceman, G. & Ewing, G. A critical review of ion mobility spectrometry for the detection of explosives and explosive related compounds. *Talanta* **54**, 515-529 (2001).
38 Bantscheff, M., Schirle, M., Sweetman, G., Rick, J. & Kuster, B. Quantitative mass spectrometry in proteomics: a critical review. *Analytical and bioanalytical chemistry* **389**, 1017-1031 (2007).
39 Wagner, M. S., McArthur, S. L., Shen, M., Horbett, T. A. & Castner, D. G. Limits of detection for time of flight secondary ion mass spectrometry (ToF-SIMS) and X-ray photoelectron spectroscopy (XPS): detection of low amounts of adsorbed protein. *Journal of Biomaterials Science, Polymer Edition* **13**, 407-428 (2002).
40 Vickerman, J. C. & Gilmore, I. S. *Surface analysis: the principal techniques*. (Wiley Online Library).

41 Kraj, A., Desiderio, D. M. & Nibbering, N. M. *Mass spectrometry: instrumentation, interpretation, and applications*. Vol. 20 (Wiley, 2008).
42 Fenn, J. B., Mann, M., Meng, C. K., Wong, S. F. & Whitehouse, C. M. Electrospray ionization for mass spectrometry of large biomolecules. *Science (New York, NY)* **246**, 64 (1989).
43 Wilm, M. Principles of electrospray ionization. *Molecular & cellular proteomics : MCP* **10**, M111 009407, doi:10.1074/mcp.M111.009407 (2011).
44 Harper, J. D. *et al.* Low-temperature plasma probe for ambient desorption ionization. *Analytical chemistry* **80**, 9097-9104 (2008).
45 Cox, T. F. *et al. An introduction to multivariate data analysis*. (Hodder Arnold, 2005).
46 Wold, S., Esbensen, K. & Geladi, P. Principal component analysis. *Chemometrics and intelligent laboratory systems* **2**, 37-52 (1987).
47 Yendle, P. W. & Macfie, H. J. H. Discriminant principal components analysis. *Journal of chemometrics* **3**, 589-600 (1989).
48 Wold, S., Sjöström, M. & Eriksson, L. PLS-regression: a basic tool of chemometrics. *Chemometrics and intelligent laboratory systems* **58**, 109-130 (2001).
49 Tobias, R. D. in *Proc. Ann. SAS Users Group Int. Conf., 20th, Orlando, FL.* 2-5.
50 Dole, M. *et al.* Molecular beams of macroions. *The Journal of Chemical Physics* **49**, 2240 (1968).
51 Emmett, M. R., White, F. M., Hendrickson, C. L., Shi, S. D. H. & Marshall, A. G. Application of micro-electrospray liquid chromatography techniques to FT-ICR MS to enable high-sensitivity biological analysis. *Journal of the American Society for Mass Spectrometry* **9**, 333-340 (1998).
52 Walker, H. K., Hall, W. D., Hurst, J. W. & Ackerman, G. L. Serum Sodium. (1990).
53 Cody, R. B., Laramée, J. A. & Durst, H. D. Versatile new ion source for the analysis of materials in open air under ambient conditions. *Analytical Chemistry* **77**, 2297-2302 (2005).
54 Kpegba, K., Spadaro, T., Cody, R. B., Nesnas, N. & Olson, J. A. Analysis of self-assembled monolayers on gold surfaces using direct analysis in real time mass spectrometry. *Analytical chemistry* **79**, 5479-5483 (2007).
55 Yu, S., Crawford, E., Tice, J., Musselman, B. & Wu, J. T. Bioanalysis without sample cleanup or chromatography: the evaluation and initial implementation of direct analysis in real time ionization mass spectrometry for the quantification of drugs in biological matrixes. *Analytical chemistry* **81**, 193-202 (2008).
56 Li, Y. J. *et al.* The evaluation and implementation of direct analysis in real time quadrupole time-of-flight tandem mass spectrometry for characterization and quantification of geniposide in Re Du Ning Injections. *Rapid communications in mass spectrometry* **26**, 1377-1384 (2012).
57 Collins, L. & Wendlandt, W. The detection of ignition temperatures of various materials by photothermal analysis. *Thermochimica Acta* **7**, 201-207 (1973).
58 Liu, Y., Lin, Z., Zhang, S., Yang, C. & Zhang, X. Rapid screening of active ingredients in drugs by mass spectrometry with low-temperature plasma probe. *Analytical and bioanalytical chemistry* **395**, 591-599 (2009).
59 Jackson, A. U. *et al.* Analysis of drugs of abuse in biofluids by low temperature plasma (LTP) ionization mass spectrometry. *Analyst* **135**, 927-933 (2010).
60 Zhang, Y. *et al.* Direct detection of explosives on solid surfaces by low temperature plasma desorption mass spectrometry. *Analyst* **134**, 176-181 (2008).
61 García-Reyes, J. F. *et al.* Direct olive oil analysis by low-temperature plasma (LTP) ambient ionization mass spectrometry. *Rapid communications in mass spectrometry* **23**, 3057-3062 (2009).

62 Chew, A. *et al.* Considerations for Primary Vacuum Pumping in Mass Spectrometry Systems-Mass spectrometry systems have specific vacuum requirements. New developments in oil-free, or dry primary vacuum pumps have. *Spectroscopy-Eugene* **20**, 44-51 (2005).
63 Taylor, P. J. Matrix effects: the Achilles heel of quantitative high-performance liquid chromatography-electrospray-tandem mass spectrometry. *Clinical biochemistry* **38**, 328-334, doi:10.1016/j.clinbiochem.2004.11.007 (2005).
64 Brown, B. N. *et al.* Surface characterization of extracellular matrix scaffolds. *Biomaterials* **31**, 428 (2010).
65 Harper, J. D. *et al.* Low-Temperature Plasma Probe for Ambient Desorption Ionization. *Anal. Chem.* **80**, 9097-9104 (2008).
66 Ratcliffe, L. V. *et al.* Surface Analysis under Ambient Conditions Using Plasma-Assisted Desorption/Ionization Mass Spectrometry. *Analytical Chemistry* **79**, 6094-6101 (2007).
67 Stoffels, E., Flikweert, A. J. & Kroesen, G. M. W. Plasma needle: a non-destructive atmospheric plasma source for fine surface treatment of (bio)materials. *Plasma Sources Sci. Technol.* **11**, 383-388 (2002).
68 Stoffels, E., Gonzalvo, Y. A., Whitmore, T. D. & Seymour, D. L. Mass spectrometric detection of short-living radicals produced by a plasma needle *Plasma Sources Sci. Technol.* **16**, 549 (2007).
69 Horbett, T. A. in *Techniques of Biocompatibility Testing* Vol. II (ed D. F. Williams) 183–214 (CRC Press, Inc., 1986).
70 Horbett, T. A. & Brash, J. L. in *Proteins at Interfaces: Physicochemical and Biochemical Studies, ACS Symposium Series* Vol. 343 (eds T. A. Horbett & J. L. Brash) 1–33 (American Chemical Society, 1987).
71 Wagner, M. S. & Castner, D. G. Characterization of Adsorbed Protein Films by Time-of-Flight Secondary Ion Mass Spectrometry with Principal Component Analysis. *Langmuir* **17**, 4649-4660 (2001).
72 Wise, B. M. & Gallagher, N. B. *PLS_Toolbox Version 2.0 Manual*. (Eigenvector Research, 1998).
73 Doumas, B. T., Ard Watson, W. & Biggs, H. G. Albumin standards and the measurement of serum albumin with bromcresol green. *Clinica Chimica Acta* **31**, 87-96 (1971).
74 Besarab, A. *et al.* The effects of normal as compared with low hematocrit values in patients with cardiac disease who are receiving hemodialysis and epoetin. *New England Journal of Medicine* **339**, 584-590 (1998).
75 Liu, Y. *et al.* Imaging Mass Spectrometry with a Low-Temperature Plasma Probe for the Analysis of Works of Art. *Angewandte Chemie* **122**, 4537-4539 (2010).
76 Chan, G. C. *et al.* Elucidation of reaction mechanisms responsible for afterglow and reagent-ion formation in the low-temperature plasma probe ambient ionization source. *Analytical chemistry* **83**, 3675-3686, doi:10.1021/ac103224x (2011).
77 Keenan, M. R. & Kotula, P. G. Accounting for Poisson noise in the multivariate analysis of ToF-SIMS spectrum images. *Surface and interface analysis* **36**, 203-212 (2004).
78 Begley, I. S. & Sharp, B. L. Characterisation and correction of instrumental bias in inductively coupled plasma quadrupole mass spectrometry for accurate measurement of lead isotope ratios. *Journal of Analytical Atomic Spectrometry* **12**, 395-402 (1997).
79 Coombes, K. R. *et al.* Quality control and peak finding for proteomics data collected from nipple aspirate fluid by surface-enhanced laser desorption and ionization. *Clinical Chemistry* **49**, 1615-1623 (2003).
80 Benninghoven, A. Chemical Analysis of Inorganic and Organic Surfaces and Thin Films by Static Time-of-Flight Secondary Ion Mass Spectrometry (TOF-SIMS). *Angewandte Chemie International Edition in English* **33**, 1023-1043 (1994).

81 Hart, G. L., Hager, G. J., Barinaga, C. J. & Duckworth, D. C. Market Research Survey of Commercial Off-The-Shelf (COTS) Portable MS Systems for IAEA Safeguards Applications. (Pacific Northwest National Laboratory (PNNL), Richland, WA (US), 2013).
82 Gao, L., Song, Q., Patterson, G. E., Cooks, R. G. & Ouyang, Z. Handheld rectilinear ion trap mass spectrometer. *Analytical chemistry* **78**, 5994-6002, doi:10.1021/ac061144k (2006).
83 Dalgleish, J. K., Hou, K., Ouyang, Z. & Cooks, R. G. In situ explosive detection using a miniature plasma ion source and a portable mass spectrometer. *Analytical Letters* **45**, 1440-1446 (2012).
84 Sokol, E. *et al.* Miniature mass spectrometer equipped with electrospray and desorption electrospray ionization for direct analysis of organics from solids and solutions. *International Journal of Mass Spectrometry* **306**, 187-195 (2011).
85 Burtis, C. A., Ashwood, E. R., Bruns, D. E. & Tietz, N. W. *Tietz textbook of clinical chemistry and molecular diagnostics*. 5th edn, (Saunders, 2013).
86 Harper, J. D. *et al.* Low-temperature plasma probe for ambient desorption ionization. *Analytical chemistry* **80**, 9097-9104, doi:10.1021/ac801641a (2008).
87 Stein, M. J., Lo, E., Castner, D. G. & Ratner, B. D. Plasma pencil atmospheric mass spectrometry detection of positive ions from micronutrients emitted from surfaces. *Analytical chemistry* **84**, 1572-1578, doi:10.1021/ac2028134 (2012).
88 Albert, A. & Engelhard, C. Characteristics of low-temperature plasma ionization for ambient mass spectrometry compared to electrospray ionization and atmospheric pressure chemical ionization. *Analytical chemistry* **84**, 10657-10664, doi:10.1021/ac302287x (2012).
89 Garcia-Reyes, J. F. *et al.* Detection of explosives and related compounds by low-temperature plasma ambient ionization mass spectrometry. *Analytical chemistry* **83**, 1084-1092, doi:10.1021/ac1029117 (2011).
90 Huang, G., Xu, W., Visbal-Onufrak, M. A., Ouyang, Z. & Cooks, R. G. Direct analysis of melamine in complex matrices using a handheld mass spectrometer. *The Analyst* **135**, 705-711, doi:10.1039/b923427f (2010).
91 Zhang, J. I., Tao, W. A. & Cooks, R. G. Facile determination of double bond position in unsaturated fatty acids and esters by low temperature plasma ionization mass spectrometry. *Analytical chemistry* **83**, 4738-4744, doi:10.1021/ac1030946 (2011).
92 Van Breemen, R. B. & Huang, C. R. High-performance liquid chromatography-electrospray mass spectrometry of retinoids. *FASEB J* **10**, 1098-1101 (1996).
93 van Breemen, R. B. *et al.* Development of a method for quantitation of retinol and retinyl palmitate in human serum using high-performance liquid chromatography-atmospheric pressure chemical ionization-mass spectrometry. *J Chromatogr A* **794**, 245-251 (1998).
94 Shelley, J. T., Stindt, A., Riedel, J. & Engelhard, C. Time-resolved mass-spectral characterization of ion formation from a low-frequency, low-temperature plasma probe ambient ionization source. *Journal of Analytical Atomic Spectrometry* **29**, 359-366, doi:10.1039/C3JA50318F (2014).
95 McMaster, M. C. in *GC/MS: A Practical User's Guide* 165-166 (John Wiley & Sons, Inc., 2007).
96 Shelley, J. T., Stindt, A., Riedel, J. & Engelhard, C. Time-resolved mass-spectral characterization of ion formation from a low-frequency, low-temperature plasma probe ambient ionization source. *J. Anal. At. Spectrom.* **29**, 359-366 (2014).
97 MacCoss, M. J., Toth, M. J. & Matthews, D. E. Evaluation and optimization of ion-current ratio measurements by selected-ion-monitoring mass spectrometry. *Analytical chemistry* **73**, 2976-2984 (2001).
98 Fliegl, H. & Sundholm, D. Aromatic pathways of porphins, chlorins, and bacteriochlorins. *The Journal of organic chemistry* **77**, 3408-3414, doi:10.1021/jo300182b (2012).

99 Sharkey, T. D. Isoprene synthesis by plants and animals. *Endeavour* **20**, 74-78 (1996).
100 Ceglowski, M., Jasiecki, S. & Schroeder, G. Laser desorption/ionization mass spectrometric analysis of folic acid, vancomycin and Triton(R) X-100 on variously functionalized carbon nanotubes. *Rapid communications in mass spectrometry : RCM* **27**, 2631-2638, doi:10.1002/rcm.6728 (2013).
101 Eicke, A., Anders, V., Junack, M., Sichtermann, W. & Benninghoven, A. Secondary ion mass spectrometry of folic acid analogs. *Analytical chemistry* **55**, 178-182 (1983).
102 McArthur, S. L., Vendettuoli, M. C., Ratner, B. D. & Castner, D. G. Methods for generating protein molecular ions in ToF-SIMS. *Langmuir : the ACS journal of surfaces and colloids* **20**, 3704-3709 (2004).
103 Hillenkamp, F. & Peter-Katalinic, J. *MALDI MS: a practical guide to instrumentation, methods and applications*. (John Wiley & Sons, 2013).
104 Brouwer, I. A. *et al.* Low-dose folic acid supplementation decreases plasma homocysteine concentrations: a randomized trial. *The American journal of clinical nutrition* **69**, 99-104 (1999).
105 Giles, W. H., Croft, J. B., Greenlund, K. J., Ford, E. S. & Kittner, S. J. Total homocyst(e)ine concentration and the likelihood of nonfatal stroke: results from the Third National Health and Nutrition Examination Survey, 1988-1994. *Stroke; a journal of cerebral circulation* **29**, 2473-2477 (1998).
106 Jamil Akhtar, M., Ataullah Khan, M. & Ahmad, I. Identification of photoproducts of folic acid and its degradation pathways in aqueous solution. *Journal of pharmaceutical and biomedical analysis* **31**, 579-588 (2003).
107 Off, M. K. *et al.* Ultraviolet photodegradation of folic acid. *Journal of photochemistry and photobiology. B, Biology* **80**, 47-55, doi:10.1016/j.jphotobiol.2005.03.001 (2005).
108 Shelley, J. T. & Hieftje, G. M. Ionization matrix effects in plasma-based ambient mass spectrometry sources. *Journal of Analytical Atomic Spectrometry* **25**, 345-350 (2010).
109 Kloepfer, A., Quintana, J. B. & Reemtsma, T. Operational options to reduce matrix effects in liquid chromatography-electrospray ionization-mass spectrometry analysis of aqueous environmental samples. *Journal of chromatography. A* **1067**, 153-160 (2005).
110 Smeraglia, J., Baldrey, S. F. & Watson, D. Matrix effects and selectivity issues in LC-MS-MS. *Chromatographia* **55**, S95-S99, doi:10.1007/BF02493363 (2002).
111 Fitzgerald, R. L., O'Neal, C. L., Hart, B. J., Poklis, A. & Herold, D. A. Comparison of an ion-trap and a quadrupole mass spectrometer using diazepam as a model compound. *Journal of analytical toxicology* **21**, 445-450 (1997).
112 Contreras, J. A. *et al.* Hand-portable gas chromatograph-toroidal ion trap mass spectrometer (GC-TMS) for detection of hazardous compounds. *Journal of the American Society for Mass Spectrometry* **19**, 1425-1434, doi:10.1016/j.jasms.2008.06.022 (2008).
113 Dalgleish, J. K. *et al.* Arrays of low-temperature plasma probes for ambient ionization mass spectrometry. *Rapid communications in mass spectrometry : RCM* **27**, 135-142, doi:10.1002/rcm.6435 (2013).
114 Chan, G. C.-Y. *et al.* Spectroscopic plasma diagnostics on a low-temperature plasma probe for ambient mass spectrometry. *Journal of Analytical Atomic Spectrometry* **26**, 1434-1444 (2011).
115 Marikovsky, Y. & Danon, D. Electron microscope analysis of young and old red blood cells stained with colloidal iron for surface charge evaluation. *The Journal of cell biology* **43**, 1-7 (1969).

9 Appendices

9.1 Appendix A: Additional ESI-MS data

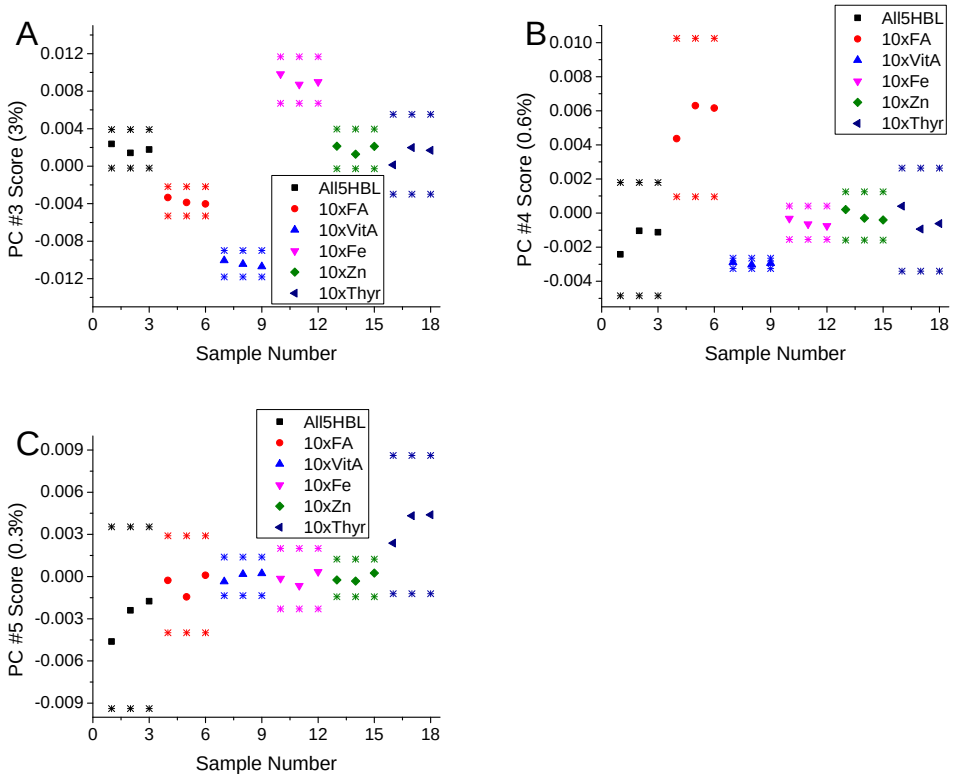

Figure 9-1 Scores plots for PC #3-5 for ESI-MS data. Single nutrients were added to solution at 10x HBLC, with the remaining nutrients added at 1x HBLC. A) Scores for PC#3 separate both 10x iron and 10x vitamin A from the other sample types. Iron separates towards the positive scores, while vitamin A separates towards the negative. Both separate to 95% confidence. B) Scores for PC#4 largely separate 10x folic acid from the other sample types towards the positive score, with a slight overlap in the confidence intervals. C) Scores for PC#5 separate the 10x thyroxine data points from the other nutrients. However, high overlap exists in the 95% confidence intervals. * indicates 95% confidence intervals.

9.2 Appendix B: Nutrient structure

Table 9-1 Nutrient structure

Nutrient	Structure
Iron	$FeCl_2$
Zinc	$ZnCl_2$
Vitamin A	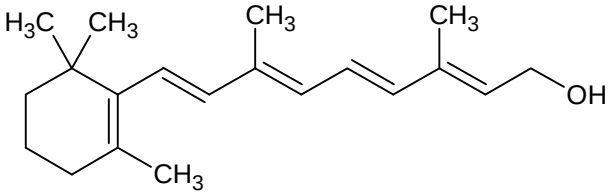
Folic Acid	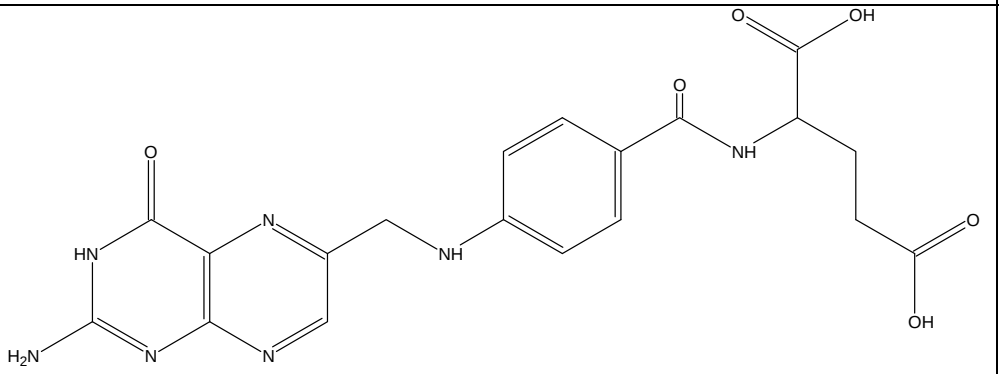
Thyroxine	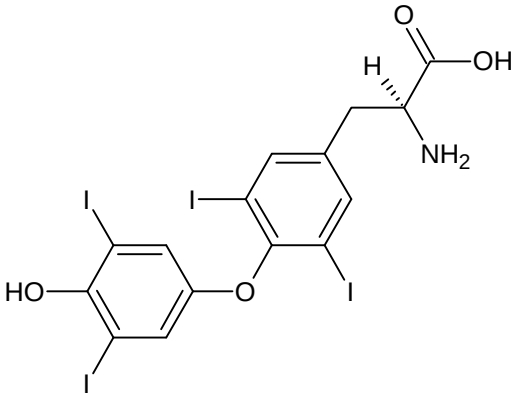

9.3 Appendix C: Sample nutrient matrix

Table 9-2 Nutrient concentration matrix

Sample	FolA	Thyr	VitA
1	H	H	H
2	H	H	L
3	H	L	L
4	H	L	H
5	L	H	H
6	L	H	L
7	L	L	H
8	L	L	L
9	M	M	M
10	M	M	L
11	M	L	L
12	M	L	M
13	L	M	M
14	L	M	L
15	L	L	M
16	H	H	M
17	H	M	M
18	H	M	H
19	M	H	H
20	M	H	M
21	M	M	H
22	H	M	L
23	H	L	M
24	M	H	L
25	M	L	H
26	L	H	M
27	L	M	H

*H: High blood level; M: Medium blood level; L: Low blood level

9.4 Appendix D: Nutrient content in blood

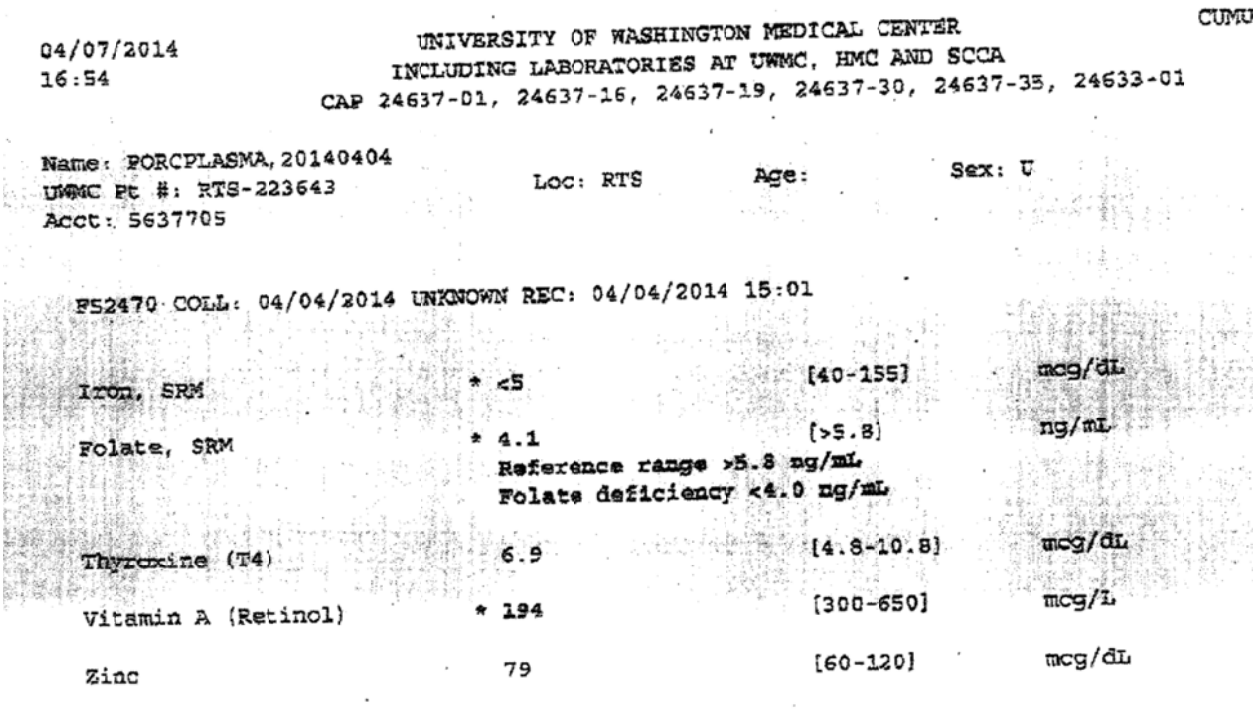

CUMU

04/07/2014
16:54

UNIVERSITY OF WASHINGTON MEDICAL CENTER
INCLUDING LABORATORIES AT UWMC, HMC AND SCCA
CAP 24637-01, 24637-16, 24637-19, 24637-30, 24637-35, 24633-01

Name: PORCPLASMA, 20140404
UWMC Pt #: RTS-223643 Loc: RTS Age: Sex: U
Acct: 5637705

FS2470 COLL: 04/04/2014 UNKNOWN REC: 04/04/2014 15:01

Iron, SRM	* <5	[40-155]	mcg/dL
Folate, SRM	* 4.1	[>5.8]	ng/mL
	Reference range >5.8 ng/mL		
	Folate deficiency <4.0 ng/mL		
Thyroxine (T4)	6.9	[4.8-10.8]	mcg/dL
Vitamin A (Retinol)	* 194	[300-650]	mcg/L
Zinc	79	[60-120]	mcg/dL

Figure 9-2 Nutrient content in raw porcine plasma. Samples were sent to the University of Washington Research Testing Service to measure nutrient content in samples using current standard of detection. For 10% porcine plasma solutions, concentrations were multiplied by 0.1, and samples were then supplemented with additional nutrients.

9.5 Appendix E: Peaks removed from spectra

m/z 36, 37, 54, 55, 73, 79, 88, 91, 135, 149, 157, 159, 219, 236, 257, 275, 285, 303, 350-355, 370-375 and 390-395